Avalanches in insulating gases

AVALANCHES IN INSULATING GASES

H.F.A. VERHAART

AVALANCHES IN INSULATING GASES

PROEFSCHRIFT

TER VERKRIJGING VAN DE GRAAD VAN DOCTOR IN DE TECHNISCHE WETENSCHAPPEN AAN DE TECHNISCHE HOGESCHOOL EINDHOVEN, OP GEZAG VAN DE RECTOR MAGNIFICUS, PROF. DR. S. T. M. ACKERMANS, VOOR EEN COMMISSIE AANGEWEZEN DOOR HET COLLEGE VAN DEKANEN IN HET OPENBAAR TE VERDEDIGEN OP DINSDAG 14 SEPTEMBER 1982 TE 16.00 UUR

DOOR

HENRICUS FERDINANDUS ANNA VERHAART

GEBOREN TE HILVERSUM

Dit proefschrift is goedgekeurd
door de promotoren:

prof.dr.ir. P.C.T. van der Laan
prof.dr.ir. W.M.C. van den Heuvel

CIP-gegevens

Verhaart, Henricus Ferdinandus Anna

Avalanches in insulating gases / Henricus Ferdinandus
Anna Verhaart. - [S.l. : s.n.].-Fig.-Proefschrift
Eindhoven. - Met lit. opg., reg.
ISBN 90-9000356-8
SISO 661.1 UDC 621.315.61.027.3
Trefw.: hoogspanningstechniek / isolatiemateriaal.

Aan mijn ouders

Aan Nelly en Marcel

VOORWOORD

Het in dit proefschrift beschreven onderzoek is uitgevoerd in de vakgroep "Technieken van de Energievoorziening" van de Technische Hogeschool te Eindhoven.
De leden van de vakgroep dank ik voor de geboden hulp.
In het bijzonder ben ik prof.dr.ir. P.C.T. van der Laan erkentelijk voor de begeleiding van het onderzoek.
Voor de technische assistentie ben ik veel dank verschuldigd aan A.J. Aldenhoven.
Ook dank aan studenten die op deelgebieden van dit onderzoek werkzaam zijn geweest, met name zou ik ir. C.G.A. Koreman willen noemen die in het kader van zijn afstudeerwerk dit onderzoek mede van de grond heeft geholpen.
Voor het numeriek werk gedaan door ir. G.G. Wolzak ter verkrijging van Figuur 3.3.2 dank ik hem hartelijk.
Het typewerk was in goede handen bij mevr. M. Marrevée en mevr. M. Verbeek; het tekenwerk werd verzorgd door F.M. van Gompel.

CONTENTS

SUMMARY

Avalanches of charged particles in gases are often studied with the "electrical method", the measurement of the waveform of the current in the external circuit. In this thesis a substantial improvement of the time resolution of the measuring setup, to be used for the electrical method, is reported. The avalanche is started by an N_2-laser with a pulse duration of only 0.6 ns. With this laser it is possible to release a high number of primary electrons (some 10^8) which makes it possible to obtain sizeable signals, even at low E/p values. The high-frequency response of the measuring system has been significantly improved by the use of a subdivided cathode. The diameter of the circular measuring part of this electrode determines a maximum gap distance for reliable measurements which can be determined experimentally and calculated from theories of Ramo and Shockley.
With this setup it is possible to analyze current waveforms with a time resolution down to 1.4 ns, determined by both the laser and the measuring system. Furthermore it is possible to distinguish between the current caused by the electrons and the current caused by the ions in the avalanche and to monitor these currents simultaneously.

Avalanche currents are measured in N_2, CO_2, O_2, H_2O, air of varying humidity, SF_6 and SF_6/N_2 mixtures.
Depending on the nature of the gas and the experimental conditions, processes as diffusion, ionization, attachment, detachment, conversion and secondary emission are observed. Values of parameters with which these processes can be described, are derived from an analysis of the current waveforms. For this analysis already published theories and new theories described in this thesis are used. The drift velocity of both the electrons and the ions could be easily determined from measured avalanche currents.
Special attention is paid to avalanches in air because of the practical importance of air insulation. An observed influence of the water vapor content on the avalanche current waveform is explained by the occurence of conversion reactions between initially unstable negative ions and water molecules. Up till now the effect of humidity on the breakdown voltage of air was generally attributed to a change in the effective ionization coefficient.

As a possible start for further research currents caused by avalanches near a solid insulator were measured.

SAMENVATTING

Lawines van geladen deeltjes in gassen worden vaak bestudeerd met de zogenaamde "electrical method", waarbij de stroom in het externe circuit als funktie van de tijd wordt gemeten. In dit proefschrift wordt een aanzienlijke verbetering van het tijdoplossend vermogen van een meetopstelling voor de electrical method beschreven. De lawine wordt gestart met het licht van een N_2-laser die een pulsduur van slechts 0.6 ns heeft. Met deze laser is het mogelijk een groot aantal primaire elektronen (enige malen 10^8) vrij te maken, waardoor signalen van goed meetbare grootte kunnen worden verkregen, zelfs voor lage E/p waarden. De frequentieresponsie van het meetsysteem is belangrijk verbeterd door het gebruik van een onderverdeelde kathode. Bij de diameter van het schijfvormige meetgedeelte van deze elektrode behoort een maximale afstand tussen de elektroden waarbij betrouwbare metingen mogelijk zijn. Deze afstand kan zowel experimenteel worden bepaald, als worden berekend met theorieën van Ramo en Shockley.

Met deze opstelling kan het stroomverloop worden geanalyseerd met een tijdoplossend vermogen van slechts 1.4 ns, bepaald door de laser en het meetsysteem. Bovendien is het mogelijk onderscheid te maken tussen de stroom veroorzaakt door de elektronen en de stroom veroorzaakt door de ionen en kunnen deze stromen gelijktijdig geregistreerd worden.

Stromen ten gevolge van lawines zijn gemeten in N_2, CO_2, O_2, H_2O, lucht met variërend vochtgehalte, SF_6 en SF_6/N_2 mengsels.

Afhankelijk van de aard van het gas en de experimentele omstandigheden zijn processen zoals diffusie, ionisatie, attachment, detachment, conversie en secondaire emissie waargenomen. Waarden van parameters waarmee deze processen kunnen worden beschreven, zijn verkregen door de stroomoscillogrammen te analyseren en te vergelijken met eerder gepubliceerde en nieuw ontwikkelde theorieën.

De driftsnelheid van zowel de elektronen als de ionen kan simpel worden afgeleid uit gemeten lawinestromen.
Speciale aandacht wordt geschonken aan lawines in lucht vanwege het praktische belang van lucht als isolerend medium. Een waargenomen invloed van het waterdampgehalte op de stroom ten gevolge van de lawine wordt verklaard door het optreden van conversie-reakties tussen aanvankelijk instabiele negatieve ionen en water-moleculen.
Tot nu toe werd het effekt van de vochtigheid op de doorslagspanning van lucht in het algemeen toegeschreven aan een verandering van de effektieve ionisatie-coëfficiënt.
Als een mogelijke aanloop voor verder onderzoek werden stromen, veroorzaakt door lawines in de nabijheid van vast isolatiemateriaal, gemeten.

1. INTRODUCTION

In electrical power engineering gas is often used as an insulating medium. In practice atmospheric air plays an important role in for instance high-voltage transmission lines and open air sub-stations. Disadvantages of systems operating in open air are the dependence on atmospheric conditions and the objections against their environmental impact. Therefore nowadays much interest is given to closed systems such as cables and metal enclosed SF_6 gas insulated sub-stations. In a closed system gases with better electrical properties can be used. From the mechanical point of view these systems require in addition to the gas rigid insulators, the so-called spacers. These spacers have a limiting influence on the breakdown voltage of the entire system. To obtain more insight in the mechanisms which cause this influence it is necessary to have more knowledge about the processes in the gas itself.

The aim of the work described in this thesis is to study the processes in which charged particles are involved, during the early stage of the electrical discharge. These so-called "pre-breakdown phenomena" are investigated at atmospheric pressures, whenever this is feasible, to make the results more relevant for the practical applications.

During the pre-breakdown stage a single free electron can produce a number of electrons and ions in the gas under the influence of the applied electric field. These so-called avalanches cause a current in the external circuit which can be measured and analyzed. To study these avalanches two significantly different methods are used: Townsend's method (see for example Ref. [Me 78])in which primary free electrons are formed continuously and the electrical method (see for example Ref. [Ra 64])in which a number of primary electrons are formed in a single short pulse. The first method results in the flow of a small steady current while with the second method a time-dependent current is obtained.

We used for our experiments the electrical method because this method can give more direct information on processes occurring in an avalanche, especially if more processes in rapid succession are involved. A problem is however, to construct a measuring setup for this method with sufficient time and amplitude resolution. Technical

problems with this resolution led in the past to the suggestion that the timeconstant of the measuring system should equal the characteristic time of the processes in the avalanche (the so-called "balanced case", see Ref. [Ra 64]). This is however, only meaningful for relatively simple gases in which only ionization and attachment are important. Other authors integrate the current with respect to time (see for example Ref. [Fr 64]); the thus obtained signals are difficult to analyze and processes occurring in rapid succession do not show up well in the integrated currents.
We made a thorough analysis of the limiting factors of the electrical method and achieved a considerable improvement of the time resolution (see Ref. [Ve 82]). In addition a laser was used with which a large number of photoelectrons could be released from the cathode in a very short pulse. This made it possible to observe avalanches in a very direct way and to study a large number of processes in various gases which led to many new results.

2. THEORY OF COLLISIONAL PROCESSES IN AN AVALANCHE AND THEIR EFFECT ON THE CURRENT IN THE EXTERNAL CIRCUIT

2.1. Introduction

In a gas-discharge configuration electrons released from the cathode drift to the anode under the influence of the applied E-field. Several collisional processes play a role in the formation of an avalanche. This chapter firstly describes briefly the most important processes in an avalanche. In the following sections calculations are given for the current caused by the motion of charge carriers in an avalanche between plane electrodes. In these calculations it is assumed that the primary electrons which start the avalanche are released from the cathode in a pulse of negligibly short duration. The density is assumed to be low enough to keep the field distortion by space-charge effects small. In the last section the transition of a non-selfsustaining discharge into a complete breakdown is discussed.

2.2. Collisional processes in an avalanche

Electrons released from the cathode will gain energy from the E-field and lose energy by collisions with heavy particles. At practical pressures these two processes balance each other very rapidly [Fo 73]. When an equilibrium velocity distribution of the electrons has been established several inelastic collisions become possible in which the electrons lose part of their energy. An ionizing collision is an example of such a collision. In this process a positive ion and a free electron are formed. The ionization process can be described by Townsend's first ionization coefficient α, defined as the mean number of ionizing collisions of one electron travelling 1 cm in the direction of the field. There are however also interactions between electrons and heavy particles in which the electron brings the heavy particle in an excited state. When this state is unstable the particle falls back to a lower state and emits a photon. Dependent on the geometry there is a chance for this photon to strike the cathode. The photon then can release an electron from the cathode if the energy of the photon is higher than the workfunction of the cathode material. This process can

be described by the coefficient γ_{photon}, defined as the mean number of secondary photoelectrons emitted from the cathode per ionizing collision.

An electron can also attach itself to a neutral atom so that a negative ion is formed. This is called attachment and can be described by the attachment coefficient η, defined as the mean number of attachments produced by a single electron travelling 1 cm in the direction of the field. A stable negative ion travels to the anode where it is neutralized. If the negative ion is unstable the attached electron can be released after a certain time. This process is called detachment and can be described by the detachment coefficient δ, here defined as the mean number of detachments per unstable negative ion in a time an electron travels 1 cm in the direction of the field. In the literature δ is often defined as the mean number of detachments per unstable negative ion in a time the ion travels a distance of 1 cm in the direction of the field. The relation between these two definitions can be obtained from the ratio of the drift velocities of the electrons and the ions. An initially unstable negative ion may upon collision with a neutral particle be transformed into a heavier and stable negative ion. This process is called conversion and can be described by the conversion coefficient β, defined here as the mean number of conversions per unstable negative ion in a time an electron travels 1 cm in the direction of the field. When a negative ion strikes the anode or a positive ion strikes the cathode it is neutralized. An electron leaves the gap when it strikes the anode. In Table 2.1.1 the forementioned processes are summarized. The table also shows the gain or loss processes for the various charge carriers.

The last process mentioned here is diffusion, the random-walk motion of a specific type of particle which causes a net velocity from regions with a high concentration to regions with a lower concentration. The diffusion coefficient D with which this process can be described is defined as the net number of particles passing in unit time through a unit area perpendicular to a concentration gradient of magnitude one.

charge carriers	gain	loss
electrons	ionization photo-emission detachment	attachment reaching the anode
positive ions	ionization	neutralized at cathode
stable negative ions	attachment conversion	neutralized at anode
unstable negative ions	attachment	detachment conversion neutralized at anode

Table 2.1.1.: Gain and loss processes for the various charge carriers

2.3. A constant number of electrons crossing a gap

When n_o electrons are released instantaneously from a certain area of the cathode ($x = 0$) under such conditions that none of the collisional processes described in the previous section take place, the number of electrons stays constant. Under the influence of the E-field they move with the drift velocity, v_e, to the anode ($x = d$) as a very thin disk. At $t = T_e$, where T_e is the transit time of the electrons, $T_e = d/v_e$, all electrons leave the gap at the anode. For

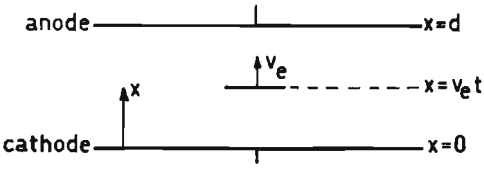

Fig. 2.3.1 Electrons moving across a gap at time t

$0 \leq t \leq T_e$ the position of the electrons in the gap is given by $x = v_e t$ (see Fig. 2.3.1).

These moving electrons cause an electrical current, i_e, in the external circuit. To calculate this current we consider the work done on the n_o electrons during their motion over a distance dx in the direction of the E-field in a time dt. This energy equals $n_o eEdx$ - in which e is the elementary charge - and is provided by the external circuit:

$$U\, i_e(t)\, dt = n_o\, e\, E\, dx \tag{2.3.1}$$

$$i_e(t) = n_o\, e\, \frac{E}{U}\, \frac{dx}{dt} = n_o\, e\, v_e\, \frac{E}{U} \tag{2.3.2}$$

For a homogeneous field and a constant voltage U, v_e will be constant also and Eq.(2.3.2) simplifies to:

$$i_e(t) = n_o\, e\, v_e/d = n_o\, e/T_e \tag{2.3.3}$$

After $t = T_e$ the current is zero. Fig. 2.3.2 shows the current as a function of time.
The current in the external circuit can also be interpreted as the current necessary to bring the appropriate image charges to the electrodes when the motion of the electrons causes changes in the electric field pattern.

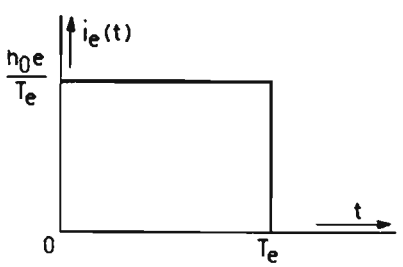

Fig. 2.3.2 The current in the external circuit caused by n_o electrons crossing a gap

2.4. A constant number of electrons crossing a gap with diffusion taking place

In this section the same conditions are assumed as in the previous section with the exception that diffusion is taken into account. Consider at $t = 0$, $x = 0$ a very thin disk of electrons in a gas atmosphere between electrodes. The disk increases in diameter and thickness by diffusion while the center of the disk moves with the drift velocity towards the anode because of the applied E-field. This process can be described by:

$$\frac{\partial C(x,y,z,t)}{\partial t} = D\nabla^2 C(x,y,z,t) - v_e \frac{\partial C(x,y,z,t)}{\partial x} \qquad (2.4.1)$$

in which $C(x,y,z,t)$ is the density of electrons in the disk. In case the diameter of the disk is much larger than its thickness the diffusion in the radial direction can be neglected. The density C is then a function of x and t only. Eq. (2.4.1) simplifies to:

$$\frac{\partial C(x,t)}{\partial t} = D \frac{\partial^2 C(x,t)}{\partial x^2} - v_e \frac{\partial C(x,t)}{\partial x} \qquad (2.4.2)$$

with the solution:

$$C(x,t) = \frac{A}{\sqrt{4\pi Dt}} \exp\{-(x - v_e t)^2/4Dt\} \qquad (2.4.3)$$

where A is a constant of dimension m^{-2} and value $n_o/\pi r^2$, which follows from the radius r of the disk and the number of initially present electrons n_o in the disk since at $t = 0$:

$$n_o = \iiint_{gap} C(x,t)\,dx\,dy\,dz \qquad (2.4.4)$$

We introduce a new quantity $\rho(x,t)$ which is defined by:

$$d n_e(x,t) = \rho(x,t)\,dx \qquad (2.4.5)$$

in which $d n_e(x,t)$ is the number of electrons between x and $x + dx$. The total number of electrons at any time is given by:

$$n_e(t) = \iiint_{gap} C(x,t)\,dx\,dy\,dz = \int_o^d \rho(x,t)\,dx \qquad (2.4.6)$$

From this equation and Eq.(2.4.3) we conclude:

$$\rho(x,t) = \frac{n_o}{\sqrt{4\pi Dt}} \exp\{-(x - v_e t)^2/4Dt\} \qquad (2.4.7)$$

which can be written as:

$$\rho(x,t) = \frac{n_o}{\sigma\sqrt{2\pi}} \exp(-u^2/2\sigma^2) \qquad (2.4.8)$$

where

$$\sigma = \sqrt{2Dt} \qquad (2.4.9)$$

and

$$u = x - v_e t \qquad (2.4.10)$$

Eq.(2.4.8) shows that $\rho(x,t)$ is a Gaussian curve at any time. Tables in which values of integrals of the Gaussian curve are given show that 68.26 % of the electrons are situated between $u = \sigma$ and $u = -\sigma$. Figure 2.4.1 shows $\rho(x,t)$ at different times.

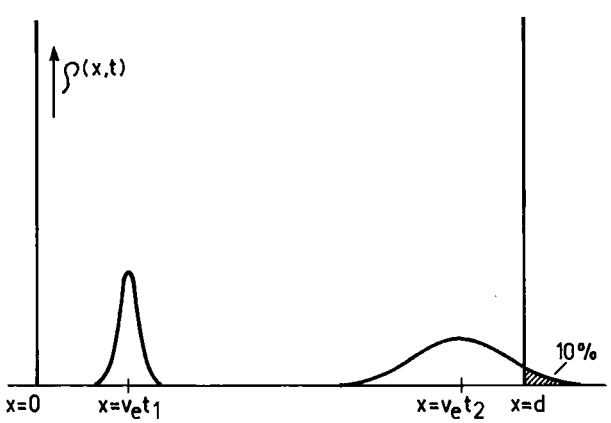

Fig. 2.4.1 The quantity $\rho(x,t)$ at $t = t_1$ and $t = t_2$ while the "cloud" of electrons moves across the gap

After a certain time the "first" electrons reach the anode and leave the gap. Let t_2 be the time at which 10 % of the initially present electrons have left the gap (see Fig. 2.4.1). From the above-mentioned tables we find that in this case:

$$d - v_e t_2 = 1.28\sigma = 1.28\sqrt{2 D t_2} \tag{2.4.11}$$

At $t = T_e$ the center of the disk has just reached the anode and 50 % of the initial electrons have left the gap. Eventually all electrons leave the gap. The current caused by these moving electrons can be calculated from (see Eq.(2.3.3) with n_o replaced by $n_e(t)$):

$$i_e(t) = \frac{n_e(t)e}{T_e} \tag{2.4.12}$$

Measurements of $i_e(t)$ in an experiment will give an $i_e(t)$ waveform as schematically shown in Fig. 2.4.2.

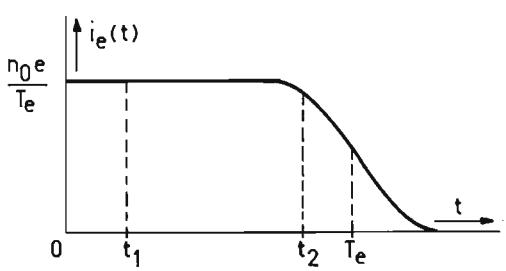

Fig. 2.4.2 Current caused by n_o electrons crossing a gap when diffusion takes place

From this waveform we obtain the values of t_2 and T_e and insert them in Eq.(2.4.11):

$$d - v_e t_2 = d - \frac{d\, t_2}{T_e} = 1.28\sqrt{2 D t_2} \tag{2.4.13}$$

From this equation we calculate the diffusion coefficient D:

$$D = \frac{1}{2t_2}\left\{\frac{d}{1.28}\,\frac{(T_e - t_2)}{T_e}\right\}^2 \tag{2.4.14}$$

Of course it is also possible to obtain from Fig. 2.4.2 moments at which other percentages of the electrons have left the gap. For

example if t_3 is the moment at which 20 % of the initially present electrons have left the gap, the diffusion coefficient follows from:

$$D = \frac{1}{2t_3}\left\{\frac{d}{0.84}\,\frac{(T_e - t_3)}{T_e}\right\}^2 \qquad (2.4.15)$$

A second relation between D and the current caused by the electrons can be derived as follows. The number of electrons which leaves the gap at the anode between t and t + dt is given by (see Eq. 2.4.5):

$$dn_e(t) = -\rho(d,t)\,v_e\,dt \qquad (2.4.16)$$

and since $i_e(t) = e\,n_e(t)/T_e$:

$$\begin{aligned}\frac{d\,i_e(t)}{dt} &= \frac{e}{T_e}\,\frac{d\,n_e(t)}{dt} = -\frac{e\,v_e}{T_e}\,\rho(d,t)\\ &= -\frac{e\,v_e}{T_e}\,\frac{n_o}{\sqrt{4\pi Dt}}\,\exp\{-(d - v_e t)^2/4Dt\}\\ &= -\frac{I_o\,v_e}{\sqrt{4\pi Dt}}\,\exp\{-(d - v_e t)^2/4Dt\} \qquad (2.4.17)\end{aligned}$$

in which $I_o = e\,n_o/T_e$.

At $t = T_e$, Eq.(2.4.17) becomes:

$$\left(\frac{d\,i_e(t)}{dt}\right)_{t=T_e} = -\frac{I_o\,ve}{\sqrt{4\pi DT_e}} \qquad (2.4.18)$$

from which follows:

$$D = \frac{I_o^2\,v_e^2}{4\pi T_e}\left\{\left(\frac{d\,i_e(t)}{dt}\right)_{t=T_e}\right\}^{-2} \qquad (2.4.19)$$

From a measured current $(d\,i_e(t)/dt)_{t=T_e}$ can be determined and expressed into I_o and T_e (see Fig. 2.4.3):

$$\left(\frac{d\,i_e(t)}{dt}\right)_{t=T_e} = -\frac{a\,I_o}{b\,T_e} \qquad (2.4.20)$$

Equation (2.4.19) can now be written as:

$$D = \frac{b^2}{a^2}\,\frac{d^2}{4\pi T_e} \qquad (2.4.21)$$

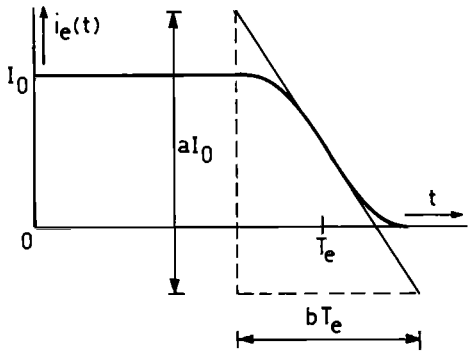

Fig. 2.4.3 Current caused by a constant number of electrons crossing a gap while diffusion takes place. From the tangent at $t = T_e$ the diffusion coefficient can be derived

The Eqs. (2.4.15), (2.4.16) and (2.4.21) are used in Chapter 4 to derive numerical values for D from measured $i_e(t)$ curves.

Assumptions made in the above treatment of the diffusion process are:

- The back diffusion of the electrons into the cathode is neglected. In fact the velocity distribution of the electrons leaving the cathode is not isotropic, so that a diffusion description is not immediately applicable. From measurements reported by Folkard and Haydon [Fo 73] it can be concluded that for pd values above 1 Torr cm and $E/p < 50$ Vcm^{-1} $Torr^{-1}$ the isotropic velocity distribution is established after a distance which is short compared to the gap distance.
- Similarly the interaction of the anode with the approaching electrons is simplified to a counting process as if the anode were a perfectly transparent grid.
- The electrostatic repulsion between the electrons is neglected.

This last assumption is justified when the "diffusion velocity" exceeds the drift velocity in the space-charge field. The characteristic length, L_{dif}, for the diffusion process is (see Eq.(2.4.9)):

$$L_{dif} = \sqrt{2\,Dt} \qquad (2.4.22)$$

From this length a "diffusion velocity" can be derived:

$$v_{dif} = \frac{d L_{dif}}{dt} = \sqrt{\frac{D}{2t}} \qquad (2.4.23)$$

The drift velocity, v_{dif}, acquired by an electron at the surface of the disk of electrons is:

$$v_{dif} = K E_d \qquad (2.4.24)$$

in which K is the mobility and E_d is the electrostatic field caused by the electrons in the disk.
The condition that the electrostatic repulsion can be neglected is given by:

$$t << \frac{D}{2K^2 E_d^2} \qquad (2.4.25)$$

In Chapter 4 it is shown empirically that this condition can be satisfied.

2.5. Avalanches in which ionization and attachment take place

In this section we discuss collisional processes which result in the formation of ions. Positive ions are formed by ionization and negative ions by attachment. Here it is assumed that only one type of positive ions and one type of negative ions are important. The negative ions are stable which means that no detachment takes place. Diffusion of both electrons and ions is neglected.
The avalanche is started by n_o electrons released from the cathode in a very short time.
When the electrons travel a distance dx in the direction of the E-field in a time dt with velocity $v_e = dx/dt$, the change in the number of electrons is given by:

$$d n_e(t) = (\alpha - \eta) n_e(t) dx = (\alpha - \eta) n_e(t) v_e \, dt \qquad (2.5.1)$$

Note that the change in number can be positive as well as negative depending on whether $\alpha > \eta$ or $\alpha < \eta$. In the case $\alpha = \eta$ the number of electrons is constant.
The increase in the number of positive ions in the same time is given by:

$$d n_p(t) = \alpha n_e(t) dx = \alpha n_e(t) v_e dt \qquad (2.5.2)$$

The increase in the number of negative ions is:

$$d n_n(t) = \eta n_e(t) dx = \eta n_e(t) v_e dt \qquad (2.5.3)$$

These new ions $d n_p(t)$ and $d n_n(t)$ are situated between $x = v_e t$ and $x + dx = v_e(t + dt)$. At any time $0 \leq t \leq T_e$ a very thin disk containing electrons is situated at $x = v_e t$ whereas the positive and negative ions are spread out between $x = 0$ and $x = v_e t$ (see Fig. 2.5.1).

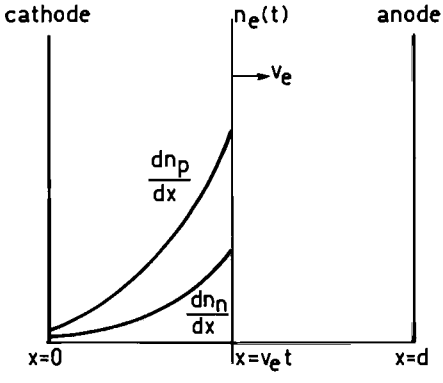

Fig. 2.5.1 The total number of electrons situated at $x = v_e t$ and the distribution of positive and negative ions in the case $\alpha > \eta$

The total number of electrons for $0 \leq t \leq T_e$ is calculated by integration of Eq.(2.5.1):

$$n_e(t) = n_o \exp\{(\alpha - \eta) v_e t\} \qquad (2.5.4)$$

We assume that the ions do not drift during the time electrons are present in the gap, which is reasonable since the drift velocity of the electrons is about 200 times larger than the drift velocity of the positive and negative ions. The distribution of the ions along x can then be described for $x \leq v_e t$ by:

$$\frac{d n_p(t)}{dx} = \alpha n_o \exp\{(\alpha - \eta) x\} \qquad (2.5.5)$$

$$\frac{d\,n_n(t)}{dx} = \eta\, n_o \exp\{(\alpha - \eta)x\} \tag{2.5.6}$$

The total number of positive and negative ions in the case $\alpha \neq \eta$ is:

$$n_p(t) = \int_0^{v_e\,t} \frac{d\,n_p(t)}{dx}\,dx = \frac{\alpha\, n_o}{\alpha - \eta}\left[\exp\{(\alpha - \eta)\,v_e\,t\} - 1\right] \tag{2.5.7}$$

$$n_n(t) = \int_0^{v_e\,t} \frac{d\,n_n(t)}{dx}\,dx = \frac{\eta\, n_o}{\alpha - \eta}\left[\exp\{(\alpha - \eta)\,v_e\,t\} - 1\right] \tag{2.5.8}$$

for $\alpha = \eta$ the corresponding equations are:

$$n_p(t) = \int_0^{v_e\,t} \alpha\, n_o\,dx = \alpha\, n_o\, v_e\, t \tag{2.5.9}$$

$$n_n(t) = \int_0^{v_e\,t} \eta\, n_o\,dx = \eta\, n_o\, v_e\, t \tag{2.5.10}$$

At $t = T_e$ the electrons reach the anode and leave the gap. The formation of ions stops and the positive and negative ions are now supposed to start their drift motion to the cathode with velocity v_p or to the anode with velocity v_n

The situation at $t = T_e$ is shown in Fig. 2.5.2.

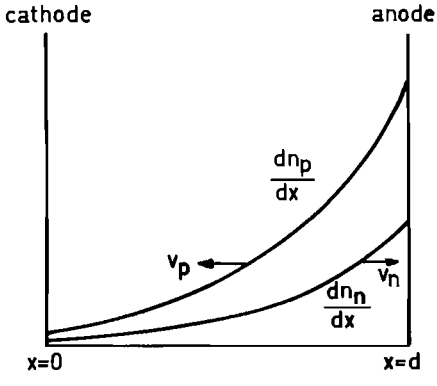

Fig. 2.5.2 The distribution of positive and negative ions at $t = T_e$ in the case $\alpha > \eta$

When the origin of the time scale is now changed to the original moment T_e the time dependence of the total number of ions can be easily derived. In case $\alpha \neq \eta$:

$$n_p(t) = \int_{v_p t}^{d} \alpha n_o \exp\{(\alpha - \eta)x\}dx$$

$$= \frac{\alpha}{\alpha - \eta} n_o[\exp\{(\alpha - \eta)d\} - \exp\{(\alpha - \eta)v_p t\}] \qquad (2.5.11)$$

$$\text{for} \quad 0 \leq t \leq T_p$$

$$n_n(t) = \int_{o}^{d-v_n t} \eta n_o \exp\{(\alpha - \eta)x\}dx$$

$$= \frac{\eta}{\alpha - \eta} n_o[\exp\{(\alpha - \eta)(d - v_n t)\} - 1] \qquad (2.5.12)$$

$$\text{for} \quad 0 \leq t \leq T_n$$

In case $\alpha = \eta$ the numbers are given by:

$$n_p(t) = \alpha n_o (d - v_p t) \qquad 0 \leq t \leq T_p \qquad (2.5.13)$$

$$n_n(t) = \eta n_o (d - v_n t) \qquad 0 \leq t \leq T_n \qquad (2.5.14)$$

in which T_p and T_n are the transit times of the positive and negative ions.

The exact equations in which the drift of ions for $0 \leq t \leq T_e$ is taken into account are, for example, given by Raether [Ra 64].

The currents caused by the moving charges can be calculated from Eq.(2.3.3):

$$i_e(t) = \frac{e\, n_e(t)}{T_e} \qquad (2.5.15)$$

$$i_p(t) = \frac{e\, n_p(t)}{T_p} \qquad (2.5.16)$$

$$i_n(t) = \frac{e\, n_n(t)}{T_n} \qquad (2.5.17)$$

Figure 2.5.3 shows schematic plots of these currents for the essentially different cases, $\alpha < \eta$, $\alpha = \eta$ and $\alpha > \eta$.

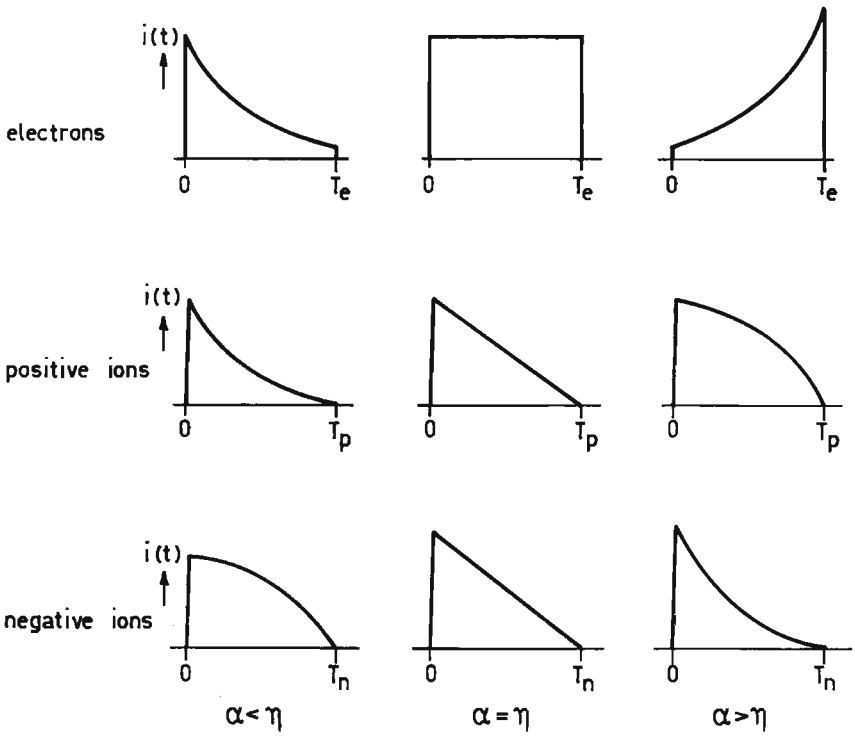

Fig. 2.5.3 The currents caused by the three types of charge carrier for $\alpha < \eta$, $\alpha = \eta$ and $\alpha > \eta$. Note the difference in time scales

In practice the three components of the current are measured as one current (see Fig. 2.5.4); the electron and ion contributions can often be distinguished because of the higher amplitude and the shorter duration of the electron current.

In Chapter 4, which deals with the experimental results, examples are given of actually measured currents. The procedure to determine the discharge parameters from the current is:

v_e : electron drift velocity from the electron transit time.

$\alpha-\eta$: "effective" ionization coefficient from the e-folding time, $\{(\alpha-\eta)v_e\}^{-1}$, of the electron current (see Eq.(2.5.4)).

v_p : positive ion drift velocity from the positive ion transit time.

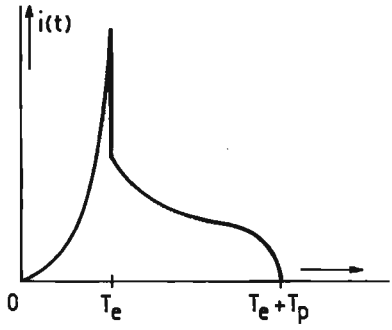

Fig. 2.5.4 The total current caused by the various particles for $\alpha > \eta$. Up to $t = T_e$ the time scale has been stretched and the vertical scale has been compressed for the sake of clarity.

v_n : negative ion drift velocity from the e-folding time, $\{(\alpha-\eta)v_n\}^{-1}$, of the negative ion current. Note that this is only possible when $\alpha-\eta \gg 0$ or $\alpha-\eta \ll 0$ (see Eq.(2.5.12)).

α/η : ratio of ionization and attachment coefficient from the ratio of the positive and negative ion currents at $t = T_e$ and from the ratio of their transit times (see Eqs.(2.5.7), (2.5.8), (2.5.16) and (2.5.17)).

α,η : determined separately from $\alpha-\eta$ and α/η.

2.6. Avalanches in which ionization, attachment and secondary emission take place

In the preceding section it was assumed that the electron cloud moves as a thin disk to the anode with a constant drift velocity. After one electron transit time all electrons have left the gap. When however, secondary electrons are released from the cathode by photons travelling back from the avalanche new electrons enter the gap, spread in time and start individual avalanches.

Schlumbohm [Sc 60] and Auer [Au 58] gave analytical solutions for the current caused by these electrons. These analytical solutions are only approximations and become very complicated if several generations are involved. In section 2.7 of this chapter a numerical solution for this

problem is worked out. In this section relations are derived between the value of γ_{photon} and the current caused by the avalanche. For simplicity γ_{photon} will be denoted as γ.
The current caused by electrons, when secondary emission by photons takes place, will generally have a shape as shown in Fig. 2.6.1.

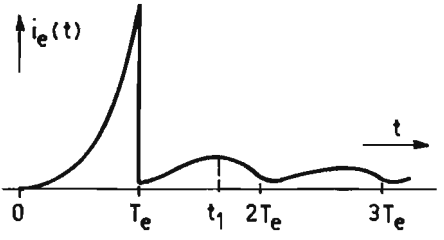

Fig. 2.6.1 Current caused by electrons if secondary emission takes place

The photons are emitted by particles which are excited by collisions with electrons. The excited state often has a mean life time τ, before the particle falls back to a lower state and a photon is emitted. The decay of the excited particles, M^*, in a time dt can be described by $dM^*(t) = -M^*(t)dt/\tau$. If $m^*(t)$ is only the number of excited particles of which the emitted photons release electrons from the cathode, the differential equation for $m^*(t)$ is:

$$dm^*(t) = \alpha \gamma n_e(t) v_e \, dt - \frac{m^*(t)}{\tau} dt \qquad (2.6.1)$$

For $0 \leq t \leq T_e$ the change in the number of electrons in a time dt can be subdivided into three components:

- by ionization

$$d n_e(t)\Big|_1 = \alpha n_e(t) v_e \, dt \qquad (2.6.2)$$

- by photoemission from the cathode

$$d n_e(t)\Big|_2 = \frac{m^*(t)}{\tau} dt \qquad (2.6.3)$$

- by attachment

$$d n_e(t)\Big|_3 = -\eta n_e(t) v_e \, dt \qquad (2.6.4)$$

The total change in n_e is the sum of the three components:

$$d\,n_e(t)\big|_{123} = (\alpha-\eta)\,n_e(t)\,v_e\,dt + \frac{m^*(t)}{\tau}\,dt \qquad (2.6.5)$$

With $n_e(0) = n_o$ and $m^*(0) = 0$ the solution of Eqs.(2.6.1) and (2.6.5) is:

$$m^*(t) = \frac{\alpha\,\gamma\,v_e n_o}{s_1 - s_2}\,\{\exp(s_1 t) - \exp(s_2 t)\} \qquad (2.6.6)$$

$$n_e(t) = \frac{n_o}{s_1 - s_2}\,\{(s_1 + 1/\tau)\exp(s_1 t) - (s_2 + 1/\tau)\exp(s_2 t)\} \qquad (2.6.7)$$

in which

$$s_{1,2} = \tfrac{1}{2}\{(\alpha-\eta)\,v_e - 1/\tau\} \pm \tfrac{1}{2}\left[\{(\alpha-\eta)\,v_e - 1/\tau\}^2 + 4v_e(\alpha-\eta+\alpha\,\gamma)/\tau\right]^{\frac{1}{2}} \qquad (2.6.8)$$

If $\alpha\,\gamma << \alpha - \eta$ this can be simplified to:

$$s_1 = (\alpha-\eta)\,v_e \qquad (2.6.9)$$

$$s_2 = -1/\tau \qquad (2.6.10)$$

$$m^*(t) = \frac{\alpha\,\gamma\,v_e\,n_o}{(\alpha-\eta)\,v_e + 1/\tau}\left[\exp\{(\alpha-\eta)\,v_e\,t\} - \exp(-t/\tau)\right] \qquad (2.6.11)$$

$$n_e(t) = n_o \exp\{(\alpha-\eta)\,v_e\,t\} \qquad (2.6.12)$$

After $t = T_e$ a fourth component, $d\,n_e(t)\big|_4$, corresponding to electrons leaving the gap at the anode should be added.
Let $t = t_1$ be the time at which $d\,i_e(t)/dt = d\,n_e(t)/dt = 0$ for the first time (see Fig. 2.6.1); this means that in a time dt after $t = t_1$ the number of electrons produced by ionization and secondary emission and lost by attachment ($d\,n_e(t)\big|_{123}$ of Eq.(2.6.5)) equals the number of electrons which leaves the gap at the anode ($d\,n_e(t)\big|_4$). Between t_1 and $t_1 + dt$ those electrons leave the gap which are emitted from the cathode between $t_1 - T_e$ and $t_1 - T_e + dt$ together with the electrons they have formed by ionization minus the electrons they have lost by attachment. The number of electrons which started from the cathode between $t_1 - T_e$ and $t_1 - T_e + dt$ follows from Eqs.(2.6.3) and (2.6.11):

$$d\,n_e(t_1 - T_e)\big|_2 = \frac{\alpha\,\gamma\,v_e\,n_o\,dt}{(\alpha-\eta)\,v_e\,\tau+1}\left[\exp\{(\alpha-\eta)\,v_e(t_1 - T_e)\} - \exp\{-(t_1 - T_e)/\tau\}\right] \tag{2.6.13}$$

For $\tau << T_e$ the second term on the right hand side is small compared to the first one:

$$d\,n_e(t_1 - T_e)\big|_2 = \frac{\alpha\,\gamma\,v_e\,n_o\,dt}{(\alpha-\eta)\,v_e\,\tau+1}\exp\{(\alpha-\eta)\,v_e(t_1 - T_e)\} \tag{2.6.14}$$

$$= \frac{\alpha\,\gamma\,v_e\,dt}{(\alpha-\eta)\,v_e\,\tau+1}\,n_e(t_1 - T_e) \tag{2.6.15}$$

During the crossing of the gap in the time T_e ionization and attachment occur, so that between t_1 and $t_1 + dt$ the number of electrons which leave the gap is given by:

$$d\,n_e(t_1)\big|_4 = \frac{-\alpha\,\gamma\,v_e\,dt}{(\alpha-\eta)\,v_e\,\tau+1}\,n_e(t_1 - T_e)\exp\{(\alpha-\eta)\,d\} \tag{2.6.16}$$

The increase of the number of electrons between $t = t_1$ and $t = t_1 + dt$ follows from Eq.(2.6.5):

$$d\,n_e(t_1)\big|_{123} = (\alpha-\eta)\,n_e(t_1)\,v_e\,dt + m^*(t_1)\,dt/\tau \tag{2.6.17}$$

In general the second term on the right hand side will be much smaller than the first one so that this equation simplifies to:

$$d\,n_e(t_1)\big|_{13} = (\alpha-\eta)\,n_e(t_1)\,v_e\,dt \tag{2.6.18}$$

Since the total $d\,n_e(t_1)$ is zero the right hand sides of Eqs.(2.6.16) and (2.6.18) should be equal and opposite:

$$(\alpha-\eta)\,n_e(t_1)\,v_e\,dt = \frac{\alpha\,\gamma\,v_e\,dt}{(\alpha-\eta)\,v_e\,\tau+1}\,n_e(t_1 - T_e)\exp\{(\alpha-\eta)\,d\} \tag{2.6.19}$$

$$\frac{n_e(t_1)}{n_e(t_1 - T_e)} = \frac{1}{\alpha-\eta}\,\frac{\alpha\,\gamma}{(\alpha-\eta)\,v_e\,\tau+1}\exp\{(\alpha-\eta)\,d\} \tag{2.6.20}$$

from which follows:

$$\gamma = \frac{(\alpha-\eta)\{(\alpha-\eta)\,v_e\,\tau + 1\}}{\alpha\exp\{(\alpha-\eta)\,d\}}\,\frac{n_e(t_1)}{n_e(t_1 - T_e)} \tag{2.6.21}$$

or $$\gamma = \frac{(\alpha-\eta)\{(\alpha-\eta)v_e\tau+1\}}{\alpha\exp\{(\alpha-\eta)d\}}\,\frac{i_e(t_1)}{i_e(t_1-T_e)} \qquad (2.6.22)$$

A second relation between γ and the current caused by the electrons can be derived as follows. For $T_e < t < 2T_e$ the total change of the number of electrons is the sum of Eqs.(2.6.16) and (2.6.18):

$$d\,n_e(t)\big|_{134} = (\alpha-\eta)\,n_e(t)\,v_e\,dt - \frac{\alpha\gamma\,v_e\,dt}{(\alpha-\eta)v_e\tau+1}\,n_e(t-T_e)\exp\{(\alpha-\eta)d\} \qquad (2.6.23)$$

$$d\,n_e(t)\big|_{134} = (\alpha-\eta)\,n_e(t)\,v_e dt - \frac{\alpha\gamma\,v_e\,n_o\,dt}{(\alpha-\eta)v_e\tau+1}\exp\{(\alpha-\eta)v_e(t-T_e)\}\exp\{(\alpha-\eta)d\} \qquad (2.6.24)$$

$$\frac{d\,n_e(t)\big|_{134}}{dt} = (\alpha-\eta)\,n_e(t)\,v_e - \frac{\alpha\gamma\,v_e\,n_e(T_e)}{(\alpha-\eta)v_e\tau+1}\exp\{(\alpha-\eta)v_e(t-T_e)\} \qquad (2.6.25)$$

For $t = t_1$, $d\,n_e(t)\big|_{134}/dt = 0$ (see Fig. 2.6.1):

$$(\alpha-\eta)\,n_e(t_1)\,v_e = \frac{\alpha\gamma\,v_e\,n_e(T_e)}{(\alpha-\eta)v_e\tau+1}\exp\{(\alpha-\eta)v_e(t_1-T_e)\} \qquad (2.6.26)$$

from which follows:

$$\gamma = \frac{n_e(t_1)}{n_e(T_e)}\,\frac{(\alpha-\eta)\{(\alpha-\eta)v_e\tau+1\}}{\alpha\exp\{(\alpha-\eta)v_e(t_1-T_e)\}} \qquad (2.6.27)$$

or $$\gamma = \frac{i_e(t_1)}{i_e(T_e)}\,\frac{(\alpha-\eta)\{(\alpha-\eta)v_e\tau+1\}}{\alpha\exp\{(\alpha-\eta)v_e(t_1-T_e)\}} \qquad (2.6.28)$$

Finally a third relation between γ and the current caused by the avalanche is derived. We start the avalanche again at $t = 0$ with n_o electrons at the cathode. During their motion to the anode the electrons experience $\alpha\,n_o[\exp\{(\alpha-\eta)d\}-1]/(\alpha-\eta)$ ionizing collisions (see previous section) and produce a proportional number of photons. So the number of new electrons which start from the cathode is $\alpha\gamma\,n_o[\exp\{(\alpha-\eta)d\}-1]/(\alpha-\eta)$, these electrons experience $\alpha^2\gamma\,n_o[\exp\{(\alpha-\eta)d\}-1]^2/(\alpha-\eta)^2$ ionizing collisions and release in turn $\alpha^2\gamma^2\,n_o[\exp\{(\alpha-\eta)d\}-1]^2/(\alpha-\eta)^2$ electrons from the cathode which again ionize and release electrons and so on. The total number of positive ions is the sum of the positive ions produced in the series of generations:

$$\Sigma\, n_p = \frac{\alpha}{\alpha-\eta}\, n_o[\exp\{(\alpha-\eta)d\}-1] + \left(\frac{\alpha}{\alpha-\eta}\right)^2 \gamma\, n_o[\exp\{(\alpha-\eta)d\}-1]^2 + \ldots\ldots$$

$$= \frac{\alpha}{\alpha-\eta}\, n_o[\exp\{(\alpha-\eta)d\}-1] \sum_{i=0}^{\infty} \left[\frac{\alpha\gamma}{\alpha-\eta}\, \exp\{(\alpha-\eta)d\}-1\right]^i$$

For $\alpha\gamma\,[\exp\{(\alpha-\eta)d\}-1]/(\alpha-\eta) < 1$ this can be written as:

$$\Sigma\, n_p = \frac{\alpha}{\alpha-\eta}\, n_o \frac{[\exp\{(\alpha-\eta)d\}-1]}{1-\alpha\gamma\,[\exp\{(\alpha-\eta)d\}-1]/(\alpha-\eta)} \qquad (2.6.29)$$

Note that in the case $\alpha\gamma\,[\exp\{(\alpha-\eta)d\}-1]/(\alpha-\eta) \geq 1$ the sum of the series becomes infinite which means that the gap breaks down.
Since in general $\exp\{(\alpha-\eta)d\} >> 1$, Eq.(2.6.29) can be simplified to:

$$\Sigma\, n_p = \frac{\alpha}{\alpha-\eta}\, n_o \frac{\exp\{(\alpha-\eta)d\}}{1-\alpha\gamma\exp\{(\alpha-\eta)d\}/(\alpha-\eta)}$$

$$= \frac{n_o \exp\{(\alpha-\eta)d\}}{\{(\alpha-\eta)/\alpha\}-\gamma\exp\{(\alpha-\eta)d\}} \qquad (2.6.30)$$

In practice only a few generations are important and $\Sigma\, n_p$ reaches its maximum after a few times T_e, which will be denoted as t_m (see Fig. 2.6.2 and the previous section).

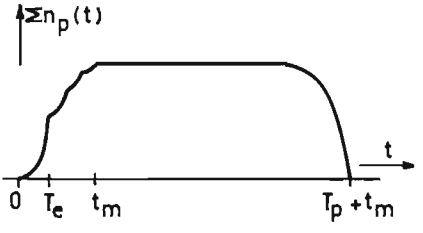

Fig. 2.6.2 The total number of positive ions in the gap as a function of time if secondary emission by photons is taken into account

The number of electrons of the second generation at $t = T_e$ is very small in comparison to the number of the first generation at $t = T_e$ which leads to the approximation of the total number of electrons at $t = T_e$:

$$n_e(T_e) = n_o \exp\{(\alpha-\eta)d\} \tag{2.6.31}$$

From Eqs.(2.6.30) and (2.6.31) follows:

$$\frac{i_e(T_e)}{i_p(t_m)} = \frac{n_e(T_e)}{\sum n_p} \cdot \frac{T_p}{T_e} = \frac{T_p}{T_e} \exp\{(\alpha-\eta)d\} \frac{\frac{\alpha-\eta}{\alpha} - \gamma \exp\{(\alpha-\eta)d\}}{\exp(\alpha-\eta)d}$$

$$= \frac{T_p}{T_e} \left[\frac{\alpha-\eta}{\alpha} - \gamma \exp\{(\alpha-\eta)d\} \right] \tag{2.6.32}$$

and from this:

$$\gamma = \left(\frac{\alpha-\eta}{\alpha} - \frac{i_e(T_e)}{i_p(t_m)} \cdot \frac{T_e}{T_p} \right) \frac{1}{\exp\{(\alpha-\eta)d\}} \tag{2.6.33}$$

The Eqs.(2.6.22), (2.6.28) and (2.6.33) are used in Chapter 4 to derive numerical values for γ from measured currents.

2.7. Avalanches in which ionization, attachment and secondary emission take place. Numerical solution

In the preceding section the process of secondary emission was discussed and some relations were given between the secondary ionization coefficient γ_{photon}, further denoted here as γ, and the current caused by the moving charges. These relations were derived from analytical calculations.
However, the current waveforms at late times were not given. In this section a numerical method is worked out to compute the complete current waveforms.
It is assumed in this section that excited particles fall back to the lower state under the emission of a photon, immediately after excitation; i.e. the mean life time τ is taken to be zero.
The increase of the number of electrons in the avalanche caused by ionizing collisions during a time Δt is:

$$\Delta n_e(t)\Big|_1 = \alpha n_e(t) v_e \Delta t \tag{2.7.1}$$

In a time Δt the number of newly formed photoelectrons is:

$$\Delta n_e(t)\Big|_2 = \alpha \gamma n_e(t) v_e \Delta t \tag{2.7.2}$$

In a time Δt the decrease of the number of electrons by attachment is:

$$\Delta n_e(t)\Big|_3 = -\eta n_e(t) v_e \Delta t \qquad (2.7.3)$$

The total change of the number of electrons in a time Δt follows from the combination of Eqs.(2.7.1), (2.7.2) and (2.7.3):

$$\Delta n_e(t)\Big|_{123} = (\alpha + \alpha\gamma - \eta) n_e v_e \Delta t \qquad (2.7.4)$$

In the numerical calculation the electrode distance d is divided into N equal parts, each Δx long. The electrons travel the distance Δx in a time Δt:

$$\Delta x = d/N \qquad (2.7.5)$$

$$\Delta t = \Delta x / v_e = T_e/N \qquad (2.7.6)$$

The avalanche starts with n_o electrons released in a very short time from the cathode, $n_e(0) = n_o$. After Δt this number has changed to $n_e(\Delta t)$:

$$n_e(\Delta t) = n_e(0) + (\alpha + \alpha\gamma - \eta) n_e(0) \Delta x$$

$$= n_e(0)\{(1 + (\alpha + \alpha\gamma - \eta) d/N\} \qquad (2.7.7)$$

Of these electrons the number $\alpha\gamma n_e(0) d/N$ is situated at the cathode $(x = 0)$.

In general the total number of electrons in the gap for $t = p\Delta t \leq T_e$ is:

$$n_e(p\Delta t) = n_e((p-1)\Delta t)\{1 + (\alpha + \alpha\gamma - \eta) d/N\} \qquad (2.7.8)$$

Of these electrons the number $\alpha\gamma n_e((p-1)\Delta t) d/N$ is situated at the cathode.

At $t = N\Delta t = T_e$ the n_o electrons which departed at $t = 0$, together with the electrons they formed by the α-process minus those lost by attachment, have just reached the anode.

Their number at that time equals: $n_o\{1 + (\alpha - \eta) d/N\}^N$. In the next Δt they will leave the gap. The total number of electrons at $t = (N+1)\Delta t$ is:

$$n_e((N+1)\Delta t) = \{1 + (\alpha + \alpha\gamma - \eta) d/N\}\{n_e(N\Delta t) - n_o(1 + (\alpha - \eta) d/N)^N\} \qquad (2.7.9)$$

At $t = (N+1)\Delta t$ the $\alpha\gamma n_o d/N$ electrons which left the cathode at $t = \Delta t$, together with the electrons they formed by the α-process minus those lost by attachment have just reached the anode and leave the gap Δt later. The total number of electrons at $t = (N+2)\Delta t$ is:

$$n_e((N+2)\Delta t) = \{1+(\alpha+\alpha\gamma-\eta)d/N\}\{n_e((N+1)\Delta t) - (1+(\alpha-\eta)d/N)^N \alpha\gamma n_o d/N\} \tag{2.7.10}$$

In general the total number of electrons in the gap for $t = p\Delta t \geq N+2$ is:

$$n_e(p\Delta t) = \{1+(\alpha+\alpha\gamma-\eta)d/N\}\{n_e((p-1)\Delta t) - (1+(\alpha-\eta)d/N)^N \times \alpha\gamma n_e((p-N-2)\Delta t)d/N\} \tag{2.7.11}$$

In principle there is no upper limit to the validity of Eq.(2.7.11) and several generations of photoelectrons can be described.
To estimate the error introduced by this type of calculation with discrete steps we consider the case in which no secondary emission and attachment take place, i.e. $\gamma = 0$ and $\eta = 0$. In this case the exact solution is (see Eq.(2.5.4)):

$$n_e(t) = n_o \exp(\alpha v_e t) \qquad 0 \leq t \leq T_e \tag{2.7.12}$$

and the numerical solution is:

$$n_e(p\Delta t) = n_o(1+\alpha d/N)^p \qquad 0 \leq p \leq N \tag{2.7.13}$$

In the limit $N \to \infty$ these equations are identical. For a finite N, Eq. (2.7.13) gives a lower value than Eq.(2.7.12). For example when $\alpha = 6\ cm^{-1}$ and $d = 1$ cm the deviation at $t = T_e$ for $N = 100$ is 16 %, for $N = 1000$, 2 % and for $N = 10{,}000$, 0.2 %.
From the number of electrons we can calculate the current caused by these electrons with the equation (see section 2.3):

$$i_e(t) = e\, n_e(t)/T_e \tag{2.7.14}$$

This theory can also be extended to calculate the current caused by positive and negative ions formed in the avalanche.
For that purpose we assume that the ions do not drift during the time

electrons are present in the gap. This is an acceptable simplification when all electrons, primary as well as secondary leave the gap in a time t_m which is short compared to the ion transit times. Note that t_m will generally be several times T_e .
In a time Δt the numbers of positive and negative ions formed are:

$$\Delta n_p(t) = \alpha n_e(t) v_e \Delta t \tag{2.7.15}$$

$$\Delta n_n(t) = \eta n_e(t) v_e \Delta t \tag{2.7.16}$$

The total number of ions at time $p\Delta t$ are:

$$n_p(p\Delta t) = n_p((p-1)\Delta t) + \alpha n_e((p-1)\Delta t)\, v_e \Delta t \tag{2.7.17}$$

$$n_n(p\Delta t) = n_n((p-1)\Delta t) + \eta n_e((p-1)\Delta t)\, v_e \Delta t \tag{2.7.18}$$

After $t = t_m$ all electrons have left the gap and the numbers of ions have reached their maximum. Now the positive ions are assumed to start to drift to the cathode with velocity v_p and the negative ions to the anode with velocity v_n . After $t = t_m + T_p$ all positive ions have left the gap and after $t = t_m + T_n$ the negative ions have left the gap.
To calculate the current caused by the moving ions we have to know the total numbers of ions at any time. Each electron, primary as well as secondary which started at the cathode has left a charge distribution of ions (see section 2.5). The distributions are:

$$\frac{\Delta n_p}{\Delta x} = \alpha \exp\{(\alpha - \eta)x\} \tag{2.7.19}$$

$$\frac{\Delta n_n}{\Delta x} = \eta \exp\{(\alpha - \eta)x\} \tag{2.7.20}$$

If A is the total number of electrons which have started at the cathode, the total distribution of ions at $t = t_m$ is A times the distribution left by one electron which has started at the cathode:

$$\frac{\Delta n_p}{\Delta x} = A\alpha \exp\{(\alpha - \eta)x\} \tag{2.7.21}$$

$$\frac{\Delta n_n}{\Delta x} = A\eta \exp\{(\alpha - \eta)x\} \tag{2.7.22}$$

To calculate the ion currents we need a relation between A and the total numbers of ions at $t = t_m$. These numbers are given by Eqs. (2.7.17) and (2.7.18), but on the other hand these numbers can also be calculated by integrating the distributions between $x = 0$ and $x = d$, as we show for the positive ions:

$$n_p(t_m) = \int_0^d \frac{\Delta n_p}{\Delta x}\, dx = \int_0^d A\alpha \exp\{(\alpha - \eta)x\}dx$$

$$= \frac{A\alpha}{\alpha - \eta}\left[\exp\{(\alpha - \eta)d - 1\right] \qquad (2.7.23)$$

$$A = \frac{n_p(t_m)}{\alpha}\,\frac{\alpha - \eta}{\exp\{(\alpha - \eta)d\} - 1} \qquad (2.7.24)$$

We define now a new time variable t* which is shifted with respect to the original time t by t_m:

$$t^* = t - t_m \qquad (2.7.25)$$

In the same way as described in section 2.5 we calculate the numbers of ions as a function of time:

$$n_p(t^*) = n_p(t_m) - \int_0^{v_p t^*} A\alpha \exp\{(\alpha - \eta)x\}dx \qquad (2.7.26)$$

$$= n_p(t_m) - \frac{A\alpha}{\alpha - \eta}\left[\exp\{(\alpha - \eta)v_p t^*\} - 1\right] \qquad (2.7.27)$$

for $0 \leq t^* \leq T_p$

$$n_n(t^*) = n_n(t_m) - \int_{d - v_n t^*}^{d} A\eta \exp\{(\alpha - \eta)x\}dx \qquad (2.7.28)$$

$$= n_n(t_m) - \frac{A\eta}{\alpha - \eta}\left[\exp\{(\alpha - \eta)d\} - \exp\{(\alpha - \eta)(d - v_n t^*)\}\right] \qquad (2.7.29)$$

for $0 \leq t^* \leq T_n$

The components of the current caused by the ions are again calculated from:

$$i_p(t^*) = \frac{e\, n_p(t^*)}{T_p} \qquad (2.7.30)$$

$$i_n(t^*) = \frac{e\, n_n(t^*)}{T_n} \qquad (2.7.31)$$

Figure 2.7.1 shows, as an example, the number of electrons within the gap as a function of time computed with the method described in this section. Figure 2.7.2 shows the number of ions as a function of time under the same conditions.

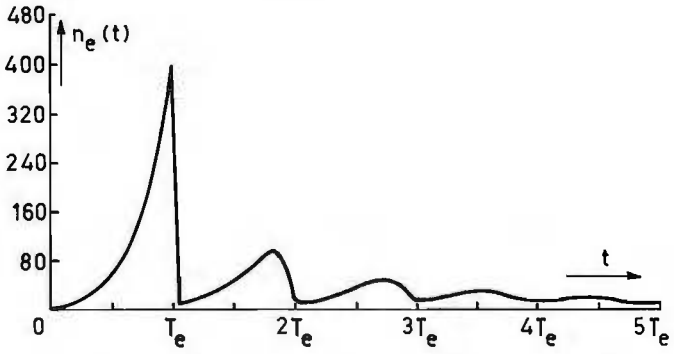

Fig. 2.7.1 The number of electrons as a function of time; $\alpha = 6$, $\eta = 0$, $\gamma = 1.67 \times 10^{-3}$, $d = 1$ cm, $N = 1000$ and $n_o = 1$

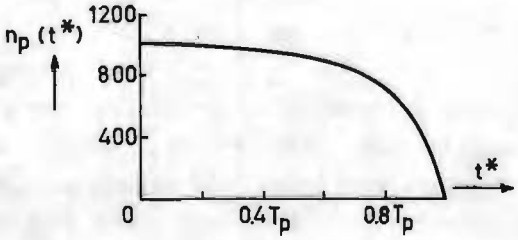

Fig. 2.7.2 The number of positive ions as a function of time under the same conditions as in Figure 2.7.1

From these figures we can demonstrate the use of the equations derived in section 2.6 to calculate γ. Under the conditions mentioned in the caption of Figure 2.7.1 and for $\tau = 0$, Eq.(2.6.21) simplifies to:

$$\gamma = \frac{1}{\exp(\alpha d)} \frac{n_e(t_1)}{n_e(t_1 - T_e)} \tag{2.7.32}$$

and Eq.(2.6.27):

$$\gamma = \frac{1}{\exp\{\alpha\, v_e(t_1 - T_e)} \frac{n_e(t_1)}{n_e(T_e)} \tag{2.7.33}$$

and Eq.(2.6.33):

$$\gamma = \frac{1}{\exp(\alpha d)} \left\{ 1 - \frac{n_e(T_e)}{n_p(t_m)} \right\} \tag{2.7.34}$$

From Figs. 2.7.1 and 2.7.2 it can be seen that $t_1 = 1.85\, T_e$, $n_e(t_1) = 100$, $n_e(t_1 - T_e) = 63$, $n_e(T_e) = 400$ and $n_p(t_m) = 1032$. With $\exp(\alpha d) = 403.4$ follows from Eq.(2.7.32) as well as from Eq.(2.7.33) and Eq.(2.7.34), $\gamma = 1.52 \times 10^{-3}$.
In comparison with the input value $\gamma = 1.67 \times 10^{-3}$ this is about 10 % lower which could be attributed to the approximations made both in this section and in section 2.6.

2.8. Avalanches in which ionization, attachment, detachment and conversion take place

In this section avalanche growth is discussed if in addition to ionization and attachment (see section 2.5), detachment and conversion are important.
For simplicity secondary processes at the cathode and diffusion are neglected. The negative ions formed by the attachment process are supposed to be unstable; they split into neutral particles and free electrons again (detachment) or they form stable negative ions upon collisions with neutral particles (conversion).
When the avalanche is started by n_o electrons released from the cathode in a very short time, the change in the number of electrons in a time dt is, for $0 \leq t \leq T_e$ given by:

$$dn_e(t) = (\alpha - \eta) n_e(t) v_e\, dt + \delta\, n_{nu}(t) v_e\, dt \tag{2.8.1}$$

in which $n_{nu}(t)$ is the total number of unstable negative ions. The

change in the number of positive ions is given by:

$$dn_p(t) = \alpha\, n_e(t)\, v_e\, dt \tag{2.8.2}$$

the change in the number of unstable negative ions by:

$$dn_{nu}(t) = \eta\, n_e(t)\, v_e\, dt - \delta\, n_{nu}(t)\, v_e\, dt - \beta\, n_{nu}(t)\, v_e\, dt \tag{2.8.3}$$

and the change in the number of stable negative ions by:

$$dn_{ns}(t) = \beta\, n_{nu}(t)\, v_e\, dt \tag{2.8.4}$$

The solution of this set of equations for the total number of electrons is:

$$n_e(t) = \frac{n_o}{A_1 - A_2}\left\{(A_1 + \delta + \beta)\exp(A_1\, v_e\, t) - (A_2 + \delta + \beta)\exp(A_2\, v_e\, t)\right\} \tag{2.8.5}$$

for $0 \leq t \leq T_e$

in which:

$$A_1 = \tfrac{1}{2}(\alpha - \eta - \delta - \beta) + \tfrac{1}{2}\left\{(\alpha - \eta - \delta - \beta)^2 - 4(\beta\eta - \alpha\beta - \alpha\delta)\right\}^{\frac{1}{2}} \tag{2.8.6}$$

$$A_2 = \tfrac{1}{2}(\alpha - \eta - \delta - \beta) - \tfrac{1}{2}\left\{(\alpha - \eta - \delta - \beta)^2 - 4(\beta\eta - \alpha\beta - \alpha\delta)\right\}^{\frac{1}{2}} \tag{2.8.7}$$

Note that for $\delta = 0$, Eq.(2.8.5) simplifies to:

$$n_e(t) = n_o \exp\{(\alpha - \eta)\, v_e\, t\} \tag{2.8.8}$$

which is identical to Eq.(2.5.4).
At $t = T_e$ the "head" of the avalanche reaches the anode and $n_o \exp\{(\alpha - \eta)\, d\}$ electrons leave the gap. The number of electrons which are still present in the gap a time dt later is:

$$n_e(T_e + dt) = n_e(T_e) - n_o \exp\{(\alpha - \eta)\, d\} \tag{2.8.9}$$

with

$$i_e(t) = \frac{e\, n_e(t)}{T_e} \tag{2.8.10}$$

and

$$i_o = \frac{e\, n_o}{T_e} \tag{2.8.11}$$

follows:

$$i_e(T_e) - i_e(T_e + dt) = \frac{e\, n_o}{T_e}\exp\{(\alpha - \eta)\, d\} = i_o \exp\{(\alpha - \eta)\, d\} \tag{2.8.12}$$

For $t > T_e + dt$ the Eqs.(2.8.1) through (2.8.4) become very complicated and have no simple analytical solution. However, there will be an aftercurrent caused by delayed electrons which were temporarily immobilized by attachment.
Measurements of $i_e(t)$ (see Chapter 4) in an experiment will give an $i_e(t)$ waveform as schematically shown in Figure 2.8.1.
The value of $(\alpha - \eta)$ can be derived from a measured current with Eq. (2.8.12). From the ratio of $i_e(T_e)$ and $i_e(T_e + dt)$ a relation between the parameters α, η, δ and β can be derived, however this relation does not give sufficient information to derive the parameters separately (see Eqs.(2.8.5), (2.8.9) and (2.8.10)).

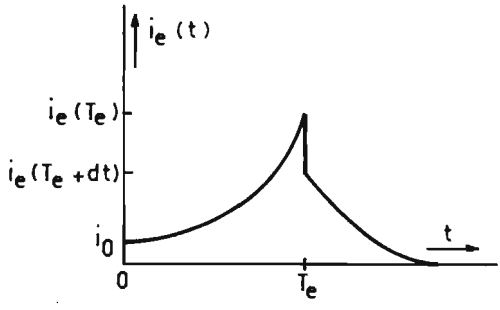

Fig. 2.8.1 Current caused by electrons in an avalanche in which ionization, attachment, detachment and conversion are important

2.9. Avalanches in which ionization, attachment, detachment, conversion and secondary emission take place. Numerical solution

In the preceding section avalanche growth was discussed when ionization, attachment, detachment and conversion are important.
The analytical solution given there for the time dependent current caused by the electrons is only valid up to $t = T_e$. In this section a numerical method is worked out to compute the complete current waveforms caused by both the electrons and the ions.
Besides the above mentioned processes, secondary emission of photoelectrons released from the cathode is taken into account. The mean

life time τ of the excited particles is taken to be zero (compare section 2.7).
Negative ions formed by attachment are supposed to be unstable; they split into neutral particles and free electrons again (detachment) or they form stable negative ions upon collisions with neutral particles (conversion).
The electrode distance d is divided into N equal parts, each Δx long. An electron travels a distance Δx in a time Δt:

$$\Delta x = d/N \tag{2.9.1}$$

$$\Delta t = \Delta x/v_e = T_e/N \tag{2.9.2}$$

Define $d n_e(p\Delta x, q\Delta t)$, $d n_p(p\Delta x, q\Delta t)$, $d n_{nu}(p\Delta x, q\Delta t)$ and $d n_{ns}(p\Delta x, q\Delta t)$ as the number of electrons, positive ions, unstable negative ions and stable negative ions situated between $p\Delta x$ and $(p+1)\Delta x$ at the time $t = q\Delta t$, where p and q are integers. The total numbers of the various charge carriers at $t = q\Delta t$ are then given by:

$$n_e(q\Delta t) = \sum_{p=0}^{N-1} d n_e(p\Delta x, q\Delta t) \tag{2.9.3}$$

$$n_p(q\Delta t) = \sum_{p=0}^{N-1} d n_p(p\Delta x, q\Delta t) \tag{2.9.4}$$

$$n_{nu}(q\Delta t) = \sum_{p=0}^{N-1} d n_{nu}(p\Delta x, q\Delta t) \tag{2.9.5}$$

$$n_{ns}(q\Delta t) = \sum_{p=0}^{N-1} d n_{ns}(p\Delta x, q\Delta t) \tag{2.9.6}$$

The avalanche starts with n_o electrons released in a very short time from the cathode, i.e. $n_e(0) = d n_e(0,0) = n_o$.
Electrons situated between $p\Delta x$ and $(p+1)\Delta x$ drift a distance Δx in a time Δt and are then situated between $(p+1)\Delta x$ and $(p+2)\Delta x$. Upon collisions with neutral particles their number increases by ionization and decreases by attachment. Their number also increases by detachment from unstable negative ions which are situated between $(p+1)\Delta x$ and $(p+2)\Delta x$:

$$dn_e((p+1)\Delta x, (q+1)\Delta t) = (1+(\alpha-\eta)\Delta x)\, dn_e(p\Delta x, q\Delta t) + \delta \Delta x\, n_{nu}((p+1)\Delta x, q\Delta t) \qquad (2.9.7)$$

for $0 \leq p \leq N-2$

At the cathode there is an increase in the number of electrons by secondary emission:

$$dn_e(0,(q+1)\Delta t) = \alpha\gamma \Delta x\, n_e(q\Delta t) \qquad (2.9.8)$$

With Eq.(2.9.3) the total number of electrons can be calculated. The relation $i_e(t) = e\, n_e(q\Delta t)/T_e$ then gives the current which flows in the external circuit.
The number of positive ions between $(p+1)\Delta x$ and $(p+2)\Delta x$ at $t=(q+1)\Delta t$ equals the number which is situated at that place at $t=q\Delta t$ increased by the number which is formed by ionizing collisions while electrons move from $p\Delta x$ to $(p+1)\Delta x$:

$$dn_p((p+1)\Delta x,(q+1)\Delta t) = dn_p((p+1)\Delta x, q\Delta t) + \alpha \Delta x\, dn_e(p\Delta x, q\Delta t) \qquad (2.9.9)$$

for $0 \leq p \leq N-2$.

$$dn_p(0,(q+1)\Delta t) = dn_p(0, q\Delta t) \qquad (2.9.10)$$

The number of unstable negative ions between $(p+1)\Delta x$ and $(p+2)\Delta x$ at $t=(q+1)\Delta t$ equals the number which is situated at that place at $t=q\Delta t$ increased by the number which is formed by attachment while electrons move from $p\Delta x$ to $(p+1)\Delta x$ and decreased by detachment and conversion:

$$dn_{nu}((p+1)\Delta x,(q+1)\Delta t) = dn_{nu}((p+1)\Delta x, q\Delta t)\{1-(\delta+\beta)\Delta x\} + \eta \Delta x\, n_e(p\Delta x, q\Delta t) \qquad (2.9.11)$$

for $0 \leq p \leq N-2$.

$$dn_{nu}(0,(q+1)\Delta t) = 0 \qquad (2.9.12)$$

The number of stable negative ions between $(p+1)\Delta x$ and $(p+2)\Delta x$ at $t=(q+1)\Delta x$ equals the number which is situated at that place at

$t = q\Delta t$ increased by the number which is formed by conversion:

$$dn_{ns}((p+1)\Delta x,(q+1)\Delta t) = dn_{ns}((p+1)\Delta x,q\Delta t) + \\ + \beta\Delta x\, n_{nu}((p+1)\Delta x,q\Delta t) \quad (2.9.13)$$

for $0 \leq p \leq N-2$.

$$dn_{ns}(0,(q+1)\Delta t) = 0 \quad (2.9.14)$$

With Eqs.(2.9.4), (2.9.5) and (2.9.6) the total numbers of the positive, unstable and stable negative ions are calculated and from them the currents which flow in the external circuit.
Since the drift velocity of ions is much smaller than the drift velocity of the electrons the ions are not supposed to drift during each time step Δt. This drift of ions is now simulated by moving the positive ions over a distance Δx in the direction of the cathode whenever $q = a\, v_e/v_p$, in which a is an integer and v_e/v_p is rounded off to an integral value, for example if $199.5 \leq v_e/v_p < 200.5$, the ions drift a distance Δx when $q = 200$, $q = 400$, $q = 600$ and so on. The drift of the negative ions is simulated in the same way.
Figure 2.9.1 shows, as an example, the number of electrons within the gap as a function of time computed with the method described in this section. Figure 2.9.2 shows the number of ions as a function of time under the same conditions. The transit times of the three ion species are all chosen equal to T_i.

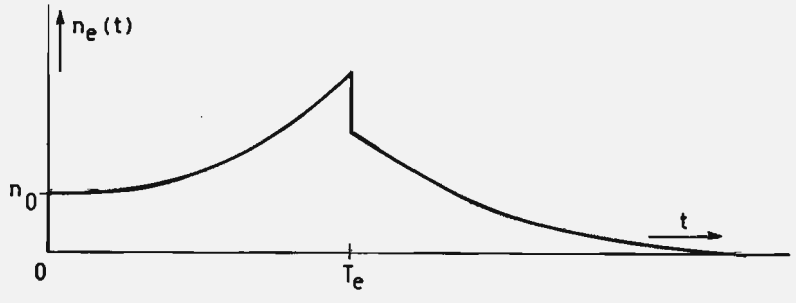

Fig. 2.9.1 The number of electrons as a function of time; $\alpha = \eta = 7.7\ cm^{-1}$, $\gamma = 0$, $\delta = 1.03\ cm^{-1}$, $\beta = 3.7\ cm^{-1}$, $d = 1\ cm$ and $N = 50$

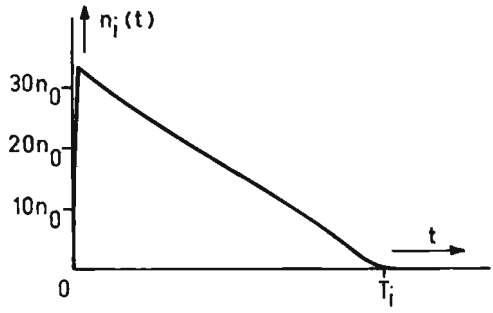

Fig. 2.9.2 The number of ions as a function of time for the same conditions as Figure 2.9.1

From Figure 2.9.1 we can see that $n_e(T_e) = 2.925\, n_o$. With the values of the parameters mentioned in the caption of Figure 2.9.1, Eq.(2.8.5) can be written as:

$$n_e(t) = \frac{n_o}{7.35}\{6.04\ \exp(1.31\, v_e\, t) + 1.31\ \exp(-6.04\, v_e\, t)\} \qquad (2.9.15)$$

from which follows $n_e(T_e) = 3.045\, n_o$ which is only 4 % higher than the value obtained by the numerical method.
Also from Figure 2.9.1 we can see that:

$$n_e(T_e + dt) - n_e(T_e) = 0.923\, n_o \qquad (2.9.16)$$

Under those conditions, i.e. $\alpha = \eta$, this should be exactly n_o (see Eq. (2.8.9)) which is about 8 % higher.
Note that from Figure 2.9.2 the maximum number of ions can be taken to be $33.2\, n_o$. In the case $\delta = 0$ this would be $(\alpha + \eta)\, n_o\, d = 15.4$ (see Eqs. (2.5.9) and (2.5.10)). Obviously the total number of ionizing collisions increases when detachment takes place.

2.10. Transition from an avalanche into a complete breakdown

In the previous sections the conditions were assumed to be such that after a certain time all electrons of the avalanche have left the gap. Since only electrons were supposed to be responsible for the formation of free charge carriers the formation of charge carriers then stops.

One ion transit time later all the charge carriers have left the gap. In this section we discuss briefly the transition of the above-mentioned non-selfsustaining discharge into a complete breakdown of the gap. Since a lot is published on the breakdown of gases (see for example Meek and Craggs [Me 78]) we restrict ourselves here to a qualitive description of the two types of breakdown and their criteria.

Townsend's mechanism of breakdown

Townsend's mechanism of breakdown is based on the generation of successive secondary avalanches. These secondary avalanches are not only started by photoelectrons from the cathode (compare section 2.6) but also by electrons released from the cathode when positive ions or metastable neutral particles strike the cathode.
The criterion for breakdown is then (see also the note near Eq. (2.6.29)):

$$\gamma \frac{\alpha}{\alpha - \eta} [\exp\{(\alpha - \eta)d\} - 1] \geq 1 \qquad (2.10.1)$$

in which γ is the "total" secondary ionization coefficient defined as the mean number of secondary electrons emitted from the cathode by photons, positive ions and metastable particles per ionizing collision. In words, this criterion states that the gap breaks down in case each avalanche, started by one electron released from the cathode, produces at least one new electron at the cathode surface.

Streamer mechanisms of breakdown

The streamer mechanisms are based on local field enhancement by space charges produced by the avalanche. When the field at the head of the avalanche reaches a certain value, the avalanche is assumed to emit highly energetic photons which are capable of photo-ionization of neutral particles just ahead of the avalanche.
Raether [Ra 40] proposed that the enhancement of the field between the avalanche and the anode caused by a large number of electrons in the avalanche is responsible for the formation of the streamer (anode-directed streamer or negative streamer).

On the other hand Loeb and Meek [Lo 41] proposed that the enhancement of the field between the head of the avalanche and the cathode caused by a large number of positive ions situated just behind the head of the avalanche is responsible for the formation of the streamer (cathode-directed streamer or positive streamer).
Both descriptions lead to a critical number of ionizing collisions above which breakdown occurs. For most gases at atmospheric pressure this critical number turns out to be several times 10^8 when the avalanche starts with one electron. If the avalanche starts from more primary electrons spread over a certain area of the cathode, this critical number is increased because the space charge density in this case is lower for the same number of charge carriers.
What type of breakdown, Townsend's or streamer occurs depends on which criterion is reached first.

3. EXPERIMENT

3.1. Introduction

The experimental setup with which we measured the current caused by the avalanche was designed for the use of the so-called "electrical method". In this method the avalanche is started by photoelectrons released from the cathode by a short UV-light pulse. The time-dependent current caused by the avalanche in the external circuit is measured as a voltage across a resistor in the ground connection of the low-voltage electrode. The time resolution of these measurements is limited by the length of the light pulse and the bandwidth with which the current can be monitored. This bandwidth is not only determined by the electronics but also very much by the lay-out of the electrodes and the experimental setup. Since high bandwidth electronics is now available, attention paid to the frequency characteristics of the circuitry of the gap can lead to significant improvements. The current shapes thus obtained give information on the processes occurring and may yield quantitative values for the parameters which describe these processes.

A different approach which is often used for the determination of discharge parameters is "Townsend's method". In this method the time-averaged current is measured in uniform field gaps with static voltage applied, while the cathode is continuously illuminated by UV-light. By analyzing a series of measurements of the current at various gap spacings, applied E-fields and pressures, quantitative values for the mentioned parameters can be obtained. When more processes are occurring at the same time the analysis becomes more complex.

In comparison to Townsend's method the electrical method, provided a high time resolution is obtained, gives more direct information about the occurring processes. In particular Townsend's method gives little information in case two processes occur in rapid succession, with no net change in the number of charged particles, such as attachment followed by rapid detachment. In this case only the electrical method will give the relevant information.

3.2. Frequency characteristics of an experimental setup to be used for the electrical method

Figure 3.2.1 is a diagram of the experimental setup which can be used for the electrical method.
The anode, at voltage V_h, is connected to the DC source by a damping resistor R_d. This resistor protects both the source and the electrodes in case of a breakdown of the gap.

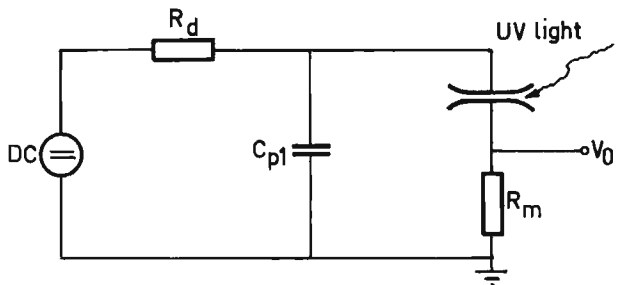

Fig. 3.2.1 Diagram of setup used for the electrical method

The capacitor C_{p1} consists of the parasitic capacitance of the high-voltage electrode and leads to ground and often includes a high-voltage capacitor at some distance from the electrodes.
The avalanche is started by photoelectrons emitted from the cathode by UV-light. The moving charges in the gap cause a current in the external circuit (see Chapter 2) which produces a voltage V_o across the measuring resistor R_m. The equivalent circuit for high frequencies of this setup is shown in Figure 3.2.2. The effect of the moving charges is represented by a current source i_g, which can be expressed in the number of charged particles and their transit times (see Eqs. (2.5.15), (2.5.16) and (2.5.17)).
The capacitance of the gap is C_g.
The current i_m through R_m and the voltage V_o can now be derived:

$$i_m = i_g + C_g \frac{dV_h}{dt} - C_g \frac{dV_o}{dt} \tag{3.2.1}$$

$$V_o = R_m i_m = R_m \left(i_g + C_g \frac{dV_h}{dt} - C_g \frac{dV_o}{dt} \right) \tag{3.2.2}$$

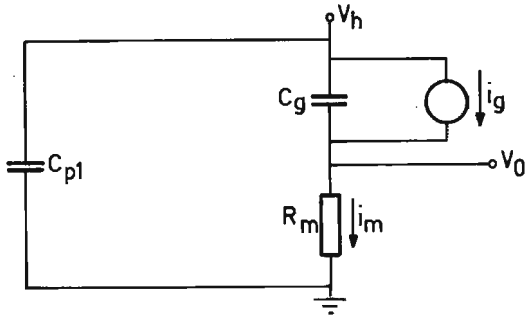

Fig. 3.2.2 Equivalent circuit for high frequencies. The avalanche is represented by the current source i_g

since

$$C_{p_1} \frac{dV_h}{dt} = - i_m \tag{3.2.3}$$

we can write Eq.(3.2.1) as:

$$i_m = i_g\left(1 - \frac{C_g}{C_{p_1} + C_g}\right) - \frac{C_{p_1} C_g}{C_{p_1} + C_g} \frac{dV_o}{dt} \tag{3.2.4}$$

and Eq. (3.2.2) as:

$$V_o = R_m i_g - \frac{R_m C_g i_g}{C_{p_1} + C_g} - R_m \frac{dV_o}{dt}\left(\frac{C_{p_1} C_g}{C_{p_1} + C_g}\right) \tag{3.2.5}$$

Equation (3.2.5) shows that the output voltage V_o reduces to zero if $C_{p_1} = 0$, in other words, when the anode is floating for high frequencies. In that case the material current in the gap is equal and opposite to the displacement current in C_g. Clearly the "coupling" capacitor C_{p_1} is an essential part of the measuring circuit.
The second term on the right hand side of Eq. (3.2.5) reduces the signal unless we make C_{p_1} large compared to C_g. A problem in high-voltage technology is however, that C_{p_1} is generally large in physical size and needs to be connected to the gap by relatively long leads. This introduces transit times and travelling waves on the leads with reflections at discontinuities of the characteristic impedance. The resulting fluctuations in the anode voltage V_h couple to the measur-

ing electrode through C_g (see second term on the right hand side of Eq. (3.2.1)). We should therefore place C_{p_1} close to the gap. For the same ratio C_{p_1}/C_g, a smaller size C_{p_1} is possible when C_g is reduced, which has the additonal advantage that the third term on the right hand side of Eq. (3.2.2) turns less important. To maintain a homogeneous E-field in the central region between the electrodes we need however, electrodes of reasonable dimensions. The solution to satisfy the three conditions (i) $C_{p_1} >> C_g$, (ii) C_{p_1} close to the gap and (iii) C_g small, is to subdivide the cathode and to place the damping resistor R_d directly above the anode (see Figure 3.2.3). The relatively small measuring part of the cathode has a capacitance C_g with

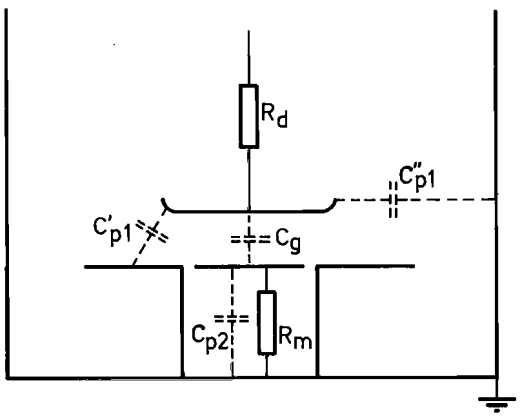

Fig. 3.2.3 Components of the equivalent circuit shown in the actual vessel

respect to the anode. The surrounding grounded ring has a capacitance C'_{p_1} with respect to the anode. Together with the capacitance C''_{p_1} between the anode and the surrounding grounded vessel, C'_{p_1} forms a compact coupling capacitor (see Figure 3.2.3). The equivalent circuit is the same as Figure 3.2.2 with $C_{p_1} = C'_{p_1} + C''_{p_1}$ and Eq. (3.2.5) becomes:

$$V_o = R_m i_g \left(\frac{C'_{p_1} + C''_{p_1}}{C'_{p_1} + C''_{p_1} + C_g} \right) - R_m C_g \frac{dV_o}{dt} \left(\frac{C'_{p_1} + C''_{p_1}}{C'_{p_1} + C''_{p_1} + C_g} \right) \qquad (3.2.6)$$

The measuring resistor R_m has a parasitic capacitance C_{p_2} parallel to it (see Figure 3.2.3). Clearly the capacitor C_{p_2} should be kept as small as possible. The value of C_{p_2} is already much reduced

since a small measuring electrode is used. To reduce the capacitance to the surrounding grounded electrode the edges of the two electrodes are beveled (see Figure 3.2.4).

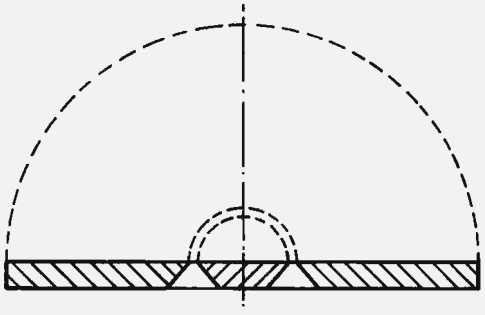

Fig. 3.2.4 Cathode with its central measuring electrode

For $C'_{p1} + C''_{p1} >> C_g$, Eq. (3.2.6) can be rewritten as:

$$V_o = R_m i_g - R_m(C_{p2} + C_g)\frac{dV_o}{dt} \qquad (3.2.7)$$

In conclusion the advantages of this configuration over a conventional one are:

- $C_{p1} >> C_g$: less loss of signal and less distortion (compare Eq. (3.2.5)).
- C_{p1} is located close to the gap and is well defined; this improves the high-frequency properties of the input circuit and travelling waves on the high-voltage leads are avoided.
- C_{p2} is small; up to high frequencies the parasatic capacitance of the measuring resistor can be neglected.

An alternative to measure i_g is to ground the central part of the cathode and to measure dV_h/dt. In that case C_{p1} is directly in parallel to C_g. Therefore:

$$\frac{dV_h}{dt} = -\frac{i_g}{C_g + C_{p1}} \qquad (3.2.8)$$

So in this case dV_h/dt is proportional to i_g.

Figure 3.2.5 shows a setup with which dV_h/dt can be measured. The circuit is similar to that of Figure 3.2.1 with the exception that R_m is omitted and a measuring network $R_{dif}C_{dif}$ is added. Note that for a purely resistive R_{dif} the network output voltage V_{dif} will be proportional to dV_h/dt. The equivalent circuit for high frequencies of this setup is shown in Figure 3.2.6.

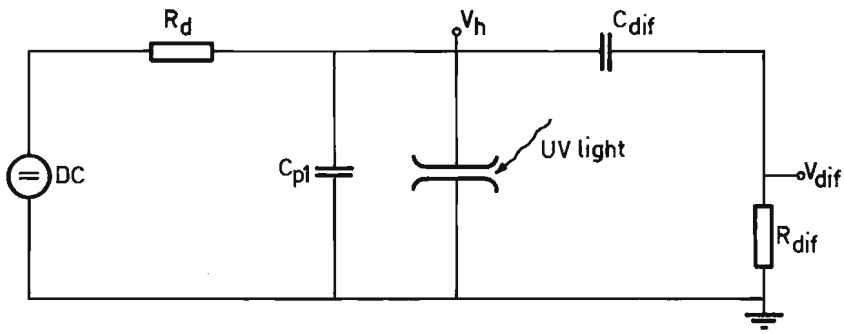

Fig. 3.2.5 Diagram of setup used for the determination of dV_h/dt

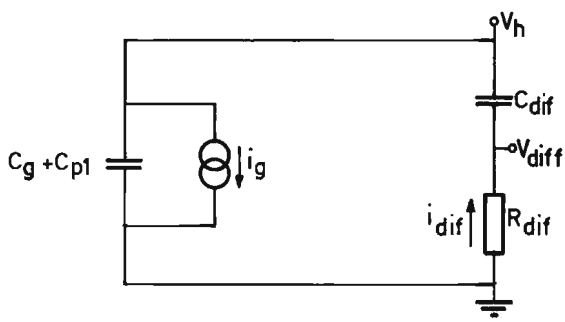

Fig. 3.2.6 Equivalent circuit for high frequencies for the dV_h/dt measurements. The avalanche is represented by the current source i_g

The current i_{dif} through R_{dif} can now be derived:

$$i_{dif} = C_{dif}\left(\frac{dV_{dif}}{dt} - \frac{dV_h}{dt}\right) \qquad (3.2.9)$$

$$i_{dif} = i_g + (C_g + C_{p_1})\frac{dV_h}{dt} \qquad (3.2.10)$$

From these equations the output voltage V_{dif} can be derived:

$$V_{dif} = -i_{dif}R_{dif} = -R_{dif}C_{dif}\left(\frac{dV_{dif}}{dt} - \frac{dV_h}{dt}\right) \qquad (3.2.11)$$

$$V_{dif} = -i_g R_{dif} - R_{dif}(C_g + C_{p_1})\frac{dV_h}{dt} \qquad (3.2.12)$$

$$V_{dif} = -\frac{R_{dif}C_{dif}}{C_{dif} + C_g + C_{p_1}} i_g - \frac{R_{dif}C_{dif}(C_g + C_{p_1})}{C_{dif} + C_g + C_{p_1}}\frac{dV_{dif}}{dt} \qquad (3.2.13)$$

When we use the surrounding ring of the subdivided cathode as the capacitor C_{dif} the circuit becomes as shown in Figure 3.2.7, and Eq. (3.2.13) can be rewritten as:

$$V_{dif} = -R_{dif}i_g\left(\frac{C'_{p_1}}{C'_{p_1} + C''_{p_1} + C_g}\right) - R_{dif}C'_{p_1}\frac{dV_{dif}}{dt}\left(\frac{C_g + C''_{p_1}}{C'_{p_1} + C''_{p_1} + C_g}\right) \qquad (3.2.14)$$

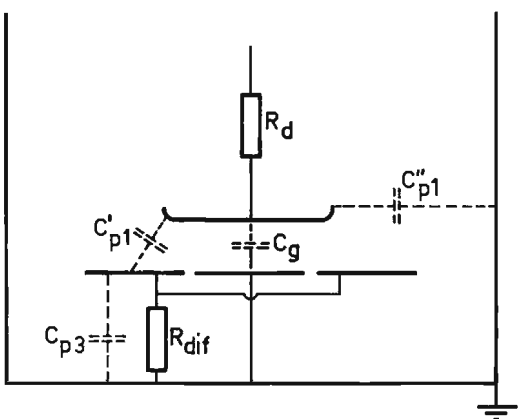

Fig. 3.2.7 Components of the equivalent circuit for the dV_h/dt measurements shown in the actual vessel

Note the similarity between this equation and Eq. (3.2.6). If in both equations the terms proportional to dV_o/dt and dV_{dif}/dt can be neglected and R_{dif} is chosen equal to R_m the ratio between the output voltages is:

$$\frac{V_o}{V_{dif}} = - \frac{C'_{p1} + C''_{p1}}{C'_{p1}} \qquad (3.2.15)$$

From Eqs. (3.2.2) and (3.2.12) we can see that V_{dif} is more sensitive than V_o for fluctuations in the anode voltage V_h. So if there are reflections in the high-voltage leads this is shown more clearly in the V_{dif} signal than in the V_o signal.
The resistor R_{dif} will have a parasatic capacitance C_{p3} (see Figure 3.2.7). For high-frequency measurements this capacitance should be small. In practice C_{p3} will be larger than C_{p2} because of the larger dimensions of the outer ring of the cathode.

3.3. Ramo-Shockley effect

The frequency response calculations of the previous section indicate that when a subdivided cathode is used the radius R of the measuring electrode should be small. However, if in a gap of width d the radius R is chosen too small the moving charge carriers induce also a current in the ground connection of the surrounding ring which reduces the current through R_m. In other words the current through R_m depends on the parameters R and d and on the position of the charge carriers in the gap and is therefore no longer a correct measure for the current caused by the avalanche. Shockley [Sh 38] and Ramo [Ra 39] gave a general formula for the current in the lead to the measuring electrode in a configuration of several electrodes:

$$i_m = \frac{E_{SR}}{U_{SR}} qv \qquad (3.3.1)$$

in which i_m is the current in the lead to a measuring electrode caused by a point charge q which moves with a velocity v. The quantity E_{SR} is the component of the E-field in the direction of v along the path of the charge q, in the hypothetical case that the measuring electrode is given a voltage U_{SR} while all other electrodes are connected to ground (see Figure 3.3.1). From Figure 3.3.1 we can see that in the case $R >> d$ and when the charge moves along the axis we obtain: $E_{SR} = U_{SR}/d$ and therefore $i_m = qv/d$, which is indeed the

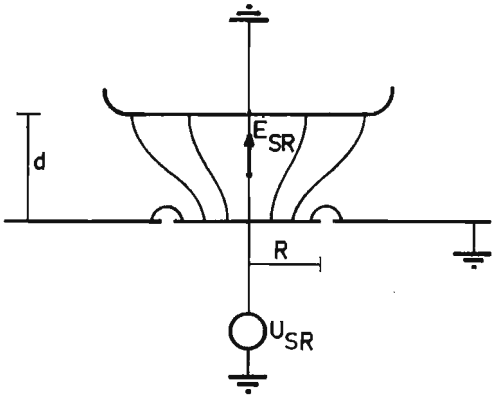

Fig. 3.3.1 Hypothetical field used in Eq.(3.3.1) to determine the current i_m

current induced in the external circuit in the real situation (see section 2.3).

When, however, R is small compared to d, E_{SR} will be a function of x and the relation between the current i_m and the charge motion becomes more complicated.

It is therefore important to determine at which ratio R/d the field E_{SR} on axis is no longer constant. For this purpose E_{SR} can be obtained by numerical methods or in an electrolytic tank (see Figure 3.3.2). From Figure 3.3.2 it can be seen that for R = 20 mm the

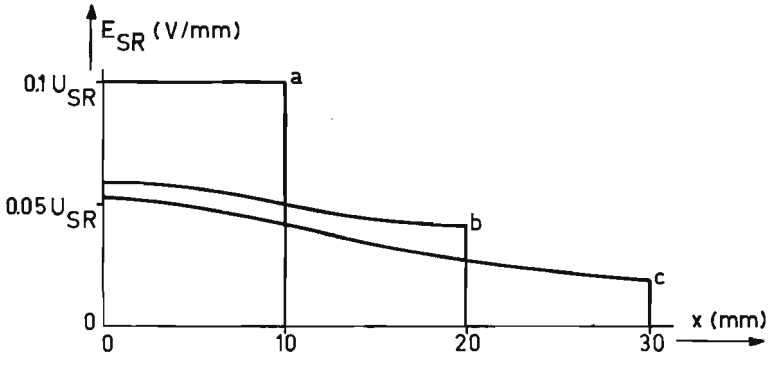

Fig. 3.3.2 Field E_{SR} to be used in Eq.(3.3.1) obtained by numerical methods. The radius of the measuring electrode is 20 mm.
(a) d = 10 mm, (b) d = 20 mm, (c) d = 30 mm.

cathode can be used up to 10 mm gap spacing.

Since E_{SR} on axis is a function of R/d only, it can be concluded that for any subdivided cathode the ratio of the radius of the measuring electrode and the gap spacing must be larger than or equal to 2. This also means that at $R/d \geq 2$ avalanches crossing along the axis do not induce a current in the lead of the surrounding ring. Therefore, it is correct to use this ring as a coupling capacitor in the current measurements, or as the differentiating capacitor in the dV_h/dt measurements of the previous section.

3.4. Start of the avalanche

After a DC voltage below the breakdown voltage has been applied to the gap the avalanche has to be started by external means. In the theoretical derivations of the avalanche growth in Chapter 2 it is assumed that the avalanche is started by n_o electrons which leave the cathode simultaneously. In practice, however, always a certain time duration is necessary to release a number of electrons, for instance by photoemission. The light source can be a spark gap, a UV flashlamp or more recently a laser. The disadvantage of the first two sources is the rather long duration of the light pulse with its inherent afterglow which cannot be readily suppressed. Also lasers which have been used for this purpose up till now, for example by Teich and Branston [Te 74] and by Jaksts and Cross [Ja 78], have a rather long light pulse (> 10 ns). In this respect the transversely excited atmospheric pressure (TEA) N_2-lasers are much more ideal. We have constructed such a laser according to the design of Patel [Pa 78] with the difference that the transmission plates were given a cylindrical shape which makes the laser more compact and mechanically more rigid.
The measured pulse duration is 0.6 ns (full width at one half maximum). Patel has measured for his laser a peak power of 1 MW at an operating voltage of 30 kV. Our laser typically operates at 20 kV so we expect a lower peak power.
The laser wavelength is 337.1 mm which corresponds to an energy of 3.68 eV per photon. This wavelength limits the choice of the cathode material to materials with a workfunction smaller than or equal to 3.68 eV. In practice aluminium turns out to be satisfactory. If the aluminium cathode is placed in oxygen or an oxygen mixture the

surface has to be polished frequently.
The laser and its high-voltage power supply are enclosed in a brass box to suppress electromagnetic interference. Also for this purpose the lightbeam leaves the box through a brass tube of 2.5 cm diameter and a length of 10 cm and the AC line voltage needed for the power supply is fed in through a filter which suppresses higher frequencies. A small antenna in the wall of the box gives an electric signal at the moment the laser is fired. This signal can be used for the triggering of the oscilloscope.

3.5. Apparatus

Figure 3.5.1 is a diagram of the experimental setup. The DC source is a Wallis, type R 603/05 P; its output voltage can be set between 1 and 60 kV, the maximum ripple is 20 ppm peak to peak.

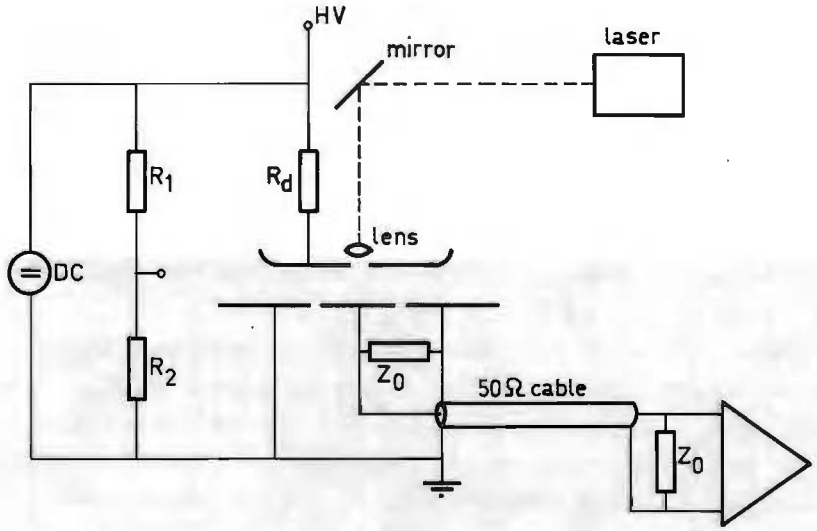

Fig. 3.5.1 Diagram of the experimental setup

The applied voltage is measured by the resistive divider formed by R_1 (2 GΩ) and R_2 (200 kΩ). The accuracy of this measurement is approximately 1%.
The light pulse of the laser (see section 3.4) strikes the cathode through a hole of 1.5 mm diameter in the center of the anode. A

positive lens in front of this hole diverges the light beam so that the electrons are released over an area of approximately 1 cm^2 for a gap spacing of 1 cm. The avalanche then starts from a large area and therefore a large number of electrons can be released without strong space-charge distortion.

The aluminium anode is of the Bruce-profile type [Br 47] with an overall diameter of 17 cm. The aluminium cathode is of the model described in section 3.2: the measuring part has a diameter of 4 cm, the total diameter of the cathode is 30 cm and the annular gap between the two parts is 0.1 mm at the cathode surface.

The damping resistor R_d which connects the HV electrode to the power source has a value of 3.3 MΩ and is placed just above the anode for reasons discussed in section 3.2.

The electrodes are placed in a stainless-steel pressure vessel with a feedthrough insulator of reinforced epoxy. The vessel can be evacuated to 10^{-3} Torr and filled to an absolute pressure of 5.3×10^3 Torr (7 bar). The pressure can be measured by the following pressure gauges: LKB type 3994 B (range 10^{-3} - 20 Torr), two Penwalts, type Fa-60 (range 0-50 Torr and 0-100 Torr) and a MKS Baratron, type 170 m - 7A with head 145 AHS - 10,000 (range 0-10^4 Torr).

The temperature inside the vessel can be measured within 0.1°C.

The water vapor content of the gasfilling is measured by an Endress and Hauser Hygrolog, type WMY 170 (dew point range from -80 to +20°C).

The electrode distance is variable and can be measured outside the vessel with an accuracy of 0.02 mm.

The vessel is provided with long rubber gloves which give the opportunity to manipulate inside the vessel without opening it. This is only possible when the inside pressure nearly equals the ambient pressure. For higher or lower pressures the holes upon which the gloves are fastened can be closed with covers, the pressure at both sides of the gloves is then kept equal by means of a by-pass.

The current measuring resistor R_m should be small, in view of the frequency response, but still large enough to retain a reasonable sensitivity. Also the long measuring cable has to be terminated with its characteristic impedance Z_o (in our case 50 Ω). Since we can start the avalanche with a large number of electrons, it was possible to measure across a terminating resistor Z_o at the end of the cable; a matching amplifier which has to be used when a higher measuring

resistor is needed, could therefore be avoided. In fact a second resistor of value Z_o is mounted at the beginning of the cable which reduces R_m and the product $R_m C_{p_2}$ (see section 3.2) by a factor two, this resistor also attenuates reflections if the cable is not exactly terminated at the far end. Parallel to this resistor two pairs of silicon diodes are mounted back to back to protect the amplifiers in case of a complete breakdown of the gap.

The output voltage is connected to a Tektronix oscilloscope system which consists of the dual beam main frame 7844 (bandwidth 0-500 MHz) with the amplifier units 7A19 (bandwidth 0-500 MHz) and 7A26 (bandwidth 0-200 MHz) and the time base units 7B80 and 7B85. For very weak signals an additional wide-band preamplifier (Avantek GPD 462, bandwidth 250 Hz - 500 MHz) can be used.

The measuring setup offers the possibility to measure, with the same R_m, the current caused by the electrons as well as the generally much smaller current caused by the ions. In fact it is possible to record the signal on both beams of the oscilloscope simultaneously, where one beam records with a small amplification and high writing speed and the other with high amplification and low writing speed. The amplitude ratio of the two currents, thus measured for the same avalanche, gives information on whether, for instance, secondary emission and detachment occur, because additionally formed electrons give rise to an after-current of electrons and so to a higher maximum current caused by the ions at later times.

The capacitors which are of importance for the frequency response (see section 3.2) were measured in the here discussed configuration for a gap spacing of 1 cm: $C'_{p_1} = 18.3$ pF, $C''_{p_1} = 3.8$ pF, $C_g = 1.1$ pF and $C_{p_2} = 33$ pF. The value for C_{p_2} has to be increased by the generally small input capacitance of the amplifiers.

Since $C'_{p_1} + C''_{p_1} >> C_g$ the input voltage is given by (see Eq. 3.2.7):

$$V_o = i_g R_m - R_m (C_{p_2} + C_g) \frac{dV_o}{dt} \qquad (3.5.1)$$

With $R_m = 25\,\Omega$ and the above mentioned values for C_{p_2} and C_g the time constant of the total input circuit turns out to be 0.9 ns.

4. EXPERIMENTAL RESULTS

4.1. Introduction

In this chapter measurements on avalanche currents are described. The currents are analyzed and values of discharge parameters are derived with the theory described in Chapter 2.
The measurements are done in nitrogen, carbon dioxide, oxygen, air, sulphur hexafluoride and sulphur hexafluoride/nitrogen mixtures.
The last section of this chapter is an introductory study of avalanches near a solid insulator.
All the experiments were carried out at room temperature (20-22 ^{o}C).

4.2. Avalanches in nitrogen

In this section measurements on avalanches in nitrogen are described. The maximum content of impurities in the nitrogen gas were: 10 ppm argon, 5 ppm oxygen and 1 ppm hydrocarbons (values given by the manufacturer) whereas the partial pressure of water vapor was lower than 0.04 Torr (own measurement).
Nitrogen is known as a nonattaching gas ($\eta = 0$) although on theoretical grounds the formation of negative ions could be possible. The life time of these negative ions should however be smaller than 10^{-12} s, [Fr 64], which is very short compared to all other characteristic times in the avalanche. The presence of negative ions can therefore be neglected, which makes the avalanche growth in nitrogen relatively simple.
In section 3.3 it was shown theoretically that when a subdivided cathode is used the ratio of the radius R of the measuring part and the gap spacing should be larger than 2. Another possibility to determine the minimum value of R/d is to measure the current in the external circuit for a well defined motion of charge carriers in the gap.
When we release n_o electrons from the center of the cathode in a very short time under such conditions that no ionization and attachment take place, a constant number of electrons will move across the gap. The current in the external circuit caused by these electrons is (see

Eq.(3.3.1)):

$$i_e(t) = n_o e v_e(t) \frac{E_{SR}}{U_{SR}} \qquad (4.2.1)$$

Since the E-field on axis between the cathode and the anode in the real situation is homogeneous and the applied voltage is kept constant, v_e will be constant also. The current $i_e(t)$ is therefore proportional to E_{SR}/U_{SR}.
The current through the measuring resistor causes a voltage V_o which can be taken from Eq.(3.2.5) where $i_e(t)$ from Eq.(4.2.1) is substituted for i_g.
If E_{SR} is constant along the path of the electrons, $V_o(t)$ will be constant also during the time electrons are present in the gap which leads to an output voltage of rectangular form. When however, E_{SR} is a function of x, the current through R_m depends on the position, $x = v_e t$, of the cloud of electrons in the gap at time t and the output voltage will be deformed.

Figure 4.2.1 shows currents caused by electrons crossing a gap in nitrogen at different gap spacings. The electric field is so low that no ionization takes place ($\alpha = 0$).
From Eq.(4.2.1) we can see that the motion of the electrons clearly transforms the $E_{SR}(x)$ plot into a perfectly similar $V_o(t)$ plot (compare Figures 3.3.2 and 4.2.1).
From these measurements we can conclude again that R/d should be larger than or equal to 2.
Since the electrons are released from the cathode in a very short time (0.6 ns, see section 3.4), the rise of the current at $t = 0$ is very fast. From Figure 4.2.1 we can see that the output voltage of our measuring setup shows an accordingly fast rise. The fall of the current is slower, especially at larger gap spacings because of diffusion and/or electrostatic repulsion in the axial direction (see section 2.4).
From the current amplitude in Figure 4.2.1.a, 100 µA, and the transit time, 130 ns, one can deduce with Eq.(4.2.1) that 8.0×10^7 photo-electrons have crossed the gap. This transport of charge carriers from the cathode to the anode causes a voltage drop $\Delta V_h = Q/(C_g + C'_{p1} + C''_{p1})$. With the values of the several capacitors given in section 3.5 this voltage drop can be determined to be 0.6 V

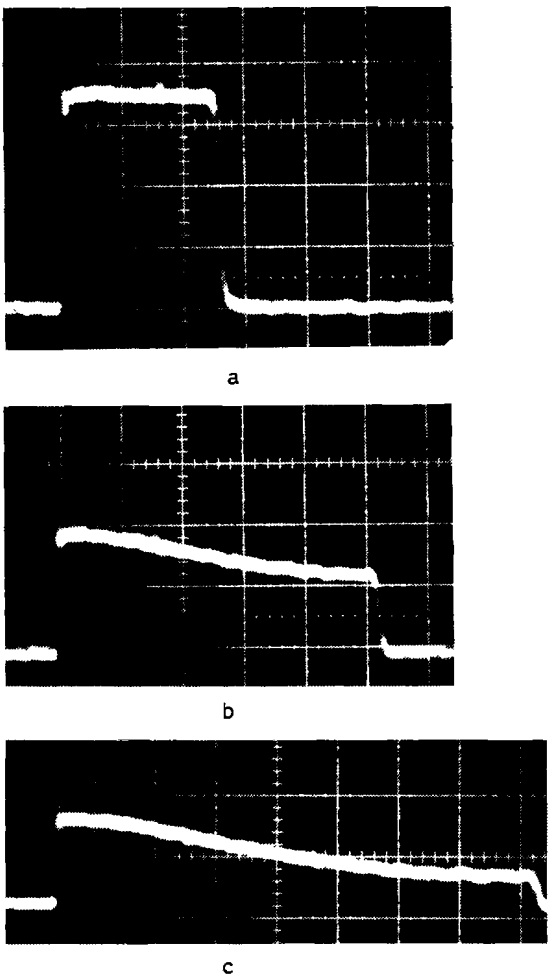

Fig. 4.2.1 Photoelectrons crossing a gap without ionization in nitrogen; p = 760 Torr, E = 17 kV/cm, 30 μA/div, 50 ns/div, (a) d = 1 cm, (b) d = 2 cm, (c) d = 3 cm. Note the similarity between this figure and Fig. 3.3.2.

which is very small compared to the total voltage applied to the gap (17 kV) .

Figure 4.2.2 shows currents caused by electrons crossing a gap without ionization at a nitrogen pressure of 5 and 20 Torr. Because the diffusion coefficient D is proportional to 1/p the effect of the

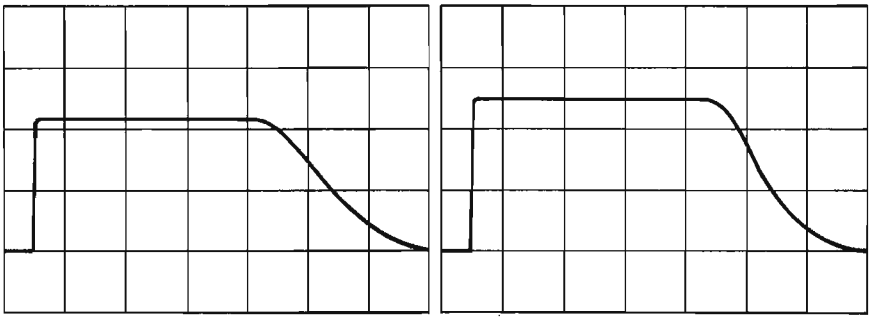

Fig. 4.2.2 Photoelectrons crossing a gap without ionization in nitrogen; $E/p = 25\ V\ cm^{-1}\ Torr^{-1}$, 30 μA/div, 20 ns/div, d = 8 mm, (a) p = 5 Torr, (b) p = 20 Torr.

diffusion process is much larger here than in Figure 4.2.1.
With the methods described in section 2.4 we can obtain values for the longitudinal diffusion coefficient D from oscillograms such as shown in Figure 4.2.2. Also the transit time can be determined and with the known gap spacing and applied E-field the mobility K can be derived.
Figure 4.2.3 shows values of D/K for different pressures at constant E/p. From the figure we can see that D/K is almost constant for $1.5 \lesssim p \lesssim 5$ Torr, increases with increasing p for $5 < p < 40$ Torr and is constant again for $p \gtrsim 40$ Torr. The value of D/K is a measure for the mean electron energy and can be interpreted as the electron temperature (kT/e, expressed in Volts) when the velocity distribution of the electrons is isotropic and Maxwellian [Me 78][1] . In a certain gas this mean electron energy should be a function of E/p only (see for example [Me 78][2]).Therefore in Figure 4.2.3 all measured D/K-values should be the same.
The explanation for the observed increase of D/K with p could be that our measurements are influenced by electrostatic repulsion (see section 2.4).
Both D and K are functions of 1/p; the space charge field E_d (see Eq.(2.4.24))depends on the number of electrons in the disk, n_o , and on the shape of the disk. Diffusion and electrostatic repulsion

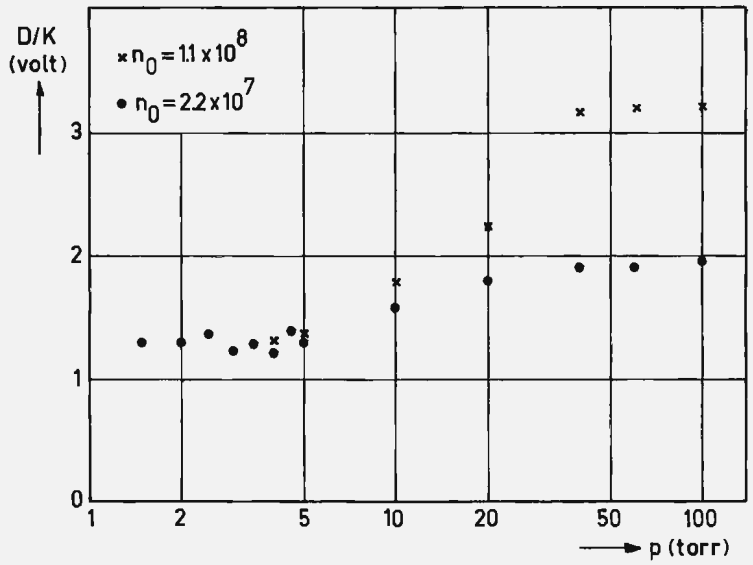

Fig. 4.2.3 D/K as a function of pressure at $E/p = 25\ V\ cm^{-1}\ Torr^{-1}$ in nitrogen.

cause a bulging of the disk which implicitly leads to a pressure dependence of E_d. The inequality (2.4.25) can now be written as:

$$t << \frac{D(1/p)}{2K^2(1/p)E_d^2(p,n_o)} = f(p,n_o) \qquad (4.2.2)$$

In the experiment T_e is kept constant (v_e is a function of E/p only and the gap spacing is kept constant) so this inequality can only be satisfied for correct combinations of n_o and p.

From Figure 4.2.3 we can now conclude that electrostatic repulsion in our experiment can be neglected for $p \lesssim 5$ Torr since for this range D/K is independent of p and n_o. For $p > 5$ Torr we find an apparent increase of D/K which depends on p and n_o.

Figure 4.2.4 shows D/K as function of E/p. In this figure also values of D/K are given which have been measured by Snelson and Lucas [Sn 75] and Saelee, Lucas and Limbeek [Sa 77]. For the range $E/p > 20\ V\,cm^{-1}\ Torr^{-1}$ our values are in good agreement with those given in Ref. [Sa 77] but for the range $E/p < 20\ V\,cm^{-1}\ Torr^{-1}$ our values are significantly larger than those given in both references.

The reason for this difference is not clear, but is certainly not

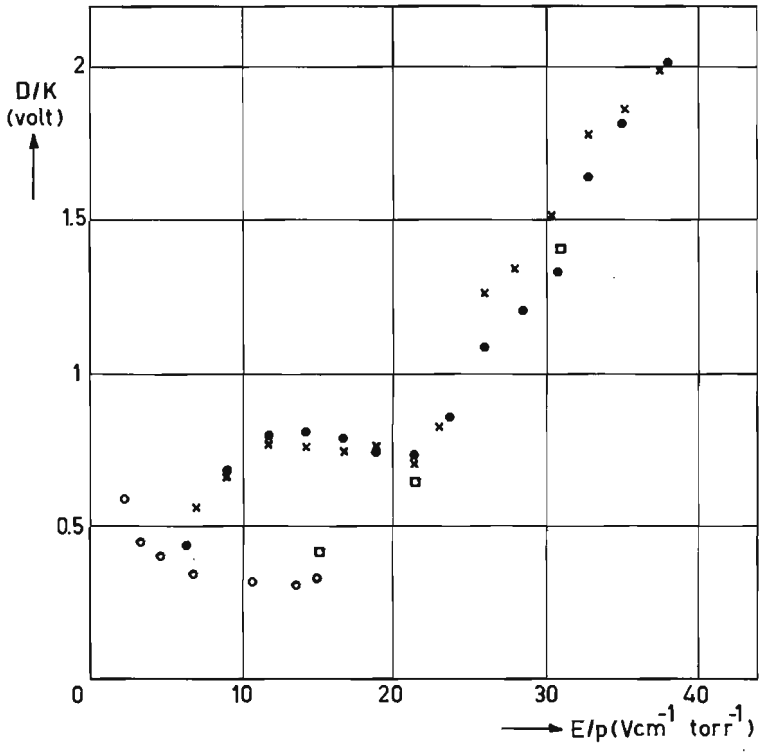

Fig. 4.2.4 D/K as a function of E/p.

- ● *our measurements with p = 2.1 Torr*
- × *our measurements with p = 4.3 Torr*
- o *measurements taken from Ref [Sn 75]*
- □ *measurements taken from Ref [Sa 77]*

caused by a loss of accuracy of our measurements in this range of E/p-values.

In practice the determination of D with Eq.(2.4.21) appears to be more accurate than with Eq.(2.4.14) or Eq.(2.4.15). The maximum error in the D/K values we estimate to be approximately 15 %, which is based on the individual errors of the quantities in Eq.(2.4.21) and the value of K.

Figure 4.2.5 shows an observed current at a pressure of approximately 0.1 Torr and without voltage applied to the gap. This current is caused by photoelectrons which leave the cathode with a kinetic energy $\frac{1}{2} m_e v^2$ caused by the difference between the energy of the incident photon and the workfunction of the cathode material.

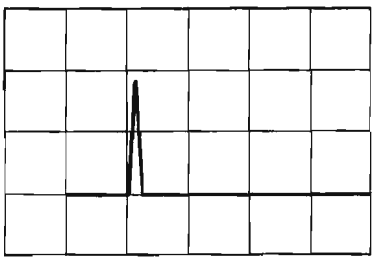

Fig. 4.2.5 Current caused by photoelectrons in nitrogen when no voltage is applied to the gap and p is approximately 10^{-1} Torr; d = 1 cm, 30 μA/div, 10 ns/div.

The directions of the velocities of the electrons have angles with the x-axis of the gap between 0 and π/2 radians. The electrons have therefore a net motion in the direction of the anode which causes a current in the external circuit. When the electrons collide with neutral particles after travelling over a mean free path, their velocities are randomized, the net drift motion of electrons drops to zero and correspondingly the current vanishes.

Figure 4.2.6 shows currents caused by electron avalanches in nitrogen at different voltages applied to the gap. From oscillograms such as shown in this figure the transit time of the electrons can be obtained and with the known gap spacing, the drift velocity v_e can be determined. We have measured v_e for the range $3.2 \leq E/p \leq 40.3$ V cm^{-1} Torr^{-1} at a constant nitrogen pressure of 769 Torr. Figure 4.2.7 shows v_e as a function of E/p.
In this figure also values of v_e are given which have been measured by Frommhold [Fr 60], Nielsen [Ni 36], Vogel and Raether [Vo 57] and Saelee, Lucas and Limbeek [Sa 77]. The accuracy of our measurements over the given E/p range is better than 3 %.
Townsend's ionization coefficient α can be derived from the measured currents as follows. The current caused by the moving electrons is given by (see Eqs.(2.3.3) and(2.5.4)):

$$i_e(t) = \frac{n_o e}{T_e} \exp(\alpha v_e t) \qquad \text{for } 0 \leq t \leq T_e \qquad (4.2.3)$$

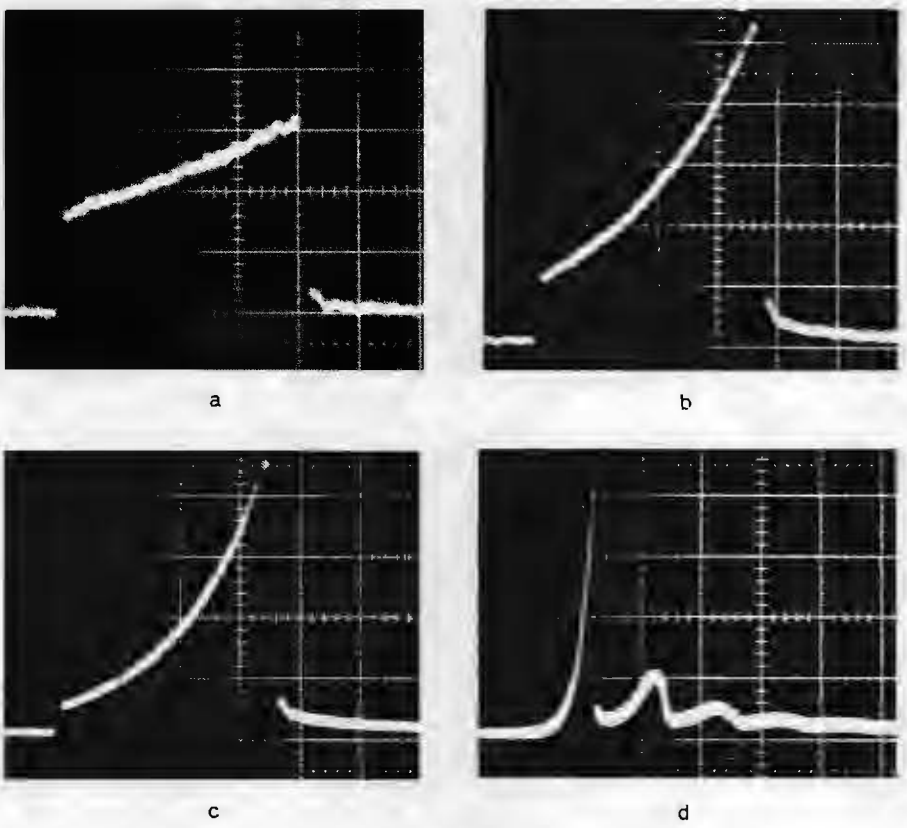

Fig. 4.2.6 Current caused by electron avalanches in nitrogen; p = 769 Torr, d = 8 mm,
(a) E = 23.20 kV/cm, 17.5 μA/div, 20 ns/div,
(b) E = 25.60 kV/cm, 35.0 μA/div, 20 ns/div,
(c) E = 26.90 kV/cm, 87.5 μA/div, 20 ns/div,
(d) E = 31.30 kV/cm, 2.0 mA/div, 50 ns/div.

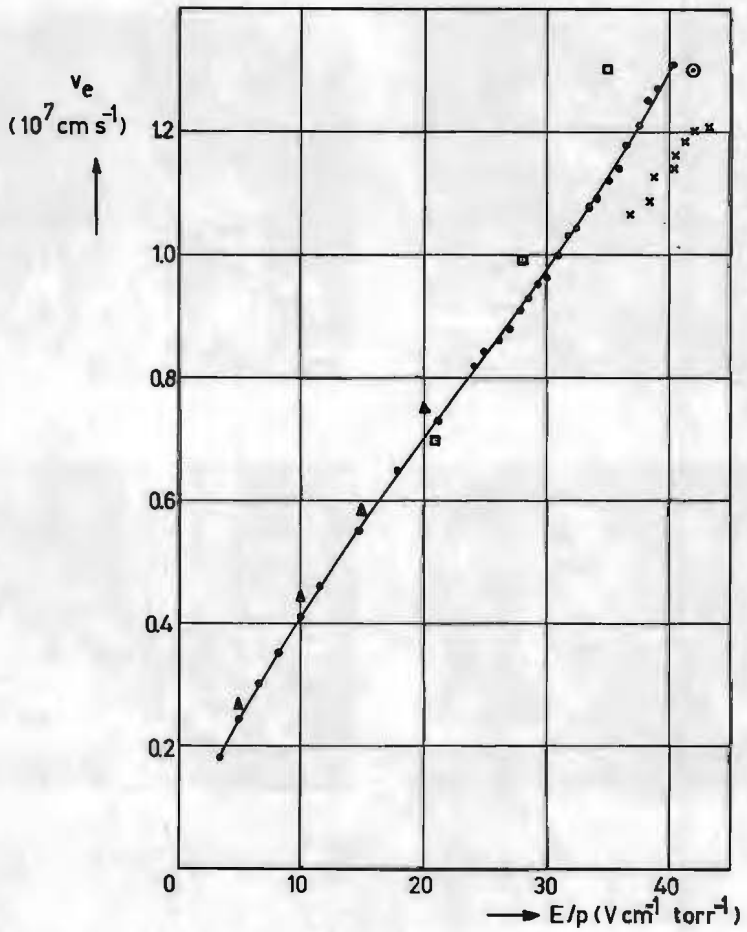

Fig. 4.2.7 Electron drift velocity v_e as a function of E/p in nitrogen at 769 Torr;
- ● *our measurements, Δ from Ref. [Ni 36]*
- □ *from Ref. [Sa 77], × from Ref. [Fr 60]*
- ⊙ *from Ref. [Vo 57].*

The coefficient α can be directly derived from the measured ratio of the currents at the end ($t = T_e$) and the beginning ($t = 0$) of the electron avalanche:

$$\frac{i_e(T_e)}{i_e(0)} = \exp(\alpha v_e T_e) = \exp(\alpha d) \qquad (4.2.4)$$

$$\alpha = \frac{1}{d} \ln \left(\frac{i_e(T_e)}{i_e(0)} \right) \qquad (4.2.5)$$

A second method is to plot the measured currents in graphs of $\ln i_e(t)$ vs t. Since:

$$\ln i_e(t) = \ln(n_o e/T_e) + \alpha v_e t \qquad (4.2.6)$$

The slope of the straight line is αv_e. With the known values of v_e and p, α/p can be derived. The first method is most suitable for low α values (see oscillograms a and b of Figure 4.2.6).For high α values $i_e(0)$ cannot be accurately measured and therefore the second method has to be used (see oscillogram d of Figure 4.2.6). For the intermediate values (see oscillogram c of Figure 4.2.6) the two methods are in very good agreement.
Figure 4.2.8 shows α/p in nitrogen as a function of E/p.

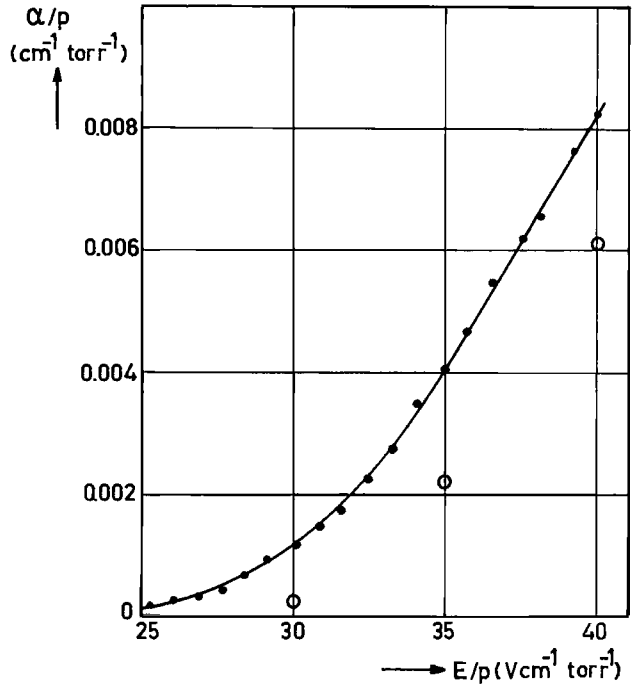

Fig. 4.2.8 Ionization coefficient as a function of E/p in nitrogen measured at 769 Torr. The continuous curve represents our measurements; the three points below the curve are taken from Ref. [Ha 76]

In this figure also values of α/p are given which have been measured by Haydon and Williams [Ha 76]. Their values are significantly smaller than our values. Haydon and Williams used Townsend's method and had to apply an indirect procedure to get values of α/p for the range $E/p \leq 50\ V\,cm^{-1}\,Torr^{-1}$ which is just the range shown in Figure 4.2.8.

The accuracy in our measurements of α/p is $10^{-4}\ cm^{-1}\,Torr^{-1}$ for the range $E/p \leq 29\ V\,cm^{-1}\,Torr^{-1}$ and 8 % for the range $E/p > 29\ V\,cm^{-1}\,Torr^{-1}$. Note that the current shown in Figure 4.2.6 d clearly demonstrates the onset of secondary avalanches by photo-emission (compare Figure 2.7.1).

Figure 4.2.9 shows simultaneously measured electron and ion currents in nitrogen. The shape of the ion currents (upper beams of oscillograms) shows clearly that nitrogen is a nonattaching gas (compare Figure 2.5.3).

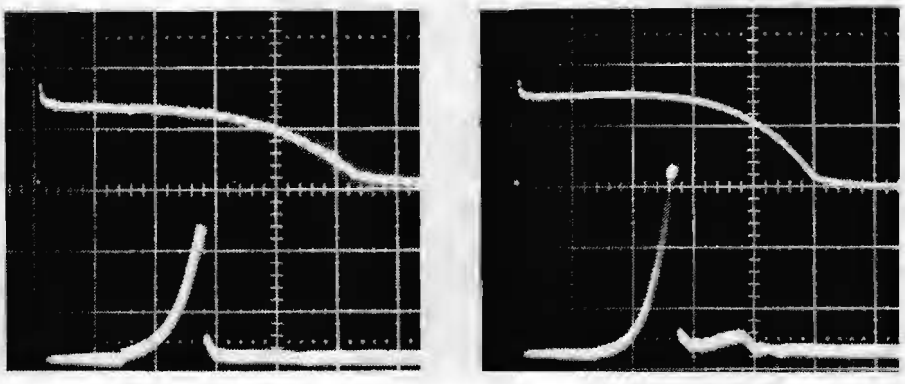

a b

Fig. 4.2.9 Avalanche currents in nitrogen; p = 760 Torr, d = 8 mm, (a) E = 28.76 kV/cm, lower beam : 0.6 mA/div, 50 ns/div, upper beam : 8.6 µA/div, 2 µs/div. (b) E = 30.31 kV/cm, lower beam : 1.2 mA/div, 50 ns/div, upper beam : 34.4 µA/div, 2 µs/div.

From pictures such as shown in this figure the transit time of the ions can be obtained and with the known gap spacing the drift velocity v_p can be determined. Figure 4.2.10 shows v_p as a function of E/p. In this figure also values measured by Frommhold [Fr 60] and Varney [Va 53] are given.

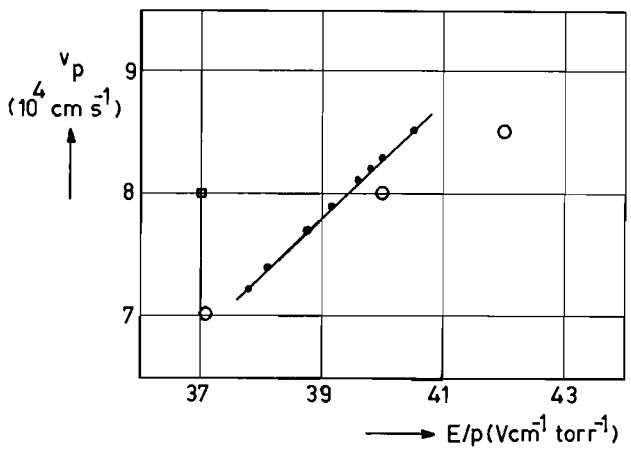

Fig. 4.2.10 Ion drift velocity v_p as a function of E/p in nitrogen at 760 Torr;
- ● *our measurements,*
- o *from Ref. [Fr 60],*
- □ *from Ref. [Va 53].*

If no secondary emission occurs the ratio of the electron current and the maximum of the ion current should almost be equal to the ratio of the transit times T_p/T_e (see section 2.5). The latter ratio can be taken to be approximately 160 in both cases. The current ratio however, equals 125 for Figure 4.2.9 a, and 72 for Figure 4.2.9 b, apparently because of secondary avalanches due to photoelectrons and the resulting increase in the amplitude of the ion current. The electron current of Figure 4.2.9 b shows the direct evidence of photo-emission quite clearly.

Since we use a subdivided cathode, not all of the secondary photo-electrons start from the measuring part of the cathode and also the current through the measuring resistor caused by secondary avalanches is deformed by the Ramo-Shockley effect (see section 3.3). Therefore the relations given in section 2.6 between γ_{photon} and the current

caused by the avalanche, cannot give accurate results. But since very little is known about γ_{photon} values for low E/p values, we give these γ_{photon} estimates anyhow.
For nitrogen Eq.(2.6.22) can be written as:

$$\gamma_{photon} = \frac{\alpha v_e \tau + 1}{\exp(\alpha d)} \frac{i_e(t_1)}{i_e(t_1 - T_e)} \tag{4.2.7}$$

and Eq.(2.6.28):

$$\gamma_{photon} = \frac{\alpha v_e \tau + 1}{\exp\{\alpha v_e (t_1 - T_e)\}} \frac{i_e(t_1)}{i_e(T_e)} \tag{4.2.8}$$

and Eq.(2.6.33):

$$\gamma_{photon} = \left\{ 1 - \frac{i_e(T_e)}{i_p(t_m)} \frac{T_e}{T_p} \right\} \frac{1}{\exp(\alpha d)} \tag{4.2.9}$$

From Figure 4.2.9 a we derive with Eq.(4.2.9), $\gamma = 4.5 \times 10^{-3}$ and from Figure 4.2.9 b with Eq.(4.2.7), $\gamma = 2.0 \times 10^{-3}$, with Eq.(4.2.8), $\gamma = 2.2 \times 10^{-3}$ and with Eq.(4.2.9), $\gamma = 3.3 \times 10^{-3}$. The value for τ was taken to be 2.5 ns which follows from measurements of Wagner [Wa 64].

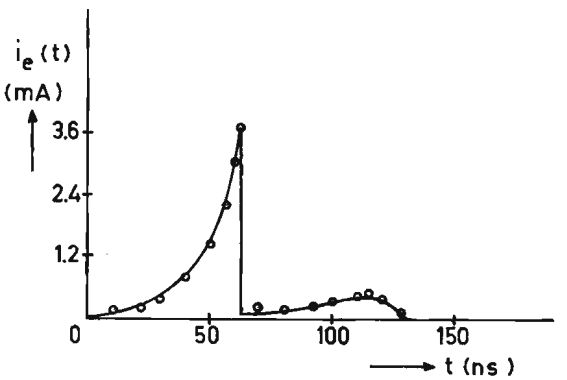

Fig. 4.2.11 Electron avalanche in nitrogen; $\alpha = 6.2\ cm^{-1}$, $\gamma = 2.0 \times 10^{-3}$, $d = 0.8\ cm$. The line represents the current waveform computed with the method given in section 2.7, the points represent measured values obtained from Figure 4.2.9 b .

Figure 4.2.11 shows an electron current waveform computed with the numerical method described in section 2.7. The parameter values were

chosen equal to the values obtained from the electron current shown in Figure 4.2.9 b. The points in Figure 4.2.11 are taken from Figure 4.2.9 b and it can be seen that these experimental values are in very good agreement with the computed values.

Figure 4.2.12 shows avalanches in nitrogen at atmospheric pressure, which lead to a complete breakdown of the 1 cm long gap although the applied voltage (30.50 kV) is only 91 % of the measured static breakdown voltage (33.50 kV). Apparently the breakdown is caused by field distortion effects due to space charges (see section 2.10).
From Figures 4.2.12 a and 4.2.12 b it can be seen that the current shape at $t = T_e$ is rounded off (compare Figure 4.2.6 d) which is probably caused by an increase of the thickness of the cloud of electrons by electrostatic repulsion.
The current waveforms given in Figures 4.2.12 c and 4.2.12 d show a deviation of the normal e-folding increase (compare Figure 4.2.6) before $t = T_e$. This is possibly caused by a lowering of the ionization efficiency since the E-field which is "seen" by the electrons situated between the formed positive ions and the anode, is lowered by the field of the positive ions.
Tholl [Th 63] observed a comparable phenomenon in his experiments and derived an "apparent" α value which decreases when more electrons are formed in the avalanche.
The positive ions also cause secondary avalanches which start from the cathode, to "see" a higher E-field which leads to a higher α value which in turn increases the number of positive ions even more. If a critical number is reached the condition for the streamer mechanism (see section 2.10) is met and the gap breaks down. This explanation implies that in our case the occurring streamer is of the cathode directed type. This is confirmed by the fact that the breakdown always occurs after one electron transit time, even in experiments where the applied voltage was only 0.1 percent below the static breakdown voltage.
It can be seen from the currents shown in Figure 4.2.12 that the time between the start of the avalanche and the breakdown of the gap (known as the formative time lag) decreases when the charge density in the primary electron cloud increases (more primary electrons and/or released from a smaller area).

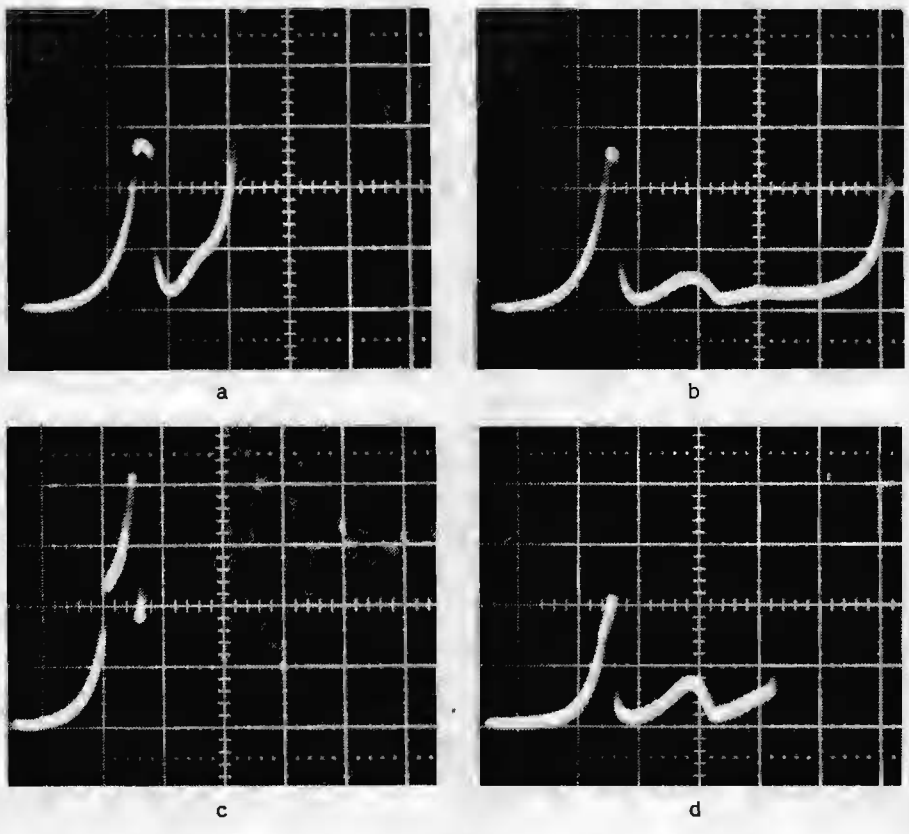

Fig. 4.2.12 Currents caused by avalanches in nitrogen at 770 Torr, which lead to a complete breakdown of the gap; E = 30.50 kV/cm, d = 1 cm, 8 mA/div, 50 ns/div.
(a) $n_o = 10^8$, (b) $n_o = 5 \times 10^7$, (c) $n_o = 10^8$, (d) $n_o = 2 \times 10^7$, (a) and (b) primary electrons released from an area of 1 cm^2, (c) and (d) primary electrons released from an area of 0.02 cm^2.

From measurements such as shown in Figure 4.2.12 we found that it was possible to initiate the breakdown with 10^8 primary electrons released from an area of 0.02 cm^2 at a minimum applied voltage of 28.50 kV (85% of the static breakdown voltage), in case the same number of electrons is released from an area of 1 cm^2 this voltage was 29.75 kV (89% of the static breakdown voltage).

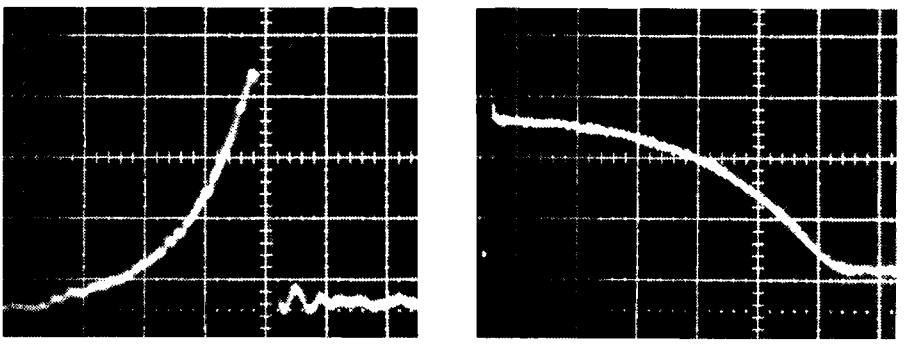

a b

Fig. 4.2.13 Currents caused by an avalanche in nitrogen at 769 Torr measured with the "differentiating method"; E = 29.37 kV/cm, d = 8 mm, (a) 1.0 mA/div, 20 ns/div, (b) 12.0 μA/div, 2 μs/div.

Figure 4.2.13 shows an example of a measurement of dV_h/dt (see section 3.2) in which the outer ring of the cathode was used as the differentiating capacitor. The input voltage of the oscilloscope was inverted to obtain a positive-going signal. From the pictures we can see that it is possible to measure the current caused by the avalanche in this manner (compare Figure 4.2.9). However, there are some differences with the signals obtained with the "normal" method: (a) the output voltage shown in Figure 4.2.13 b becomes negative after the ions have left the gap, which corresponds to the current coming from the power supply through the damping resistor to recharge the gap, (b) the oscillogram which represents the current caused by the electrons (see Figure 4.2.13 a) shows more noise and a much slower drop of the output voltage at $t = T_e$.

This differentiating method could be improved if a separate, differentiating capacitor, especially designed for this type of measurements were used.

4.3. Avalanches in carbon dioxide.

In this section measurements on avalanches in carbon dioxide are described.
The maximum content of impurities in the carbon dioxide gas were : 50 ppm oxygen, 200 ppm nitrogen and 3 ppm argon (values given by the manufacturer) whereas the partial pressure of water vapor was lower than 0.04 Torr (own measurement).

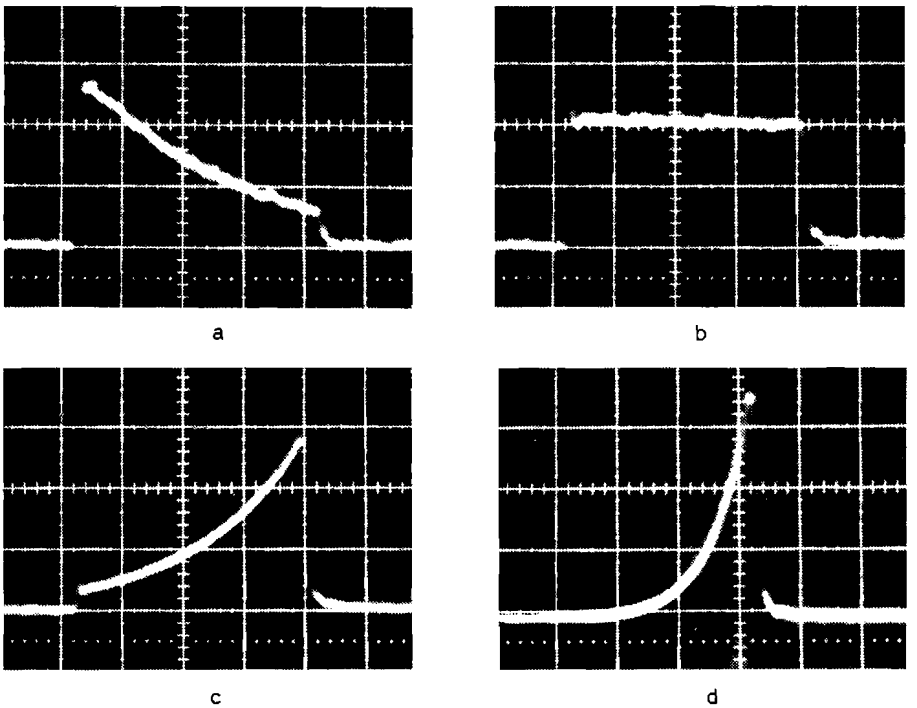

Fig. 4.3.1 Currents caused by electron avalanches in carbon dioxide; d = 1 cm, p = 750 Torr, 20 ns/div,
(a) 30 μA/div, E = 19.00 kV/cm,
(b) 30 μA/div, E = 20.80 kV/cm,
(c) 150 μA/div, E = 22.00 kV/cm,
(d) 4 mA/div, E = 24.00 kV/cm.

Figure 4.3.1 shows currents caused by electron avalanches in carbon dioxide at different voltages applied to the gap. From Figure 4.3.1 a

it is obvious that carbon dioxide is an attaching gas since the current decreases with time which means that $\eta > \alpha$ (see Figure 2.5.3 and Eq. (2.5.4)). Figure 4.3.1 b shows the current in case α just equals η while Figures 4.3.1 c and 4.3.1 d show currents for the case $\alpha > \eta$.

From oscillograms such as shown in Figure 4.3.1 the transit time of the electrons can be obtained and with the known gap spacing, the drift velocity can be determined. We have measured v_e for the range $4.0 \leq E/p \leq 34.0$ Vcm^{-1} Torr^{-1} at a constant carbon dioxide pressure of 750 Torr. Figure 4.3.2 shows v_e as a function of E/p.

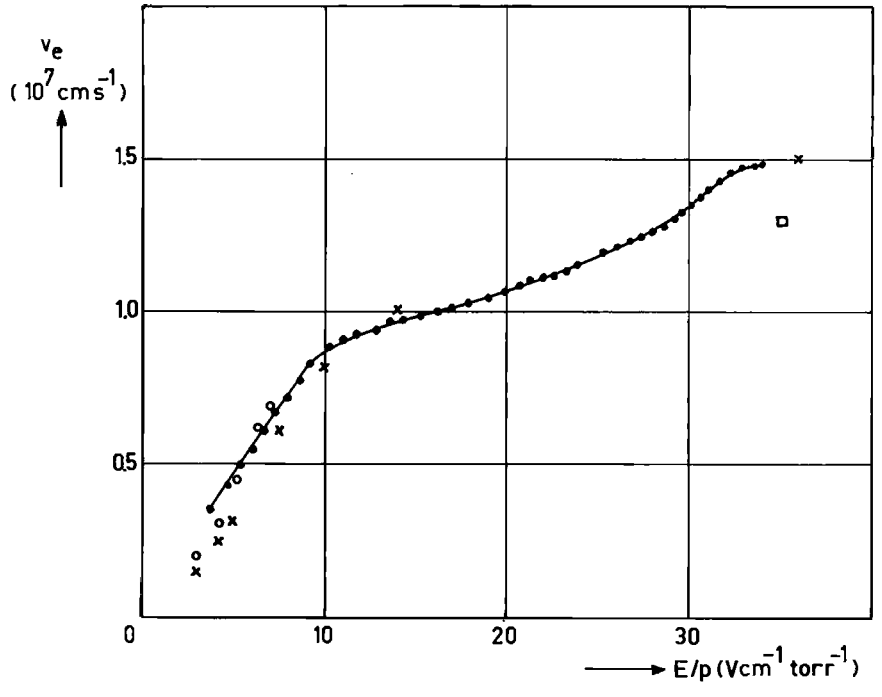

Fig. 4.3.2 Electron drift velocity v_e as a function of E/p in carbon dioxide at 750 Torr;
● *our measurements,* o *from Ref.* [*El 66*],
x *from Ref.* [*Sa 77*], □ *from Ref.* [*Fr 60*].

In this figure also values of v_e are given which have been measured by Saelee, Lucas and Limbeek [Sa 77], Elford [El 66] and Frommhold [Fr 60].

The accuracy of our measurements over the given E/p range is better than 3%.

From the measured currents we can derive the effective ionization coefficient, $\alpha-\eta$, as follows. The current caused by the moving electrons in case of an attaching gas is given by (see Eqs. (2.3.3) and (2.5.4)):

$$i_e(t) = \frac{n_o e}{T_e} \exp\{(\alpha-\eta)v_e t\} \quad \text{for} \quad 0 \leq t \leq T_e \qquad (4.3.1)$$

In the same way as described in the previous section for nitrogen we can derive $\alpha-\eta$ from the ratio of the current at $t = T_e$ and $t = 0$, and/or from graphs of $\ln i_e(t)$ vs t.

Figure 4.3.3 shows $(\alpha-\eta)/p$ in carbon dioxide as a function of E/p.

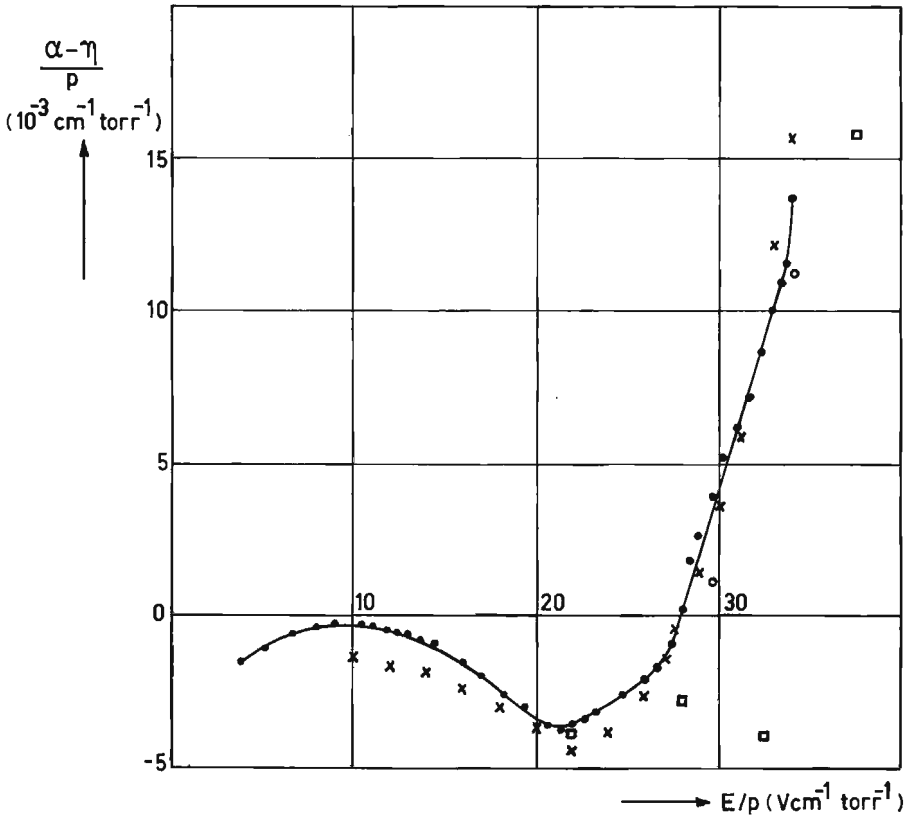

Fig. 4.3.3 Effective ionization coefficient as a function of E/p in carbon dioxide at 750 Torr.
● *our measurements,* × *from Ref.* [*Te 75*],
o *from Ref.* [*Co 75*], □ *from Ref.* [*Al 76*].

In this figure also values are given which have been measured by Teich, Jabbar and Branston [Te 75], Conti and Williams [Co 75] and Alger and

Rees [Al 76]. Our values are in reasonable agreement with the values given in Ref. [Te 75] and Ref. [Co 75] but show a significant difference with the values given in Ref. [Al 76]. The reason for this can be the fact that Alger and Rees did their experiments at pressures between 0.06 and 1.4 Torr while we have done our experiments at a pressure of 750 Torr.

In a test experiment we did at a pressure of 20 Torr we found α and η to be equal at $E/p = 35$ Vcm^{-1} Torr^{-1}, whereas at 750 Torr α and η are equal for $E/p = 27.8$ Vcm^{-1}. A rough interpolation of the values given in Ref. [Al 76] indicates that α and η should be equal for an E/p value of approximately 35 Vcm^{-1} Torr^{-1}, in good agreement with the value we found at 20 Torr.

A pressure dependence of the "critical" E/p-value where α and η are equal must be related to details of the collision processes involved. An increase of the critical E/p with pressure is for instance observed in hexafluoropropylene (C_3F_6) by Aschwanden and Biasiutti [As 81].

The accuracy in our measurements of $(\alpha-\eta)/p$ over the given E/p range is approximately 8% but not smaller than 10^{-4} cm^{-1} Torr^{-1}.

Figure 4.3.4 shows simultaneously measured electron and ion currents in carbon dioxide.
The shape of the ion currents (upper beams of oscillograms) clearly shows that carbon dioxide is an attaching gas (compare Figure 2.5.3).

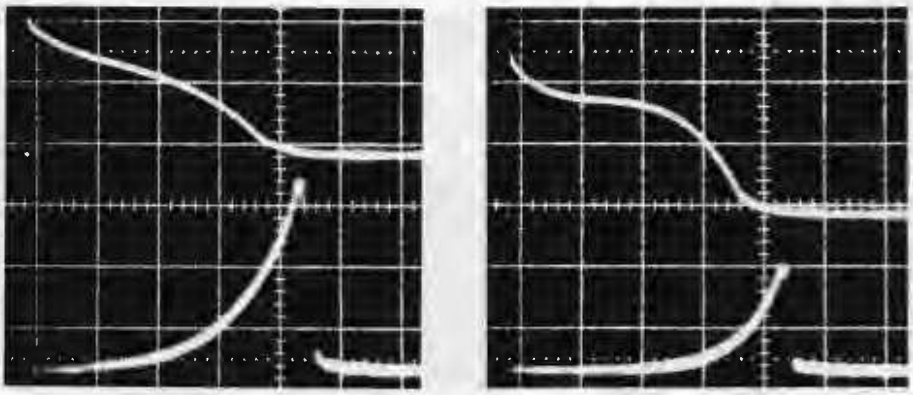

Fig. 4.3.4 Avalanche currents in carbon dioxide;
p = 750 Torr, d = 1 cm, upper beams 10 μs/div,
lower beams 20 ns/div.
(a) E = 23.20 kV/cm, upper beam 20 μA/div,
lower beam 0.6 mA/div,
(b) E = 24.00 kV/cm, upper beam 100 μA/div,
lower beam 1.2 mA/div.

We have not carried the analysis of the ion current further to obtain α and η values separately since for most practical applications the effective ionization coefficient $\alpha-\eta$ is more useful.

4.4. Avalanches in oxygen.

In this section measurements on avalanches in oxygen are described. Since pure oxygen shows a complicated behaviour and is of little interest for insulating purposes we restrict ourselves to some remarks on the shapes of the avalanche currents. In section 4.5 which deals with avalanches in air more attention is paid to processes in which oxygen is involved.

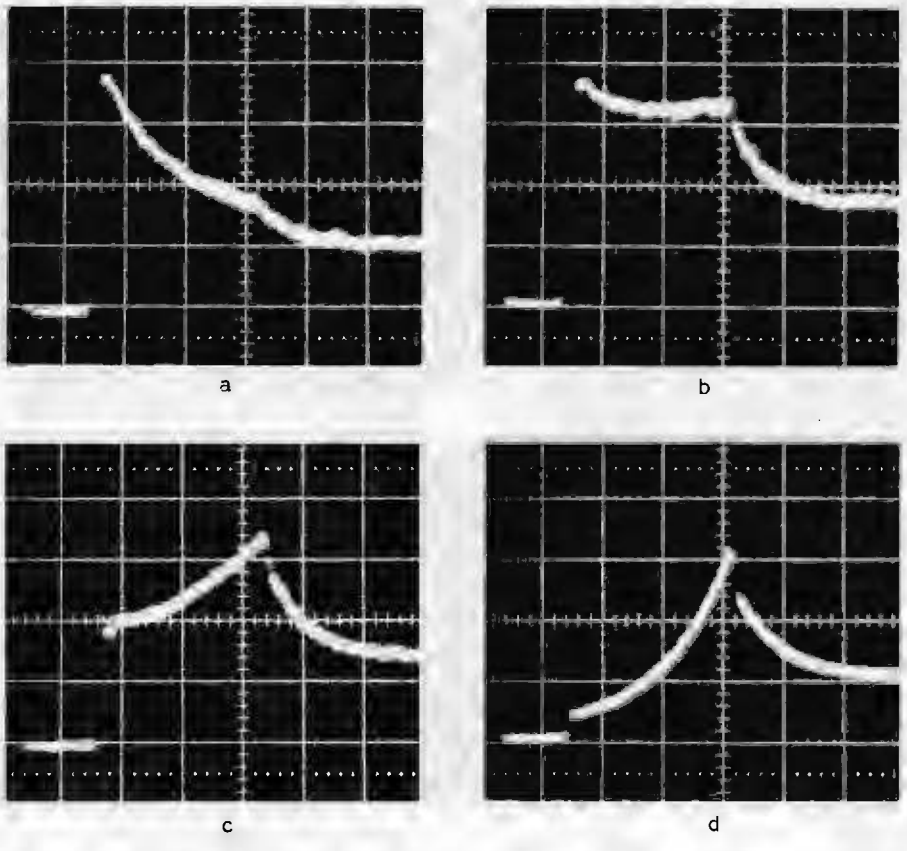

Fig. 4.4.1 Currents caused by avalanches in oxygen,
d = 1 cm, p = 765 Torr, 20 ns/div,
(a) 15 μA/div, E = 27.53 kV/cm.
(b) 15 μA/div, E = 27.72 kV/cm.
(c) 15 μA/div, E = 27.86 kV/cm.
(d) 75 μA/div, E = 28.14 kV/cm.

Figures 4.4.1 and 4.4.2 show currents caused by avalanches in oxygen. From Figure 4.4.1 a it can be seen that oxygen is an attaching gas since the current decreases with time which means that $\eta > \alpha$ (compare Figure 2.5.3). In comparison with Figure 4.3.1, which shows avalanches in carbon dioxide, Figure 4.4.1 shows a remarkable difference. While in carbon-dioxide the current drops to nearly zero after one electron transit time, in oxygen there remains a current which decreases over approximately 40 ns after T_e to reach an almost constant level. The decreasing current is caused by electrons which are detached from unstable negative ions (see sections 2.8 and 2.9). The constant level is caused by ions which can be concluded from Figure 4.4.2. For example, the constant level shown in the lower beam of Figure 4.4.2 a is 22.5 µA which is equal to the current height at the beginning of the upper beam.

From the upper beams of Figure 4.2.2 it can also be seen that there is detachment in oxygen since the ion current increases after T_e which means that there are still electrons present in the gap which

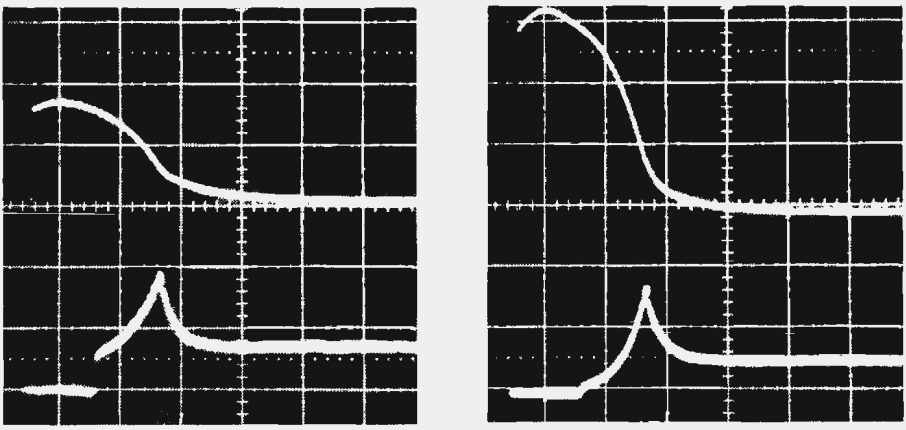

Fig. 4.4.2 Avalanche currents in oxygen,
d = 1 cm, p = 765 Torr, upper beams 5 µs/div,
lower beams 50 ns/div.
(a) E = 28.02 kV/cm, upper beam 15 µA/div,
lower beam 30 µA/div.
(b) E = 28.25 kV/cm, upper beam 30 µA/div,
lower beam 150 µA/div.

ionize. Whether also conversion takes place in oxygen cannot be immediately concluded from the pictures.

4.5 Avalanches in air.

In this section measurements on avalanches in air are described. In the literature much attention is given to the breakdown characteristics of air because of the importance of air for high-voltage engineering (see for example [Me 78]). One of the interesting features of the breakdown process in air is that the humidity content of air influences the breakdown voltage; in general the breakdown voltage increases with the water vapor content. To explain this phenomenon is not easy, because of the many possible processes in air, where many interactions between electrons, ions and molecules may take place (see list in [Ba 75]). We now describe measurements on the influence of humidity on avalanche growth and explain this influence with the theory given in the sections 2.8 and 2.9.

Figure 4.5.1 shows currents caused by avalanches in air at different water vapor pressures, p_{H_2O}, with the same voltage applied to the gap. From the pictures we can see that there is an aftercurrent after $t = T_e$ which means that detachment takes place (see section 2.8 and 2.9 and compare with the avalanches in oxygen, section 4.4). The current drop at $t = T_e$, $i_e(T_e) - i_e(T_e+dt)$, is in all cases approximately equal to $i_e(0)$ which means that $\alpha = \eta$ (see Eq. (2.8.12)). That the currents increase with time, even though α equals η, can be attributed to ionization by electrons which detach from unstable negative oxygen ions. Figure 4.5.1 also shows that $i_e(T_e)/i_e(0)$ decreases with increasing humidity. In this section we will explain that this is caused by the formation of stable negative ions upon collisions between unstable negative ions and water molecules (conversion, see sections 2.8 and 2.9).
Figure 4.5.2 shows currents caused by avalanches at different water vapor pressures with 28.00 kV applied to the 1 cm long gap. Although the current waveforms show differences (especially the aftercurrents) in all cases the current drop at $t = T_e$ equals approximately 4 $i_e(0)$, which means that $\alpha - \eta = 1.4\ cm^{-1}$ (see Eq. (2.8.12)). From oscillograms

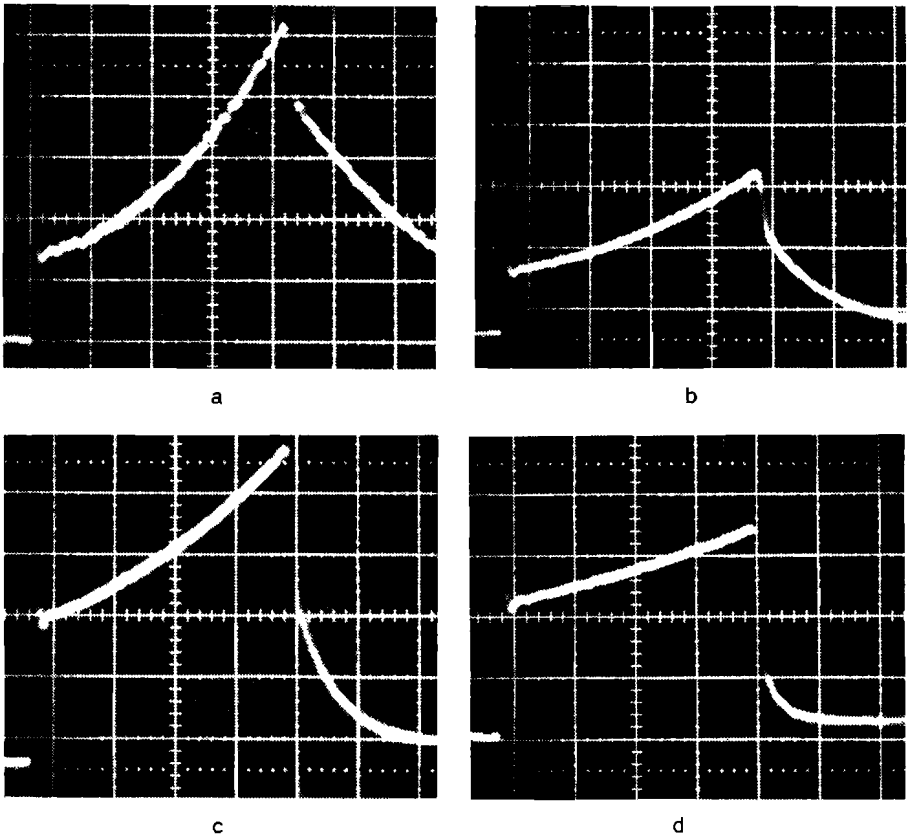

Fig. 4.5.1 Avalanches in air at different humidities;
d = 1 cm, E = 27.00 kV/cm.
p = 778 Torr, 20 ns/div.
(a) pH_2O = 0.05 Torr, 30 μA/div,
(b) pH_2O = 0.85 Torr, 75 μA/div,
(c) pH_2O = 1.79 Torr, 75 μA/div,
(d) pH_2O = 7.50 Torr, 75 μA/div.

such as shown in Figures 4.5.1 and 4.5.2 recorded at different applied voltages it is found that $\alpha-\eta$ is independent of the amount of water vapor in air. Figure 4.5.3 shows $(\alpha-\eta)/p$ as a function of E/p. Note that the thus measured $\alpha-\eta$ values differ from those quoted in the literature, because all methods used thus far had a slower frequency response and therefore tend to measure the combined electron production by ionization and detachment, rather than the real $\alpha-\eta$

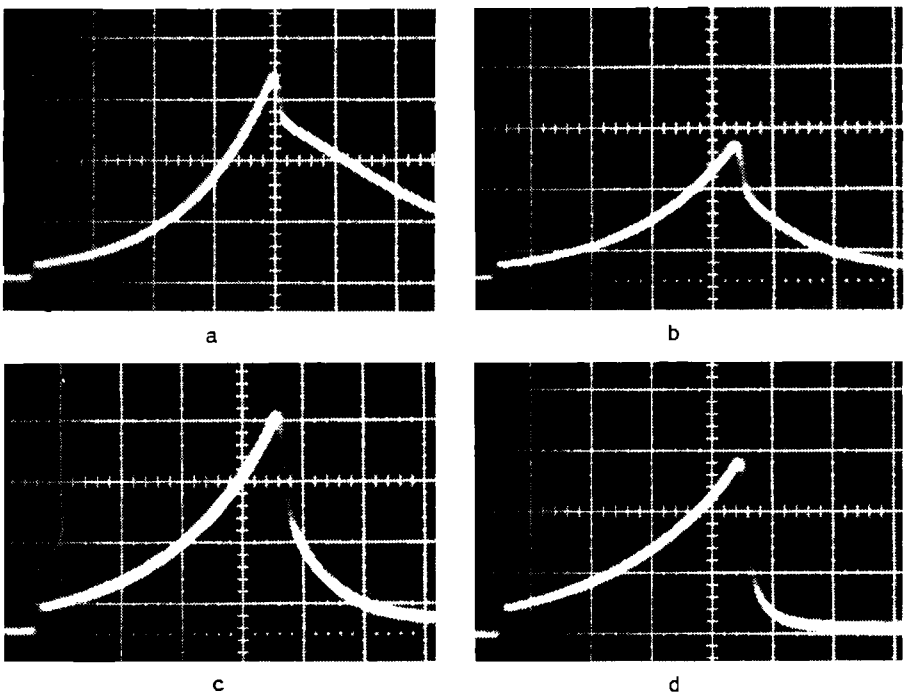

Fig. 4.5.2 Avalanche currents in air at different water vapor pressures; d = 1 cm, E = 28.00 kV/cm, p = 778 Torr, 20 ns/div, 400 µA/div, (a) pH_2O = 0.05 Torr, (b) pH_2O = 0.85 Torr, (c) pH_2O = 1.79 Torr, (d) pH_2O = 7.5 Torr.

value. Only Frommhold [Fr 64] treats detachment separately and arrives at real α-η values for dry air at high E/p.
Also from oscillograms such as shown in Figures 4.5.1 and 4.5.2 the transit time of the electrons can be taken and with the known electrode distance the drift velocity can be derived. The drift velocity is independent of the water vapor content. Figure 4.5.4 shows v_e as a function of E/p. In this figure also values of v_e are given which have been measured by Frommhold [Fr 64] in dry air.

Figure 4.5.5 shows simultaneously measured electron and ion currents in air with a water vapor pressure of 11.25 Torr. From the electron component it can be seen that the aftercurrent is very small which means that most of the formed unstable negative ions are stabilized

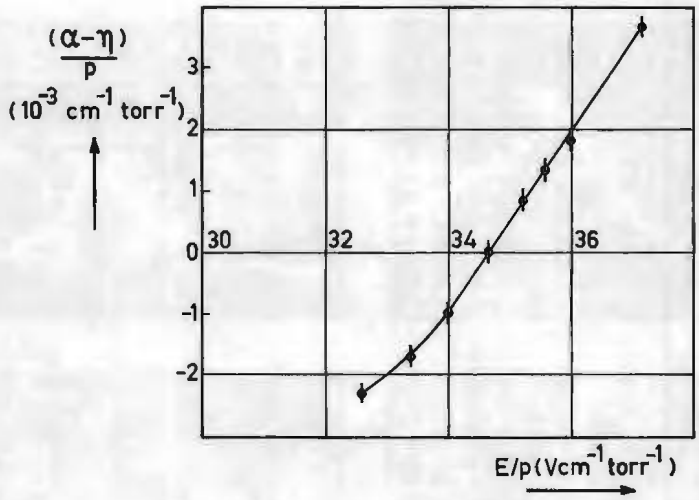

Fig. 4.5.3 Values of (α-η)/p as a function of E/p in air at 778 Torr, 0.05 < p H_2O < 11.25 Torr.

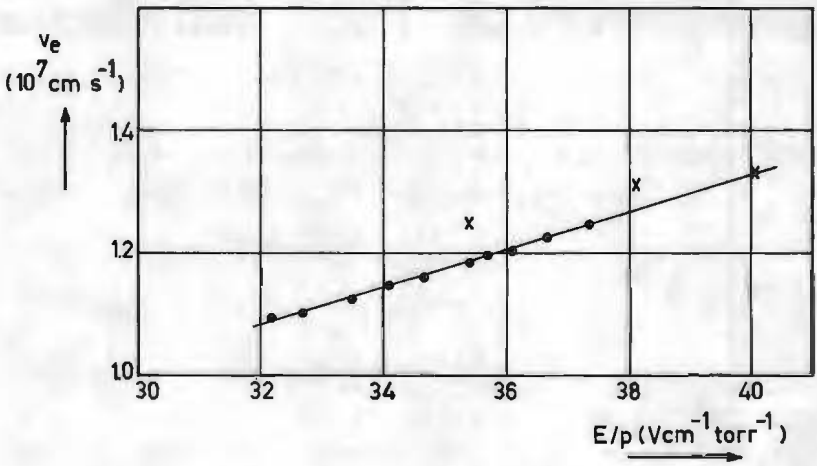

Fig. 4.5.4 Electron drift velocity as a function of E/p in air at 778 Torr;
o our measurements, 0.05 < p H_2O < 11.25 Torr.
x from Ref. [Fr 60], dry air.

by conversion so that only few electrons are produced by detachment. The humid air behaves in this case almost as a "normal" attaching gas under the condition $\alpha = \eta$ (compare Figures 2.5.3 and 4.3.1b). This can also be concluded from the ion current shape since the current

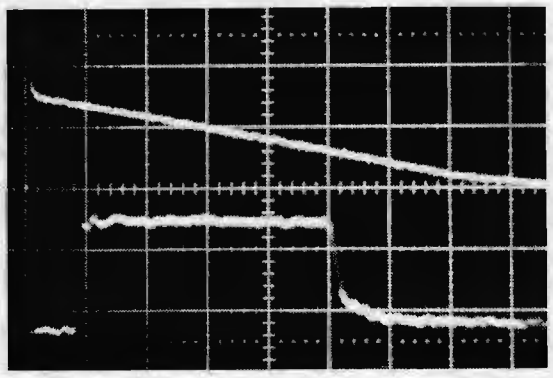

Fig. 4.5.5 Avalanche current in humid air;
d = 1 cm, p = 778 Torr, pH_2O = 11.25 Torr,
E = 27 kV/cm, upper beam
7.5 μA/div, 2 μs/div, lower beam
75 μA/div, 20 ns/div.

decreases linearly with time (see Eqs. (2.5.13) and (2.5.14) and compare Figure 2.5.3).

From Eqs. (2.5.4), (2.5.9), (2.5.10), (2.5.15), (2.5.16) and (2.5.17) follows in case $\alpha=\eta$ and $T_p=T_n$:

$$\frac{i_e(T_e)}{i_p(T_e)+i_n(T_e)} = \frac{1}{\alpha+\eta}\frac{T_p}{T_e} \qquad (4.5.1)$$

From Figure 4.5.5 the values of the currents and transit times can be taken and inserted in Eq. (4.5.1) from which follows $\alpha+\eta = 15.4\ cm^{-1}$. Since α is almost equal to η we now conclude that $\alpha = \eta = 7.7\ cm^{-1}$. Frommhold [Fr 64] found for dry air $\eta/p = 0.01\ cm^{-1}Torr^{-1}$ for the range $35 < E/p < 50\ Vcm^{-1}Torr^{-1}$ from which follows $\eta = 7.78\ cm^{-1}$ at p = 778 Torr. By extrapolating his data for α/p to $E/p = 34.7\ Vcm^{-1}Torr^{-1}$ (he gives only α/p values for $E/p > 40\ Vcm^{-1}Torr^{-1}$) we obtain $\alpha/p = 0.01\ cm^{-1}Torr^{-1}$ which results in $\alpha = 7.78\ cm^{-1}$ at p = 778 Torr in good agreement with the value we found.

The increase of the breakdown voltage of air with humidity is attributed by many authors to the attaching nature of water vapor (see [Me 78]). We found however, that attachment in pure water vapor is

negligible, in contrast to the results of [Pr 60] and [Pa 72]. Figure

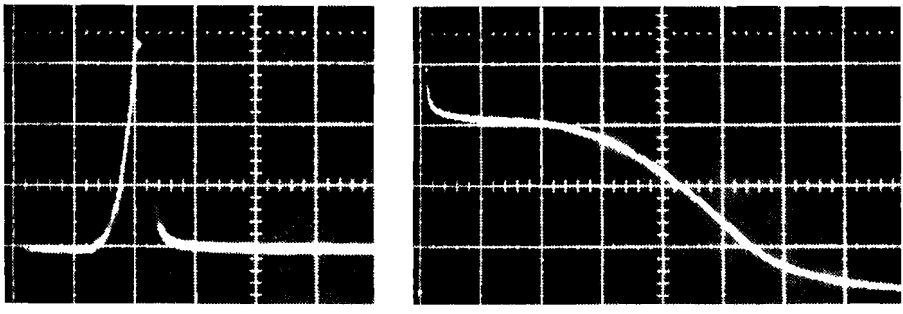

a b

Fig. 4.5.6 Avalanche currents in water vapor;
d = 5 mm, p = 14.0 Torr, E = 620 Vcm^{-1},
(a) 4 mA/div, 20 ns/div.
(b) 15 µA/div, 2 µs/div.

4.5.6 shows avalanche currents in water vapor. From the electron component (Figure 4.5.6 a) we can see that ionization takes place and from the ion component (Figure 4.5.6 b) we can see that there are no negative ions ($\eta = 0$, compare avalanches in nitrogen, Figure 4.2.9). From the combination of the results of Frommhold and our own measurements we now conclude that the attachment coefficient η of air is independent of both the applied E-field (for $32.5 < E/p < 37.5$ Vcm^{-1} Torr^{-1}) and the water vapor content ($p H_2O < 11.25$ Torr).
From oscillograms such as shown in Figures 4.5.1 and 4.5.2 obtained at different humidities and with different voltages applied to the gap the following quantity can be derived:

$$C = \frac{1}{d} \ln \{i_e(T_e)/i_e(0)\} - (\alpha-\eta) \qquad (4.5.2)$$

where now, not just the drop, but the full value of $i_e(T_e)$ is considered. We found that the value of C is only a function of the water vapor content. Figure 4.5.7 shows 1/C as a function of $p H_2O$. From this figure we conclude that for $p H_2O > 1$ Torr:

$$C = 1 / (0.75 + 0.29\ p H_2O) \qquad (4.5.3)$$

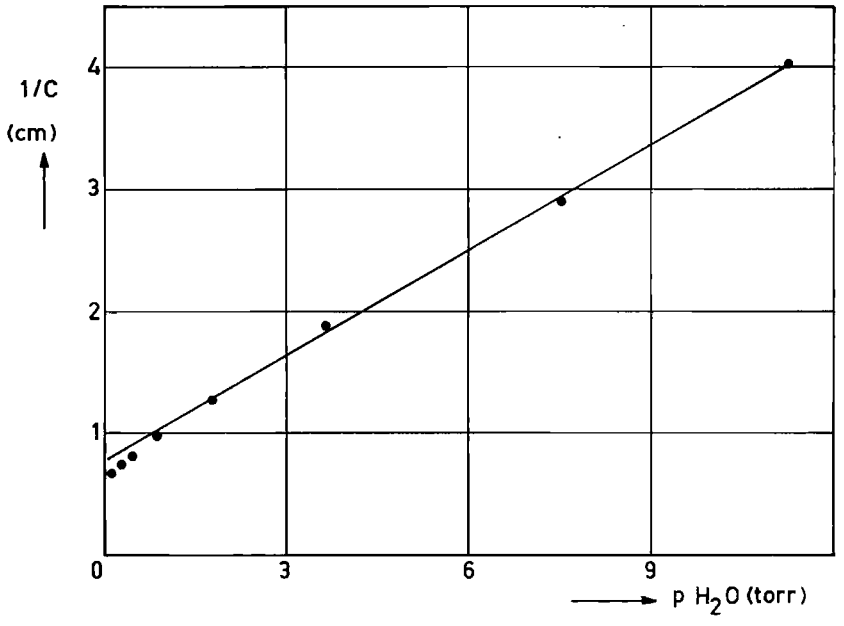

Fig. 4.5.7 The value of 1/C (C given by Eq. 4.5.2) as a function of the partial water vapor pressure in air.

in which pH_2O has to be inserted in Torr and the dimension of C is cm^{-1}.

The electron current in case of a gas in which ionization, attachment, detachment and conversion take place is given by (see Eqs. (2.8.5), (2.8.10) and (2.8.11)):

$$i_e(t) = \frac{i_o}{A_1-A_2}\{(A_1+\delta+\beta)\exp(A_1 v_e t)-(A_2+\delta+\beta)\exp(A_2 v_e t)\} \qquad (4.5.4)$$

for $0 < t < T_e$,

in which A_1 and A_2 are given by Eqs. (2.8.6) and (2.8.7).

Figure 4.5.8 shows a plot of $i_e(t)$ vs t in case $\alpha = \eta$ and $pH_2O = 0.05$ Torr (points obtained from Figure 4.5.1 a) in which the vertical axis has a logarithmic scale. From this figure and the known value of v_e we conclude that for $t \geq 20$ ns.

$$i_e(t) = 0.9\, i_o \exp(1.5\, v_e t) \qquad (4.5.5)$$

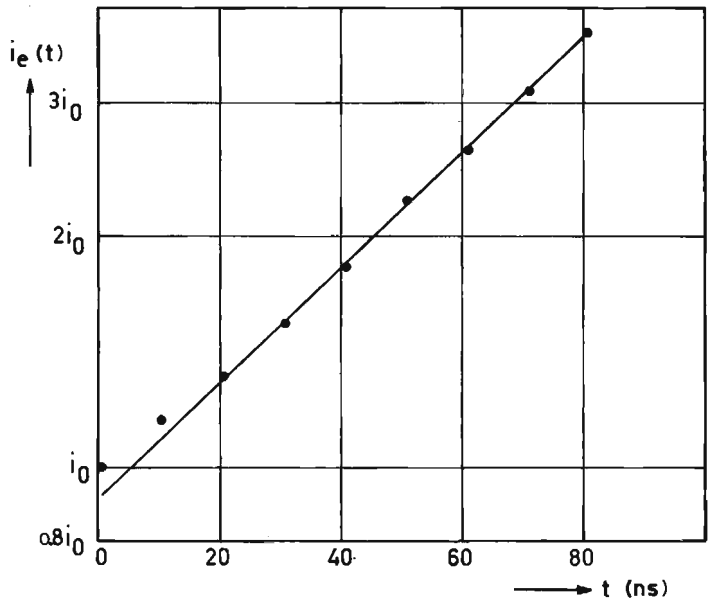

Fig. 4.5.8 The current $i_e(t)$ as a function of time for $0 < t < T_e$. The points are taken from Figure 4.5.1a.

Apparently in this case only one e-folding time is important. Later on in this section it is shown that the term in Eq. (4.5.4) with $\exp(A_1 v_e t)$, in case $\alpha = \eta$ and $pH_2O = 0.05$ Torr, is much larger than the term with $\exp(A_2 v_e t)$. Also it will turn out that $(A_1+\delta+\beta)/(A_1-A_2)$ almost equals unity. Equation (4.5.4) then simplifies to:

$$i_e(t) = i_o \exp(A_1 v_e t) \tag{4.5.6}$$

In case $\alpha = \eta$ A_1 is given by (see Eq. (2.8.6)):

$$A_1 = \frac{1}{2}\{-\delta-\beta+\sqrt{(\delta+\beta)^2+4\eta\delta}\} \tag{4.5.7}$$

From Eq. (4.5.2) follows for $\alpha = \eta$:

$$i_e(T_e) = i_o \exp(Cd) = i_o \exp(Cv_e T_e) \tag{4.5.8}$$

From the combination of Eqs. (4.5.5), (4.5.6) and (4.5.8) and by

neglecting the factor 0.9 in Eq. (4.5.5) we conclude that in this case ($\alpha = \eta$, $p H_2O$ = 0.05 Torr):

$$A_1 = C = 1.5 \text{ cm}^{-1}$$

With the known value of η we derive from Eq. (4.5.7):

$$\delta = 0.36 + 0.24\ \beta \qquad (4.5.9)$$

The next step now is to find δ and β separately in this case where $\alpha = \eta$. For this purpose current waveforms were computed with the numerical method described in section 2.9. With a trial and error procedure it was found that the computed waveform was in good agreement with the measured one if δ was chosen to be 1.03 cm^{-1} and β, 2.8 cm^{-1} (see Figure 4.5.9).

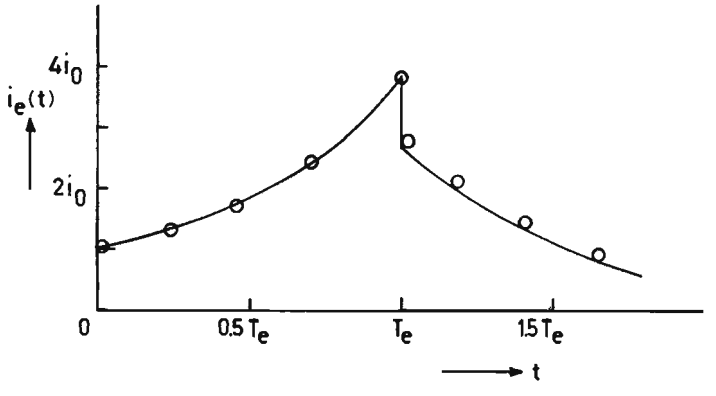

Fig. 4.5.9 The current $i_e(t)$ as a function of time. Line computed with the method described in section 2.9 with $\alpha=\eta$ = 7.7 cm^{-1}, δ = 1.03 cm^{-1}, β = 2.8 cm^{-1} and d = 1 cm. The points are taken from the measurement of Figure 4.5.1a.

With these values of δ and β we can check whether the simplification of Eq. (4.5.4) to Eq. (4.5.6) was correct. A_1 equals in this case 1.5 cm^{-1} (see Eq. (2.8.6)) and A_2 equals -5.3 cm^{-1} (see Eq. (2.8.7)). With these values Eq. (4.5.4) can be written as:

$$i_e(t) = i_o\{0.8 \exp(1.5\ v_e t) + 0.2 \exp(-5.3\ v_e t)\} \qquad (4.5.10)$$

From this equation it can be seen that for $v_e t$ not too small (say $v_e t > 0.2$ cm) the second term can be neglected and Eq. (4.5.10) simplifies to:

$$i_e(t) = 0.8\, i_o \exp(1.5\, v_e t) = 0.8\, i_o \exp(A_1 v_e t) \qquad (4.5.11)$$

which is indeed almost identical to Eq. (4.5.6).
The values of δ and β found for $p H_2O = 0.05$ Torr can lead to more general parameters if we make the plausible assumptions that δ is independent of both the applied E-field and the water vapor content, and that β is a function of $p H_2O$ only. Let us for instance write β as:

$$\beta = A + B\, p H_2O \qquad (4.5.12)$$

For $(\delta+\beta)^2 > 4\,\eta\delta$, Eq. (4.5.7) simplifies to:

$$A_1 = C = \frac{\eta\delta}{\beta+\delta} \qquad (4.5.13)$$

with Eqs. (4.5.3) and (4.5.12) follows from Eq. (4.5.13):

$$\frac{1}{C} = \frac{A}{\eta\delta} + \frac{B}{\eta\delta}\, p H_2O + \frac{1}{\eta} = 0.75 + 0.29\, p H_2O \qquad (4.5.14)$$

and from this:

$$B = 0.29\, \eta\delta = 2.30 \qquad (4.5.15)$$

Since the straight line approximation of Figure 4.5.7 is not accurate at low $p H_2O$ values we use the data for $p H_2O = 0.05$ Torr to find A. With $\beta = 2.8$ cm^{-1} for $p H_2O = 0.05$ Torr, β as a function of $p H_2O$ is given by:

$$\beta = (2.7 + 2.30\, p H_2O)\ \text{cm}^{-1} \qquad (4.5.16)$$

in which $p H_2O$ has to be inserted in Torr.
Summarizing we can say that for the conditions of our experiments, $\eta = 7.7$ cm^{-1}, $\delta = 1.03$ cm^{-1} and $\beta = (2.7 + 2.30\, p H_2O)$ cm^{-1} while α can be derived from the $(\alpha-\eta)/p$ values given in Figure 4.5.3.

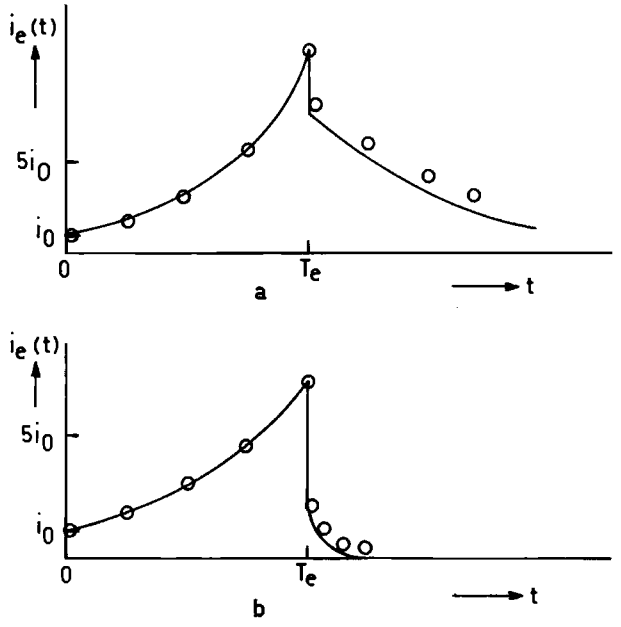

Fig. 4.5.10 Electron avalanches in air; d = 1 cm, E = 28 kV/cm, p = 778 Torr, $\alpha = 9.2\ cm^{-1}$, $\eta = 7.7\ cm^{-1}$, $\delta = 1.03\ cm^{-1}$, the lines represent the current waveforms computed with the method described in section 2.9, the points are taken from (a) Figure 4.5.2 a and (b) Figure 4.5.2 d, (a) $p H_2O = 0.05$ Torr, $\beta = 2.8\ cm^{-1}$, (b) $p H_2O = 7.5$ Torr, $\beta = 20.0\ cm^{-1}$.

Figure 4.5.10 shows current waveforms computed with the numerical method described in section 2.9 for $\alpha > \eta$. In this figure also values are given which are obtained from oscillograms shown in Figure 4.5.2. It can be seen that the computed values are in good agreement with the measured values. That, especially at late times the measured values are somewhat larger than the computed values, is caused by the ion contribution to the current (compare avalanches in oxygen, section 4.4). Also in cases $\alpha < \eta$ computed electron currents are in good agreement with measured currents.

Figure 4.5.11 shows currents caused by ions in air at different humidities and with the same voltage applied to the gap, while Figure 4.5.12 shows ion currents for the same parameters computed with the numerical method. The transit times of the three ion species are all chosen equal to T_i. In Figure 4.5.12 also points are shown

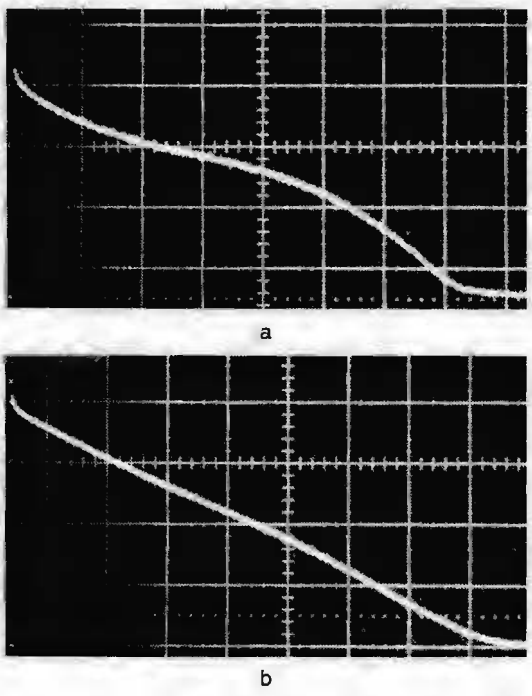

Fig. 4.5.11 Ion current in air; d = 1 cm, E = 28 kV/cm, p = 778 Torr, 15 μA/div, 2 μs/div, (a) $p H_2O$ = 0.05 Torr, (b) $p H_2O$ = 7.5 Torr.

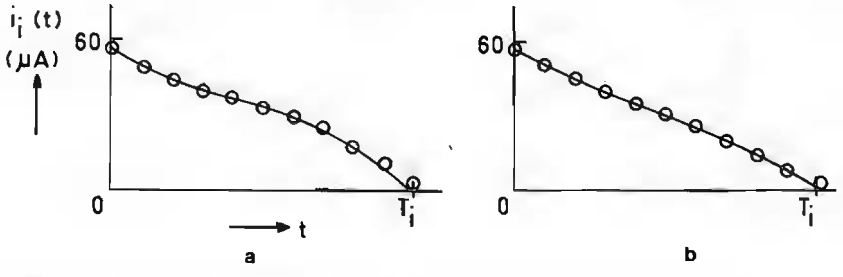

Fig. 4.5.12 Ion current in air; d = 1 cm, E = 28.00 kV/cm, p = 778 Torr, α = 9.2 cm^{-1}, η = 7.7 cm^{-1}, δ = 1.03 cm^{-1}, the lines represent the current waveforms computed with the method described in section 2.9, the points are taken from (a) Figure 4.5.11 a and (b) Figure 4.5.11 b ; (a) $p H_2O$ = 0.05 Torr, β = 2.8 cm^{-1} (b) $p H_2O$ = 7.5 Torr, β = 20.0 cm^{-1}..

which are obtained from oscillograms shown in Figure 4.5.11. The computed values are in very good agreement with the measured values.

With the numerical method it is possible to keep track of the numbers of electrons (n_e), positive ions (n_p) and negative ions (n_n) which leave the gap per electron which initially starts from the cathode. In Table 4.5.1 these numbers are given for dry air, humid air and a "normal" attaching gas in which no detachment takes place, in case $\alpha = \eta = 7.7\ cm^{-1}$ and $d = 1$ cm.

	n_e	n_p	n_n
Air, $pH_2O = 0.05$ Torr	7.45	23.50	17.05
Air, $pH_2O = 11.25$ Torr	1.30	8.74	8.44
"Normal" gas	1.0	7.7	7.7

Table 4.5.1 Numbers of electrons, positive ions and negative ions which leave the gap per electron which starts from the cathode in dry air, humid air and a "normal" attaching gas.

Since "counting" charge carriers is just what is done with Townsend's method (see section 4.1) we may derive from the numbers given in Table 4.5.1 values of α and η, α_T and η_T, which would be obtained if Townsend's method were applied without any knowledge of detachment and conversion.
The numbers of the various charge carriers which leave the gap per electron which starts from the cathode is in a case without detachment and for $\alpha \neq \eta$ given by (see section 2.5):

$$n_e = \exp\{(\alpha - \eta)\, d\} \tag{4.5.17}$$

$$n_p = \frac{\alpha}{\alpha - \eta} \left[\exp\{(\alpha - \eta)\, d\} - 1\right] \tag{4.5.18}$$

$$n_n = \frac{\eta}{\alpha - \eta} \left[\exp\{(\alpha - \eta)\, d\} - 1\right] \tag{4.5.19}$$

With the numbers given in the table it follows from these equations that for dry air $\alpha_T = 7.3\ cm^{-1}$ and $\eta_T = 5.3\ cm^{-1}$. From measurements with Townsend's method Prasad [Pr 59] obtained for dry air $\alpha_T = 7.0\ cm^{-1}$ and $\eta_T = 4.8\ cm^{-1}$, which differ not much from the above-mentioned values. For humid air follows $\alpha_T = 7.6\ cm^{-1}$ and $\eta_T = 7.4\ cm^{-1}$. For dry air the value of the attachment coefficient is clearly significantly smaller than the value for humid air, and the incorrect conclusion has therefore been drawn that adding water vapor to air increases η.

In this section as well as in sections 2.8 and 2.9 we have assumed that all negative ions formed by the attachment process are unstable. However, it may also be possible that two types of negative ions, one stable and one unstable, are formed by the attachment process. In that case two attachment coefficients have to be defined: η_1 as the mean number of unstable negative ions produced by a single electron travelling 1 cm in the direction of the E-field and likewise η_2 for stable negative ions.
The Eqs. (2.8.1) through (2.8.4) then change into:

$$dn_e(t) = (\alpha - \eta_1 - \eta_2)\, n_e(t)\, v_e dt + \delta n_{nu}(t)\, v_e dt \qquad (4.5.20)$$

$$dn_p(t) = \alpha n_e(t)\, v_e dt \qquad (4.5.21)$$

$$dn_{nu}(t) = \eta_1 n_e(t)\, v_e dt - \delta n_{nu}(t)\, v_e dt - \beta n_{nu}(t)\, v_e dt \qquad (4.5.22)$$

$$dn_{ns}(t) = \eta_2 n_e(t)\, v_e dt + \beta n_{nu}(t)\, v_e dt \qquad (4.5.23)$$

With the solution for the total number of electrons:

$$n_e(t) = \frac{n_o}{B_1 - B_2} \{ (B_1 + \delta + \beta) \exp(B_1 v_e t) - (B_2 + \delta + \beta) \exp(B_2 v_e t) \} \qquad (4.5.24)$$

for $0 \leqslant t \leqslant T_e$

in which:

$$B_1 = \frac{1}{2}\{\alpha-\eta_1-\eta_2-\delta-\beta + \sqrt{(\alpha-\eta_1-\eta_2-\beta-\delta)^2 - 4(-\alpha\delta-\alpha\beta-\beta\eta_1+\beta\eta_2+\eta_2\delta)}\} \quad (4.5.25)$$

$$B_2 = \frac{1}{2}\{\alpha-\eta_1-\eta_2-\delta-\beta - \sqrt{(\alpha-\eta_1-\eta_2-\beta-\delta)^2 - 4(-\alpha\delta-\alpha\beta-\beta\eta_1+\beta\eta_2+\eta_2\delta)}\} \quad (4.5.26)$$

Equation (2.8.12) changes into:

$$i_e(T_e)-i_e(T_e+dt)=i_o\exp\{(\alpha-\eta_1-\eta_2)\,d\} \quad (4.5.27)$$

In section 2.9 the changes in the equations are: η has to be replaced by $\eta_1+\eta_2$ in Eq. (2.9.7), by η_1 in Eq. (2.9.11) and the term $\eta_2\Delta x n_e$ $(p\Delta x, q\Delta t)$ has to be added at the right hand side of Eq. (2.9.13).

With a procedure comparable to the one described in this section it appeared to be also possible to obtain a good agreement between the computed currents and the measured currents for an appropriate set of coefficients. The value of α is unchanged, the η-value is now split up into $\eta_1 = 1.9\ cm^{-1}$ and $\eta_2 = 5.8\ cm^{-1}$ (note that $\eta = \eta_1 + \eta_2 = 7.7\ cm^{-1}$) the value of δ is changed into $5.6\ cm^{-1}$ and β is now given by:

$$\beta = 3.0\,p\,H_2O \quad (4.5.28)$$

To decide which model is the correct one is not possible with the available experimental results. Further experimental studies could include larger electrode spacings, changes in the gas composition or analysis of the various ion species.
However, both models show that the influence of water vapor on the avalanche growth in air is caused by conversion. It is therefore important to take conversion into account when an explanation is sought for the influence of water vapor on the breakdown characteristics in air. Also both models lead to the same "real" effective ionization coefficient $\alpha-\eta$ or $\alpha-\eta_1-\eta_2$.
Further analysis is needed to see how the breakdown criteria of air are influenced by the choise of parameters: the classical ones α_T and

η_T or the parameters α, η, δ and β derived in this section. Since eventually the same number of charge carriers is produced no change in Townsend's criterion is expected. In the streamer criterion changes will occur since the charge carrier distribution in space will be different for the two cases.

4.6 Avalanches in sulphur hexafluoride.

In this section avalanches in sulphur hexafluoride (SF_6) are described.

Sulphur hexafluoride is often used as an insulating gas in high-voltage equipment because of its high breakdown strength. In homogeneous E-fields the breakdown voltage of SF_6 is about three times higher than the breakdown voltage of air.

The maximum contents of the impurities in the SF_6 gas, we used, were: 900 ppm O_2, 330 ppm CF_4 and 2.2 ppm HF (values given by the manufacturer) whereas the partial pressure of water vapor was lower than 0.04 Torr (own measurement).

Figure 4.6.1 shows currents caused by avalanches in SF_6 at a pressure of 52.9 Torr with different voltages applied to the gap. From Figures 4.6.1 a and 4.6.1 b it is obvious that SF_6 is an attaching gas since the current decreases with time, which means that $\eta > \alpha$ (see Figure 2.5.3 and Eq. (2.5.4)). The drop of the current shown in Figure 4.6.1 c at $t = T_e$ just equals i_o which means that in this case $\alpha = \eta$ while Figure 4.6.1 d shows a current for the case $\alpha > \eta$. That the currents after $t = T_e$ do not drop to zero is caused by the ion contribution to the current. This can be concluded from Figure 4.6.2 which shows simultaneously measured electron and ion currents (compare avalanches in oxygen, section 4.4).

From oscillograms such as shown in Figure 4.6.1 the transit time of the electrons can be obtained and with the known gap spacing, the drift velocity can be determined.

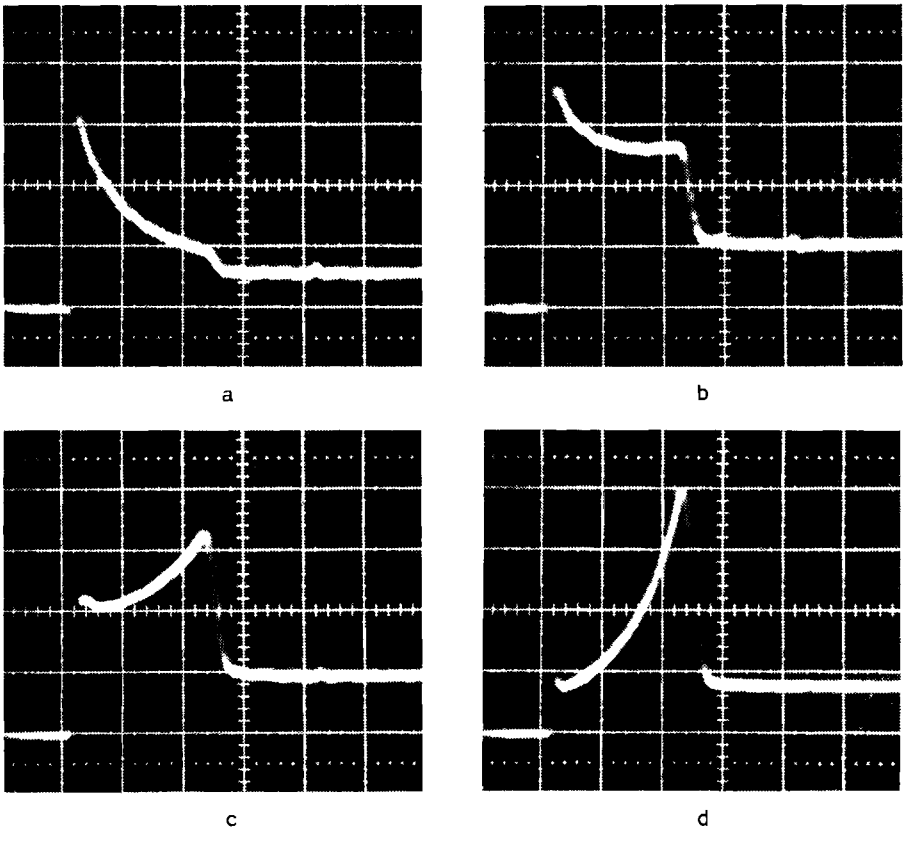

Fig. 4.6.1 Currents caused by avalanches in SF_6;
d = 1 cm, p = 52.9 Torr, 20 ns/div.
(a) E = 6.14 kV/cm, 75 μA/div.
(b) E = 6.20 kV/cm, 75 μA/div.
(c) E = 6.24 kV/cm, 150 μA/div.
(d) E = 6.32 kV/cm, 400 μA/div.

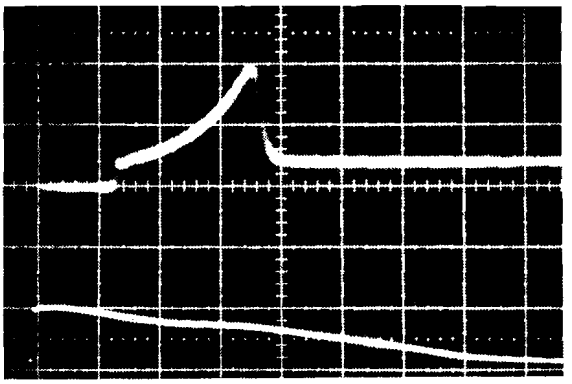

a

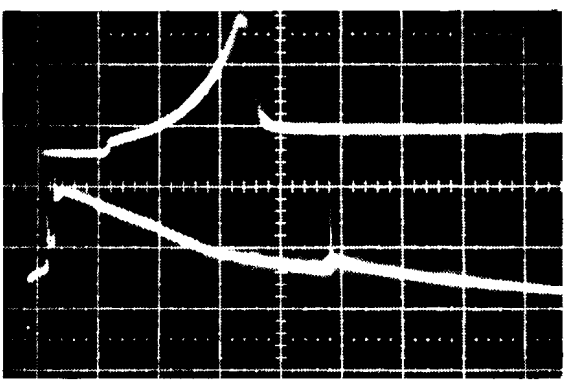

b

Fig. 4.6.2 Currents caused by avalanches in SF_6; d = 1 cm, p = 52.9 Torr;
(a) E = 6.30 kV/cm, upper beam 0.4 mA/div, 20 ns/div, lower beam 0.2 mA/div, 2 µs/div.
(b) E = 6.34 kV/cm, upper beam 0.8 mA/div, 20 ns/div, lower beam 0.4 mA/div, 5 µs/div. The spikes on the ion current are discussed at the end of this section.

Figure 4.6.3 shows v_e as a function of E/p. For reasons which will be explained later on in this section the measurements are carried out at different gas pressures; for values of E/p at which v_e could be measured, v_e appears independent of the pressure. For E/p close to 118 $Vcm^{-1}Torr^{-1}$ this conclusion holds for pressures from 5 to 100 Torr for lower and higher E/p, v_e can only be measured for a narrower pressure range.

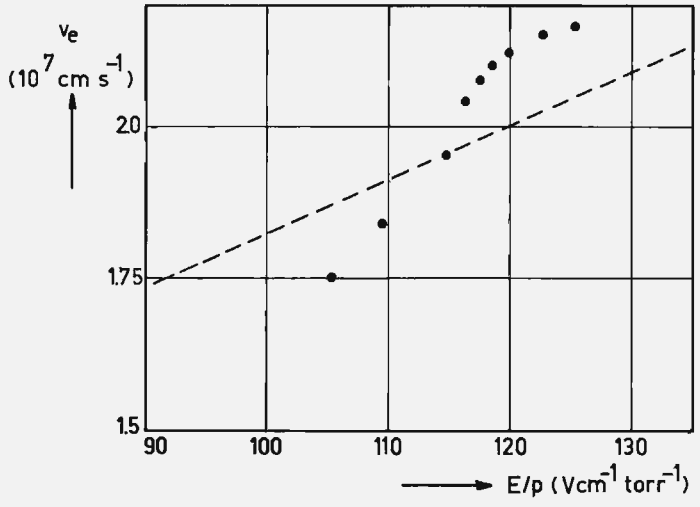

Fig. 4.6.3 Electron drift velocity v_e as a function of E/p in SF_6, 5 < p < 100 Torr; ● our measurements, dotted line from Ref. [Ha 71].

The dotted line in this figure is an extrapolation of measurements by Harris and Jones [Ha 71] for a lower E/p range, $5.3 < E/p < 53$ $Vcm^{-1}Torr^{-1}$, where the data turned out to fit the equation:

$$v_e = 1.74 \times 10^6 \, (E/p)^{0.51} \qquad (4.6.1)$$

That our measurements at high E/p do not follow this equation is not surprising since many types of inelastic collisions occur in SF_6, with efficiencies which depend strongly on E/p.

Also from oscillograms such as shown in Figure 4.6.1 the effective ionization coefficient, $\alpha - \eta$, can be derived in the same way as described for nitrogen and carbon dioxide (see sections 4.2 and 4.3).

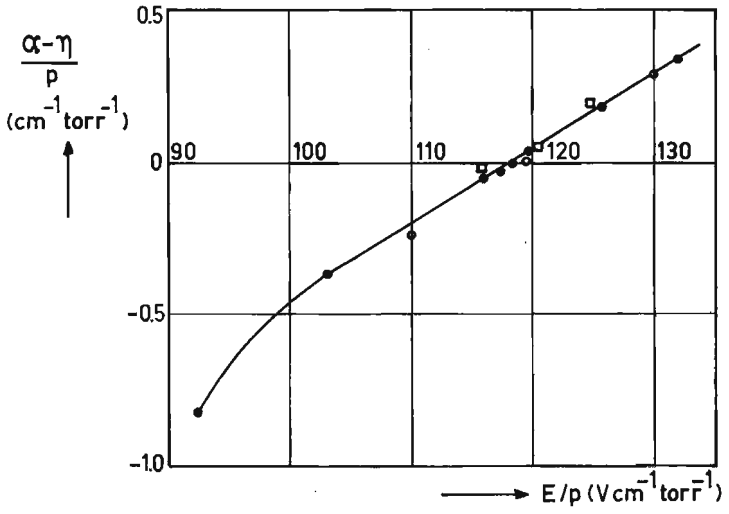

Fig. 4.6.4 Effective ionization coefficient as a function of E/p, 5 < p < 100 Torr;
- ● *our measurements,*
- □ *from Ref. [Bo 71],*
- o *from Ref. [Te 74].*

Figure 4.6.4 shows $(\alpha - \eta)/p$ in SF_6 as a function of E/p. In this figure also values are given which have been measured by Teich and Branston [Te 74] and Boyd and Crichton [Bo 71]. From the figure it can be seen that the values of our measuring points for $103 < E/p < 132$ Vcm^{-1} can be expressed by:

$$\frac{\alpha-\eta}{p} = k\,\{(E/p)-(E/p)_{crit}\} \quad cm^{-1}Torr^{-1} \qquad (4.6.2)$$

in which $(E/p)_{crit} = 118$ $Vcm^{-1}Torr^{-1}$ is the value of E/p for which α equals η, and $k = 0.024$. In the literature (see for example [Ma 81]) equations of this type are often suggested: values of $(E/p)_{crit}$ vary from 114.3 to 118.6 $Vcm^{-1}Torr^{-1}$ while k varies from 0.026 to 0.028.

The strong increase of $(\alpha - \eta)/p$ with E/p is the reason why we had to do our measurements at low pressures; the higher the pressure the smaller is the range of E/p for which we can measure avalanche currents from which v_e and $\alpha - \eta$ can be derived. With Eq. (4.6.2) it can be shown that at higher pressures even a small scale inhomo-

genity of the E-field can lead to breakdown through the streamer mechanism even though the mean E/p value is well below 118 $Vcm^{-1}Torr^{-1}$. When a single electron starts from the cathode the number of electrons when the head of the avalanche has reached a distance x_c, is given by:

$$n_e = \exp \{ \int_0^{x_c} (\alpha - \eta) dx \} \qquad (4.6.3)$$

or

$$\ell n\ n_e = \int_0^{x_c} (\alpha - \eta) dx \qquad (4.6.4)$$

with Eq. (4.6.2) this can be written as:

$$\ell n\ n_e = 0.024 \int_0^{x_c} E(x) dx - 2.83\ p x_c \qquad (4.6.5)$$

Suppose that the electric field strength exceeds the critical field 118 p over a distance $x_c < d$:

$$E(x) = 118\ a\ p \qquad (4.6.6)$$

in which $a > 1$. Equation (4.6.5) can now be written as:

$$\ell n\ n_e = 2.83\ p\ x_c\ (a-1) \qquad (4.6.7)$$

The streamer criterion is reached when n_e approximately equals 5×10^8 (see for example [Me 78]) or $\ell n\ n_e = 20$, from which follows:

$$x_c = \frac{7.07}{(a-1)p} \qquad (4.6.8)$$

For example, if a = 1.1 the gap breaks down at a pressure of 760 Torr when $x_c > 0.93$ mm.

The gap of our measuring setup broke down at a gapwidth of 5 mm and a SF_6 pressure of 769 Torr, when E/p equaled 116.19 $Vcm^{-1}Torr^{-1}$. The increase of the electric field strength near the annular gap of our

subdivided cathode could be the reason that the critical E/p value of 118 $Vcm^{-1}Torr^{-1}$ was not reached.

For a homogeneous E-field the breakdown criterion is reached for $x_c = d$, so Eq. (4.6.7) can be written as:

$$a - 1 = \frac{7.07}{pd} \qquad (4.6.9)$$

which shows that for high values of pd, a approaches unity , in other words that the gap will break down just above $E/p = 118\ Vcm^{-1}Torr^{-1}$. The relation between the sparking potential and pd is in this case given by:

$$U_s = 118\ pd = (E/p)_{crit}\ pd \qquad (4.6.10)$$

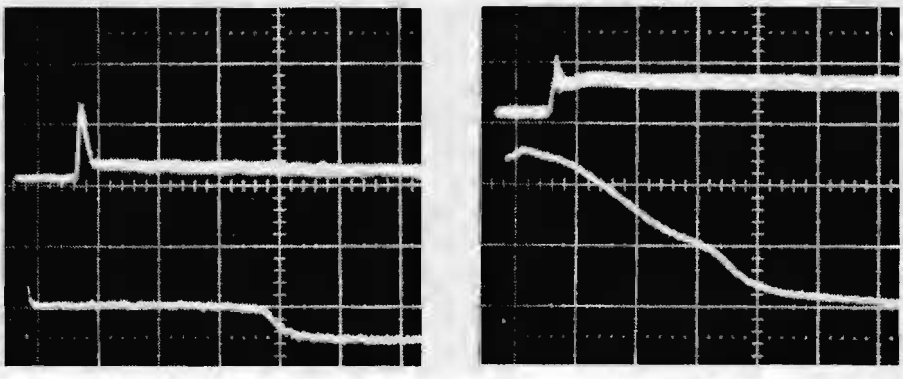

a b

Fig. 4.6.5 Currents caused by avalanches in SF_6; d = 5 mm, p = 769 Torr
(a) E = 85.2 kV/cm, upper beam 0.8 mA/div. 20 ns/div, lower beam 200 µA/div, 2 µs/div.
(b) E = 89.34 kV/cm, upper beam 2 mA/div, 20 ns/div, lower beam 400 µA/div, 2 µs/div.

Figure 4.6.5 shows avalanche currents in SF_6 at a pressure of 769 Torr. The electron components can be seen to die out very

quickly after the start of the avalanche. With Eq. (4.6.2) it can be calculated that at a pressure of 769 Torr $\alpha - \eta = -132{,}9\ cm^{-1}$ for $E/p = 110.8\ Vcm^{-1}Torr^{-1}$ (situation of Figure 4.6.5 a) and $\alpha - \eta = -33.6\ cm^{-1}$ for $E/p = 116.18\ Vcm^{-1}Torr^{-1}$ (situation of Figure 4.6.5 b). These very low $\alpha - \eta$ values are the reason of the fast decrease of the electron component.
The ion component in Figure 4.6.5 a results mostly from negative ions which were formed very close to the cathode (compare Figure 2.5.3). The ion component in Figure 4.6.5 b shows that now also positive ions contribute to the current. Also the current waveform indicates that under these conditions detachment takes place, since the current increases after $t = T_e$ (compare avalanches in oxygen, section 4.4). Also it can be seen that secondary processes take place since a current remains after one ion transit time. This also can be seen from the ion component shown in Figure 4.6.2 b which even shows current "spikes" caused by individual electron avalanches. Which secondary process causes this phenomenon is not clear, but it certainly is not photoemission of electrons from the cathode since this would occur in a time which is much shorter than the observed one (compare avalanche in nitrogen section 4.2).

These secondary processes of whatever nature will cause the apparent $(\alpha - \eta)_T$ to be larger than the real $(\alpha - \eta)$ shown in Figure 4.6.4; just as observed in air (see section 4.5). This is consistent with the fact that we found a smaller k value in Eq. (4.6.2) than other authors.

4.7 Avalanches in sulphur hexafluoride/nitrogen mixtures.

In this section measurements on avalanches in mixtures of sulphur hexafluoride and nitrogen are described.

As is mentioned in the previous section, SF_6 is often used in high-voltage equipment because of its high breakdown strength. However, since SF_6 is rather expensive and its behavior in inhomogeneous fields at high pd values is not so good, there is also much interest in the breakdown characteristics of mixtures of SF_6 with more common gases like nitrogen or air (see for a review paper on this subject Ref. [Ma 79]).

To investigate the influence of adding nitrogen to SF_6 one could measure the breakdown voltage in a homogeneous E-field, or one could determine the critical E/p value, $(E/p)_{crit}$, for which α equals η. In the previous section it is shown that for high pd values and in SF_6 the two methods lead to the same results (see Eq. (4.6.10)). When mixtures are used one should make certain that the mixture in the vessel is homogeneous. Suzuki [Su 82] has investigated the rate of mixing of SF_6 and N_2. He found that, when the mixing is only caused by the diffusion process, several hours are needed before the mixture is homogeneous. In our experiment the inlet of one gas into the other was accompanied by turbulence and in addition an electric fan was placed in the vessel to speed up the mixing process. We found that approximately 5 minutes after the vessel was filled with the two gases $(E/p)_{crit}$ had reached a stationary value from which we conclude that the mixture is homogeneous.

We measured avalanche currents in SF_6/N_2 mixtures at a total pressure of 50 Torr. Since the current waveforms were very similar to the waveforms obtained in pure SF_6 we do not show oscillograms. As we did for SF_6 we determined $\alpha - \eta$ values for several mixing ratios of SF_6 and N_2. Since the value of $(E/p)_{crit}$ is the most interesting quantity we give here only this quantity, Figure 4.7.1 shows $(E/p)_{crit}$ as a function of the partial pressure of SF_6 in percents. In this figure also values of $(E/p)_{crit}$ are given which have been measured by Aschwanden [As 79]. The full line in the figure represents the empirically derived equation which fits our measurements for $10 \leq \%SF_6 \leq 60$:

$$(E/p)_{crit} = 118.0 - 2.84\ (1.03)^{C}\ Vcm^{-1}Torr^{-1} \qquad (4.7.1)$$

in which C is the percentage of N_2 in the mixture. The dotted line represents the equation empirically derived by Aschwanden:

$$(E/p)_{crit} = 4.69\ D^{0.2}\ Vcm^{-1}Torr^{-1} \qquad (4.7.2)$$

in which D is the percentage of SF_6 in the mixture.

Pelletier, Gervais and Mukhedkar [Pe 81] have measured relative sparking potentials, RSP (sparking potential of the mixture divided by the

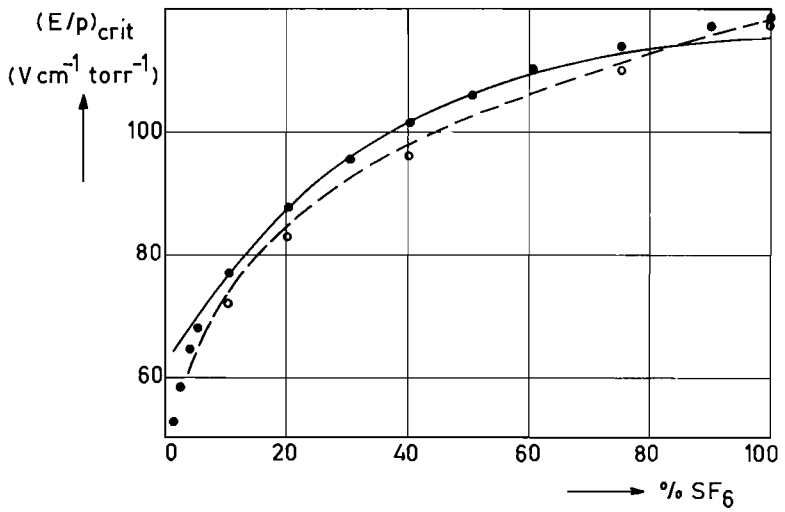

Fig. 4.7.1 The critical value of E/p as a function of the percentage of SF_6 in the SF_6/N_2 mixture, measured at a total pressure of 50 Torr,

- ● *our measurements,*
- o *from Ref. [As 79], the full line represents Eq. (4.7.1) and the dotted line Eq. (4.7.2).*

sparking potential of pure SF_6) of SF_6/N_2 mixtures in uniform fields. For 40% SF_6 they found RSP = 0.87 and for 60% SF_6, RSP = 0.92. From our measurements follows that the relative $(E/p)_{crit}$ ($(E/p)_{crit,mixt}/(E/p)_{crit,SF_6}$) for 40% SF_6 is 0.86 and for 60% SF_6, 0.93, which is in good agreement with the RSP values given in Ref. [Pe 81].

In Figure 4.7.2 the mobility K of electrons (K is defined as the ratio of the drift velocity and the applied E-field) for $(E/p)_{crit}$ at a pressure of 50 Torr is shown as a function of the percentage SF_6 in the mixture.

The addition of SF_6 to N_2 clearly slows down the electrons, which can be attributed to the many inelastic collision processes of electrons with SF_6 molecules.

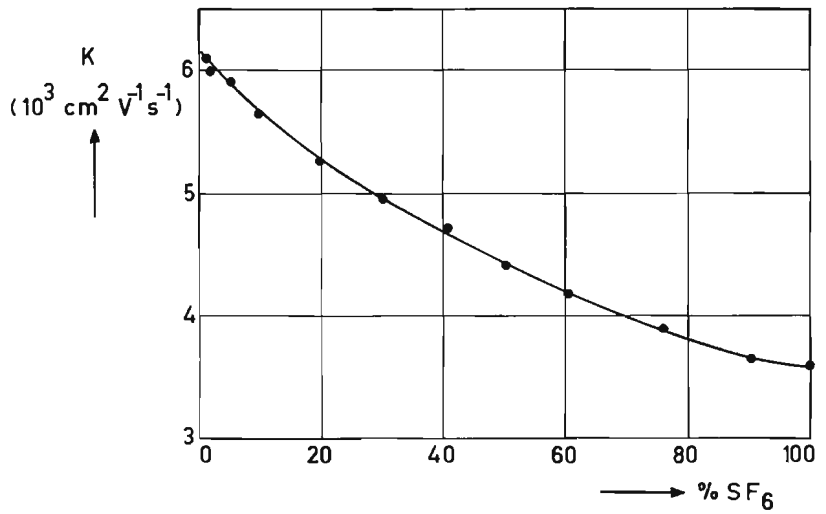

Fig. 4.7.2 The mobility K of electrons for $(E/p)_{crit}$ at a pressure of 50 Torr as a function of the percentage SF_6 in the SF_6/N_2 mixture.

4.8 Avalanches near a solid insulator.

In this section measurements on avalanches near a solid insulator are described.

Gas insulated systems require solid insulators (spacers) to support the electrodes. These spacers tend to lower the breakdown characteristics of the entire system (see for a review paper on this subject Ref. [La 81]). A study on avalanche formation in the vicinity of a spacer may give information on the mechanisms causing this influence. As a first approach to such a study we did some experiments on avalanche formation near a cylindrical teflon spacer. We placed the spacer between the electrodes so that the primary electrons were released near the cathode-solid-gas triple junction. The laser beam was focussed to a diameter of 1.5 mm. Avalanche currents measured in this way in air as well as in nitrogen showed no noticeable differences with avalanche currents measured in the absence of a spacer.

Jaksts and Cross reported an influence of a teflon spacer on the avalanche growth in air [Ja 78] and in nitrogen [Ja 81] in a comparable experiment. We suspect that the reported influence may be explained as the effect of the spacer on the response of their measuring setup. To maximize any interactions between the charge carriers in the avalanche and the spacer material we studied avalanche growth inside a hollow, cylindrical channel in the spacer material.
Figure 4.8.1 shows currents caused by such avalanches in nitrogen; the diameter of the channel in the teflon spacer was 4 mm. The current of

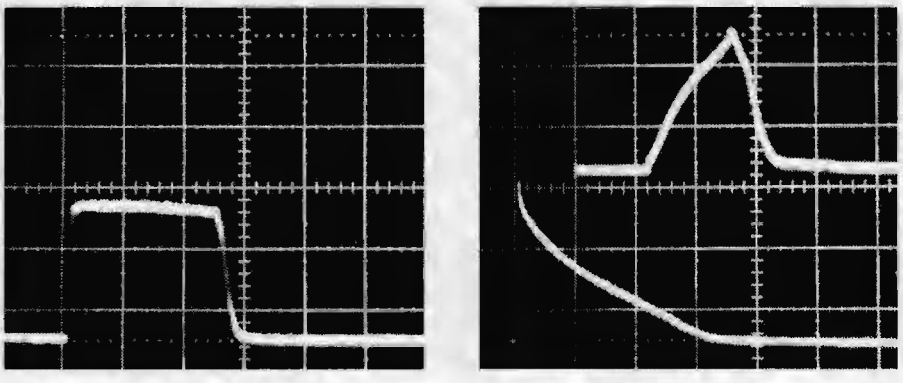

a b

Fig. 4.8.1 Avalanches in nitrogen near a teflon surface;
d = 1 cm, p = 760 Torr,
(a) U = 17.00 kV, 75 µA/div, 50 ns/div,
(b) U = 28.00 kV, lower beam 17.2 µA/div,
5 µs/div, upper beam 1.2 mA/div,
50 ns/div.

Figure 4.8.1 a, monitored at an applied E-field for which no ionization takes place, is very similar to the current which would be measured without a spacer (see Figure 4.2.1 a), although the current drop after one electron transit time is not so fast. The electron current shown in Figure 4.8.1 b clearly deviates from the normal exponential growth which occurs in the absence of the spacer, and in addition the current drop at $t = T_e$ is much slower (compare Figures 4.2.6 and 4.2.9). Also the ion current shape differs much from shapes measured without a spacer (see Figure 4.2.9).

The reason for all these differences is not clear. Perhaps the formation of surface charges on the insulator deforms the initially homogeneous E-field. This would lead to a different growth of the avalanche since the ionization coefficient α is strongly dependent on the E-field (see Figure 4.2.8). Also the relation between the motion of the charge carriers and the current in the external circuit will change (see Eqs. (2.3.1), (2.3.2) and (2.3.3)).

Figure (4.8.2) shows currents caused by avalanches in a conical channel in a teflon spacer. The diameter of the channel varies from 3 to 6 mm. In this case the E-field is inhomogeneous because of polarisation charges and possible also because of additional surface charges. From the currents shown in Figures 4.8.2 (a) and (c) it can be seen that the E-field varies in the channel.

All the electron currents show again the slower drop at $t = T_e$ than would be measured without a spacer.

How to derive more information from such currents about the interaction processes between the avalanche and the insulator surface would be an interesting subject for further research.

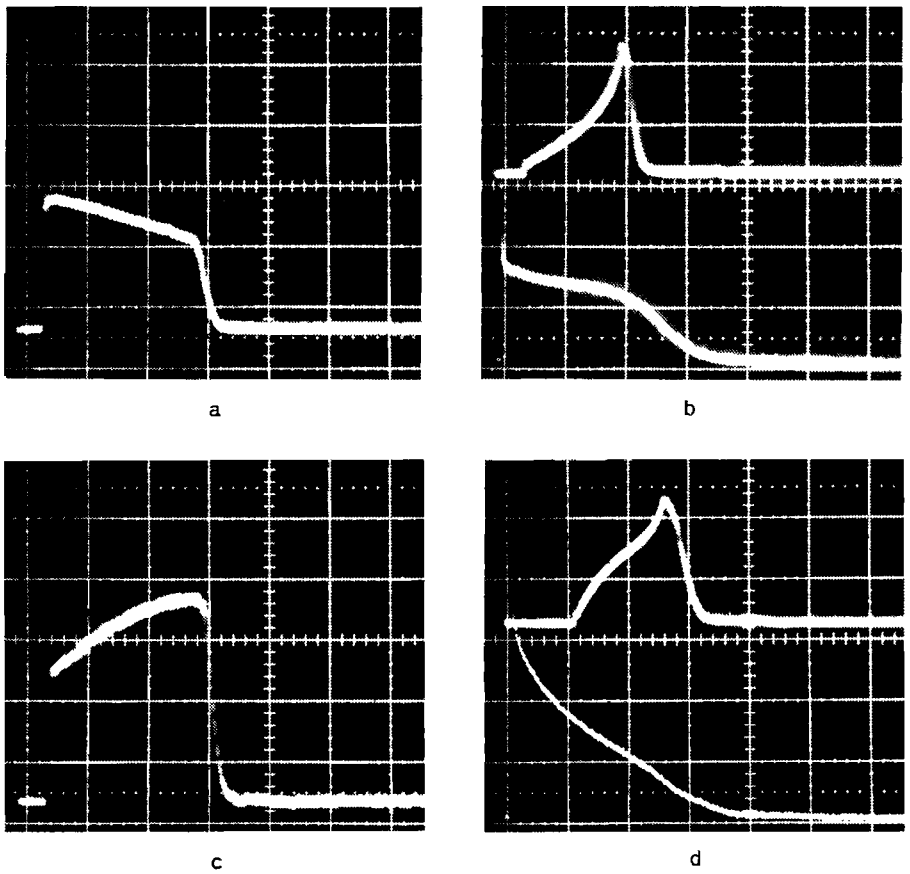

Fig. 4.8.2 Currents caused by avalanches in nitrogen in a conical channel (diameter varies from 3-6 mm) in a teflon spacer; d = 1 cm, p = 760 Torr, (a) and (b) the wider opening of the channel at the cathode, (c) and (d) spacer upside down in comparison with (a) and (b).
(a) U = 17.00 kV, 75 μA/div, 50 ns/div,
(b) U = 28.00 kV, lower beam 8.6 μA/div, 5 μs/div, upper beam 0.6 mA/div, 50 ns/div,
(c) U = 17.00 kV, 30 μA/div, 50 ns/div,
(d) U = 28.00 kV, lower beam 8.6 μA/div, 5 μs/div, upper beam 1.2 mA/div, 50 ns/div.

5. CONCLUSIONS

Improvements of the usual "electrical method" for avalanche studies have led to a setup with which direct information about processes in the avalanche can be obtained.
The main improvements are the use of a laser with 0.6 ns pulse duration to initiate the avalanche, the use of a subdivided measuring electrode and a decoupling resistor directly above the high-voltage electrode.
The limitations of a subdivided electrode, caused by the Ramo-Shockley effect, have to be properly analyzed to have both a large bandwidth and a current truly representing the motion of the charge carriers.
Under those conditions the current waveforms not only provide a direct insight into various processes in the avalanche, but give also fundamentally more information when two processes occur in rapid succession.

Since the avalanche can be started with a high number of primary electrons no ionization is needed to obtain a measurable signal and therefore measurements can be carried out at low E/p values.

The currents caused by electrons as well as by ions can be measured without changes in the setup. In fact the two components can be monitored simultaneously which gives additional information about processes as secondary emission, detachment and conversion.

For gases in which only ionization and attachment are important, the current waveforms can be calculated with the "classical" equations. If also secondary emission of photoelectrons from the cathode occurs, the numerical method of section 2.7 gives good agreement between computed and measured waveforms. For gases in which in addition to the fore-mentioned processes, detachment and conversion take place, the electron current waveform can be described by the analytical solution given in section 2.8 up to one electron transit time. At later times the numerical method given in section 2.9 gives useful results.

Measured avalanche currents in air show clearly an influence of water vapor on the avalanche growth. It is shown that this influence

is caused by conversion reactions between negative ions and water molecules and not by an increase of the attachment coefficient, as is generally assumed.

The critical E/p value of attaching gases, which is important for high-pressure gas insulated systems, can easily be determined, even if detachment and conversion occur.

At lower pressures the influence of diffusion can be clearly seen and with the theory of section 2.4 numerical values of the diffusion coefficient in nitrogen have been derived.

For some gases values of several discharge parameters derived by us differ at low E/p values significantly from values reported by other authors. Since we can work with sizeable signals, even at low E/p values, our results should be reasonably accurate.

Preliminary measurements have been done on avalanches propagating close to the surface of solid insulators. Surface charges on the insulators are important but no further conclusions can be drawn at this stage.

REFERENCES

Al 76 S.R. Alger and J.A. Rees, J. Phys. D 9, 2359 (1976).

As 79 Th. Aschwanden, Third Int. Symp. on High Voltage Engineering, Milan, 31.12 (1979).

As 81 Th. Aschwanden and G. Biasiutti, J. Phys. D 14, L 189 (1981).

Au 58 P.L. Auer, Phys. Rev. 111, 671 (1958).

Ba 75 F. Bastien, R. Haug and M. Lecuiller, Journal De Chimie Physique 72, 105 (1975).

Bo 71 H.A. Boyd and G.C. Crichton, Proc. IEE 118, 1873 (1971).

Br 47 F.M. Bruce, Proc. IEE 94, 138 (1947).

Co 75 V.J. Conti and A.W. Williams, J. Phys. D 8, 2198 (1975).

El 66 M.T. Elford, Aust. J. Phys. 19, 629 (1966).

Fo 73 M.A. Folkard and S.C. Haydon, J. Phys. B 6, 214 (1973).

Fr 60 L. Frommhold, Z. Phys. 160, 554 (1960).

Fr 64 L. Frommhold, Fortschr. Phys. 12, 597 (1964).

Ha 71 F.M. Harris and G.J. Jones, J. Phys. B 4, 1536 (1971).

Ha 76 S.C. Haydon and O.M. Williams, J. Phys. D 9, 523 (1976).

Ja 78 A. Jaksts and J.D. Cross, IEEE Int. Symp. on Electr. Insul, Philadelphia, 149 (1978).

Ja 81 A. Jaksts and J.D. Cross, Can. Elec. Eng. J. 6, 14 (1981).

La 81 J.R. Laghari, IEEE Trans. Electr. Insul. Vol EI-16, 373 (1981).

Lo 41 L.B. Loeb and J. Meek, The mechanism of the Electric Spark (Oxford University Press, 1941).

Ma 78 N.H. Malik and A.H. Qureshi, IEEE Trans. Electr. Insul. Vol. EI-13, 135 (1978).

Ma 81 N.H. Malik, IEEE Trans. Electr. Insul. Vol. EI-16, 463 (1981).

Me 78 J.M. Meek and J.D. Craggs, Electrical Breakdown of Gases (Wiley, New York, 1978).

Me 78[1] Ref. [Me 78] page 91.

Me 78[2] Ref. [Me 78] page 104.

Ni 36 R.A. Nielsen, Phys. Rev. 50, 950 (1936).

Pa 72 J.E. Parr and J.L. Moruzzi, J. Phys. D 5, 514 (1972).

Pa 78 B.S. Patel, Rev. Sci. Instrum. 49, 1361 (1978).

Pe 81 J.M. Pelletier, Y. Gervais and D. Mukhedkar, IEEE Trans. on Power Apparatus and Systems, Vol. Pas-100, 3861 (1981).

Pr 59 A.N. Prasad, Proc. Phys. Soc. 74, 33 (1959).

Pr 60 A.N. Prasad and J.D. Craggs, Proc. Phys. Soc. 76, 223 (1960).

Ra 40 H. Raether, Naturwiss. 28, 749 (1940).

Ra 64 H. Raether, Electron Avalanches and Breakdown in Gases (Butterworths, London, 1964).

Ra 39 S. Ramo, Proc. IRE 27, 584 (1939).

Sa 77 H.T. Saelee, J. Lucas and J.W. Limbeek, Solid State and Electron Devices 1, 111 (1977).

Sc 60 H. Schlumbohm, Z. Phys. 159, 212 (1960).

Sh 38 W. Shockley, J. Appl. Phys. 9, 635 (1938).

Sn 75 R.A. Snelson and J. Lucas, Proc. IEE 122, 333 (1975).

Su 82 T. Suzuki, IEEE Trans. Electr. Insul. Vol. EI-17, 34 (1982).

Te 74 T.H. Teich and D.W. Branston, Third Int. Conf. on Gas Discharges, IEE Conf. Publ. 118, 109 (1974).

Te 75 T.H. Teich, M.A.A. Jabbar and D.W. Branston, 2nd Int. High Voltage Symp., Zürich 1975, 390.

Th 63 H. Tholl, Z. Phys. 172, 536 (1963).

Va 53 R.N. Varney, Phys. Rev. 89, 708 (1953).

Ve 82 H.F.A. Verhaart and P.C.T. van der Laan, J. Appl. Phys. 53, 1430 (1982).

Vo 57 J.K. Vogel and H. Raether, Z. Phys. 147, 141 (1957).

Wa 64 K.H. Wagner, Z. Naturforschg 19a, 716 (1964).

Stellingen

behorend bij het proefschrift van

H.F.A. Verhaart

1. Dat Jaksts en Cross een hogere driftsnelheid van elektronen in stikstof meten dan andere auteurs wordt door hen ten onrechte aan ruimtelading toegeschreven.

   A. Jaksts en J.D. Cross, Can.Elec.Eng. J.6, 14 (1981).

2. Berekening van de doorslagspanning van lucht met het streamer criterium, waarbij waarden voor de effectieve ionisatie-coefficient worden gebruikt die bepaald zijn met de Townsend methode, leidt bij hoge druk en/of grote elektrodenafstand tot onjuiste resultaten.

   N.H. Malik, IEEE Trans.Electr.Insul. Vol.EI-16, 463 (1981).

3. De invloed van het waterdampgehalte op de doorslagspanning van lucht is een gevolg van de wisselwerking tussen zuurstof-ionen en water-moleculen en niet van elektronenvangst door water-moleculen. Deze conclusie wordt gesteund door het feit dat in stikstof het water-dampgehalte geen invloed heeft op de doorslagspanning.

   J. Giesenbauer, Proc. of the 2nd Int.High Voltage Symp. Zürich, p.448 (1975).
   Dit proefschrift, section 4.5.

4. Aanwezigheid van oppervlaktelading op een isolerende spacer hoeft niet noodzakelijkerwijze te leiden tot een verlaging van de door-slagspanning van het spacer-gas systeem, zoals door Knecht wordt gesteld.

   A. Knecht, Proc. of the 3rd Int.Symp. on Gaseous Dielectrics, Knoxville, USA, 1982. (to be published).

5. Vaak wordt de minimaal detecteerbare grootte van partiële ont-ladingen opgegeven als een soort kwaliteitsmaat voor een hoog-spanningslaboratorium. Hierbij dient echter tevens te worden ver-meld bij welke sample-capaciteit dit minimum haalbaar is.

6. Het model van Jüttner ter verklaring van de kathode-erosie in een metaaldampontlading in vacuüm, is principiëel onjuist.

   B. Jüttner, J.Phys.D.: Appl.Phys. 14, 1265 (1981).

7. De afbrandsnelheid van smeltlichamen in hoogspanningssmeltveiligheden wordt mede bepaald door verwarming van het smeltlichaam door ohmse dissipatie voor en tijdens de afbrand, zoals is aangetoond door Daalder en Hartings.
Indien bij berekeningen van de afbrandsnelheid, zoals bijvoorbeeld gegeven door Wilkens en Gnanalingam en Turner en Turner, geen rekening wordt gehouden met deze opwarming dienen de resultaten met de nodige reserve te worden gehanteerd.

J.E. Daalder en R.M. Hartings, Proc. of the 4th Int.Symp. on Switching Arc Phenomena, Lodz, Polen (1981).
R. Wilkens en S. Gnanalingam, Proc. of the 5th Int. Conf. on Gas Discharges, Liverpool, U.K., p.195 (1978).
H.W. Turner en C. Turner, Proc. of the 3rd Int. Symp. on Switching Arc Phenomena, Lodz, Polen, p.334 (1977).

8. Het door Ünal gepresenteerde model voor het dampbelgedrag aan een oververhitte wand in onderkoelde vloeistoffen is onvolledig gefundeerd o.a. omdat verondersteld wordt dat de warmtetoevoer alleen via een dunne vloeistoflaag tussen de bel en de wand plaatsvindt.

H.C. Ünal, Some aspects of two-phase flow, heat transfer and dynamic instabilities in medium and high pressure steam generators.
Proefschrift T.H. Delft, 1981.

9. Volgens berekeningen van Hart en Marino wordt een menselijk lichaam onder een hoogspanningslijn blootgesteld aan een energieflux die qua grootte vergelijkbaar wordt met de door sommigen maximaal toelaatbaar geachte energieflux bij bestraling met microgolven. Hun gebruik van een energieflux, zoals toegepast bij microgolven, is echter niet zinvol bij 50 Hz velden en deze energieflux is daarom zeker geen maat voor biologische beïnvloeding.

F.X. Hart en A.A. Marino, Journal of Bioelectricity 1, 129 (1982).

10. De eis dat een raskrielkip vijfmaal minder moet wegen dan zijn grote rasgenoot, onder behoud van lichaamsvorm, houdt geenszins in dat de lineaire afmetingen van lichaamsdelen met dezelfde factor dienen te verminderen.

C. Aalbers, Dwerghoenders als liefhebberij.
(Thieme, Zutphen, 1961), p.10.

11. Het aantal toeschouwers bij wedstrijden in het betaalde voetbal kan aanzienlijk stijgen indien, zoals reeds bij andere branches is ingeburgerd, een "niet goed, geld terug" garantie geboden wordt.

Eindhoven 14 september 1982.